# Estudio del comportamiento mecánico de puertas metálicas bajo fuego mediante modelización numérica

## Study of the mechanical behaviour of steel doors under fire using a numerical model

AUTOR:   CARMEN DEL MAR PÉREZ DELGADO

TITULACIÓN:   MASTER EN INGENERÍA DE CAMINOS, CANALES Y PUERTOS

TUTOR UPV:   JULIÁN ALCALÁ GONZÁLEZ

TUTOR DTU:   LUISA GIULIANI

CURSO: 2019/2020

**DTU Civil Engineering**
Department of Civil Engineering

# Study of the mechanical behaviour of steel doors under fire using a numerical model

Carmen del Mar Perez Delgado

Kongens Lyngby 2020

DTU

# Abstract

Steel fire doors are essential for the passive fire protection strategy of any building or structure. The aim of this thesis is to analyse the behaviour of a wide sliding steel door under fire by developing a FEM (Finite element method) model. According to the Fire Test Procedures Code (FTP code) of the International Maritime Organization (IMO)[1], when a fire resistance door is larger than those which can be accommodated in the standard specimen size (2.4x2.5 m) two alternatives can be followed to approve the door, accommodate it into a larger test furnace or use the procedure established in the code for evaluation of the fire performance. The method established in the code include the performance of FEM models to analysed the door and calibrate the model, thermal and mechanical, with an equivalent tested door.

The objective of this thesis is to study the behaviour of a wide steel door under fire to developed a model that approaches to reality. So, several studies of the material behaviour under fire were performed and several models were developed to ensure the validation of the final model. The main focus was to understand the behaviour, validate the model and developed a simple final model of the steel door.

The model developed represents the external structure of a sliding steel door and the model was created using ABAQUS, a FEM modelling program. The temperature field used to study the door's behaviour follows the Standard fire curve ISO 834. The common failure mechanism of this doors is buckling so the calculus and analysis was focus on this topic.
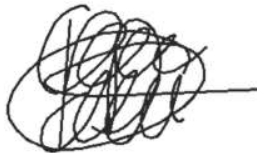
After processing the different models and developing the final one, it was found that the external structure of the steel door by itself does not provide a lot of mechanical resistance against buckling. So, internal connectors or stiffeners are necessary to connect the frontal steel plates. A proper definition of the boundary conditions is fundamental to analyse the behaviour and approach the model to a more realistic

one. It was also found that is possible to perform one way coupled analysis instead of merging a thermal model with a mechanical model. This is useful because instead of two analysis the same results can be obtained performing only one.

# Preface

This Master thesis was prepared at the department of Civil Engineering at the Technical University of Denmark in fulfillment of the requirements for acquiring a Master degree in Civil Engineering.

Kongens Lyngby, August 8, 2020

Carmen del Mar Perez Delgado

# Acknowledgements

The development of this Thesis has been a challenge and a great opportunity to develop my skills as a Civil Engineer. I want to thank my parents and friends for all their support during these months and thanks to my tutor, Luisa Giuliani, for her guidance.

# Contents

# Introduction

## 1.1 Background and motivation

Steel fire doors are one of the most common ways to avoid fire propagation in buildings and other structures. They are essential against fire and they have to ensure that flame and smoke are contained.

The thermo-mechanical behavior of steel fire doors can be studied performing laboratory tests or/and developing a Finite Element Model. However, there are limitations for the dimensions of the steel fire doors according to IMO's recommendations [2]. Large dimension fire doors cannot be tested in a laboratory due to the size of the facilities needed and the high cost. Moreover, there is no reliable FE model for doors with these dimensions. For this reason, the development of a FEM model that predicts the thermal and mechanical performance of the door during a fire will be beneficial for the industry.

It has been proven that the thermo-mechanical behavior of fire doors plays a big role in preventing flame and smoke propagation [3]. Therefore, the integrity of the door will have to be ensured, as they would limit fire propagation as well as avoid structural failure of the building where the doors are located, giving the occupants of the area sufficient time of evacuation besides giving firemen enough time to intervene and end the fire [4].

In the case of large fire doors, the non-uniform temperature distribution that leads to the bending of the door from the supporting frame is not commonly modelled due to its complexity, high computation time and non-linear behavior, leading to the uncertainty of how big the influence of the heat distribution across the door affects the mechanical properties. However, this influence can be predicted with a thermo-mechanically FEM model, which predicts the performance of a large door. This will

help the industry, because the cost of testing a large dimensions door is high as well as complex, due to security reasons and the need for special facilities.

## 1.2   Object and aim

The objective of this project is to study the mechanical behaviour of large steel doors and, at the end, create a mechanical model which predicts the behavior of a steel door during a fire. This model will be combined with a thermal model done in a brother-project by the student Ainara Sofia Franco Vergara [5]. Both documents will use synergies and exchange data from one another, with the common aim of developing a final complete model that contains the result of both projects.

The aim is to obtain results that are representative of the performance of the door during a fire scenario. In the case of merging both models, it would be one-way couple. This will create an impact on the industry in the future thermo-mechanical analysis of large fire doors, optimizing the process in time and cost.

## 1.3   Methodology

The mechanical model will start as a simple model and the complexity of it will be increased as the results obtained are validated by analytical calculations. The software used for the development of the model is the Finite Element software Abaqus.

The definition of boundary conditions that are accurate enough to represent the behavior of the door during a fire will be one of the main objectives of the model. Moreover, non-linear behaviors as plasticity, material degradation and buckling will be the key problems where the project will focus.

Different analysis will be performed during the modelling process. First, an eigenvalue analysis to obtained the differen buckling modes, then a static-transient analysis, to analysed the post-buckling behaviour. Also, the thermoplastic characteristics of the material will be taken into account, analyzing its effects on the model.

The analytical validation of the model will be done by analyzing a single plate. This plate will be representative of the behavior of the door, being its characteristics and

boundary conditions adequate.

After the mechanical model validation, the thermal and mechanical model will be merge using one-way coupling. This means that the results obtained in one of the models will determine the second model.

# Theoretical background

In this chapter the theoretical background used to developed this Thesis is going to be explained. The first section will focus in the characteristics of the fire-resistance steel doors and its importance. The next section would expose the different temperature distributions, the Standard fire curve and the material properties of the steel used in the model developed. Then, the non-linear behavior of the model, plate theory, bending of plates and buckling would be exposed.

## 2.1 Finite element method (FEM) modelling

Finite element method (FEM) is a numerical method used for solving partial differential equation in two or three space variables. These problems are known as boundary value problems because they consist of partial differential equations and boundary conditions. This method is the dominant discretization technique in structural mechanics.

To solve the problem the model is divided into components of simple geometry known as finite elements. This is accomplished by a space discretization by the development of a mesh of the object studied. The response of each element depends on a finite number of degrees of freedom characterized as the value of an unknown function at a group of nodal points.

For the development of this project a finite element modelling programmed has been used, called Abaqus, and this method has been applied for the mechanical analysis of the fire door. Regarding the types of elements and the analysis used in Section 3

it has been explained in detail.

## 2.2   Fire-resistance steel door

Fire resistance doors are fundamental in the fire protection of a structure. The objective of the door is to slow or stop the fire propagation inside a building or a construction being a key element for safety. For this reason, the study of the deformation of the door under fire action is a key element in the design of optimal and reliable doors. The door has to contain the fire and the smoke so, when the door deforms due to fire-action the space between the frame and the door has to be small enough, at least for a establish period of time.

This thesis will focus in sliding steel doors with big dimensions. This doors are usually used in industrial environments or garages. The main problem with this doors is that due to its size it is difficult and expensive to perform fire-test. For this reason a reliable finite element model of this type of doors could be really useful for the industry.

The steel door analysed during this thesis have a dimensions of 2.8x2.8 meters and a total width of 82 millimeters. The steel plates that compose the door have a thickness of 1 mm and the insulation, made of mineral wool, has a thickness of 80 millimeters and it is located inside the door. The sliding mechanism and the disposition of the door is similar to the one show in Figure 5.19.



**Figure 2.1** Industrial sliding fire resistance steel door. Picture extracted from Samson doors official website [6]

The door is subjected at top and bottom in one of the sides by rails. When the door

is closed one of the sides is in direct contact with the side wall and the frame, while the top of the door and the other side are in contact with the side walls. When the door is closed both sides are perfectly isolated from each other.

The properties of the sliding steel door used as a model was provided by DBI (Dansk Brand- og Sikringsteknisk Institut).

## 2.3   Fire

When a structure is design against fire it is a common practice to represent the temperature distribution using the Standard fire-curve. In this Thesis, it was used the Standard fire curve ISO 834 which is defined by Equation 2.1. In this Equation $t$ is the time in minutes, $T$ is the furnace temeprature (ºC) at time $t$ and $T_0$ is the initial temperature (ºC).

$$T = To + 345 \log 10(8t + 1) \tag{2.1}$$

The curve obtained with this equation is shown in Figure 2.2.
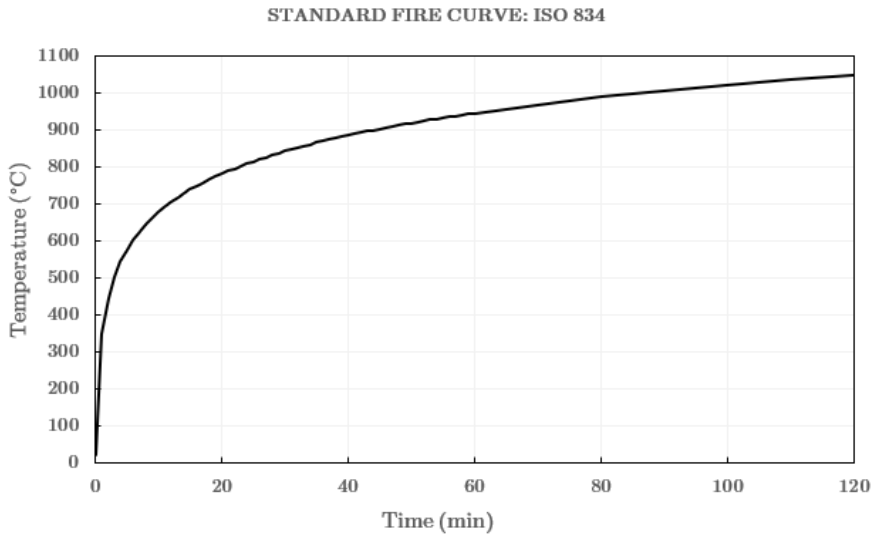


**Figure 2.2** Standard fire curve ISO 834.

## 2.4   Material properties

The material used in the model developed is galvanized steel which is a common material on the design of fire resistance steel doors. The type chosen is ASTM A525 Galvanized Steel [7] which provides sufficient resistance to the steel panels that conform the door. This type is characterized by the corrosion protection of the zinc-iron coating (galvanization process) which protects the metal as a barrier against corrosive elements.

### 2.4.1   Mechanical properties

The galvanized steel A525 is characterized by a Young modulus of 210 GPA and a Poisson's ratio of 0.3, being its density 7800 $kg/m^3$.

#### 2.4.1.1   Elasticity modulus

The Young modulus, also called elasticity modulus, is a constant that describes the elastic properties of a determined material. It is a mechanical property that measures the stiffness and its value is equal to the longitudinal stress divided by the strain. This modulus is directly related to the stress-strain curve of the material, Figure 2.3. Its value is calculated by measuring the slope of the axial stress-strain curve in the elastic zone of the diagram.

#### 2.4.1.2   Stress-strain curve

The stress-strain diagram for steel plots the elongation of the material versus the applied stress. It can be divided in two different zones: the elastic zone and the plastic zone. The elastic zone is characterized by a linear straight line and its located at the beginning of the diagram. Then, after a transition zone, when the yield strength is reach the plastic zone starts. If the material is considered perfectly plastic the elongation will increased at constant stress, Figure 2.3, but if a more realistic behavior is considered it will appear some strain hardening after yielding, Section 2.4.2.

The stress-strain curve is one of the most reliable sources to evaluate the mechanical properties of the material.
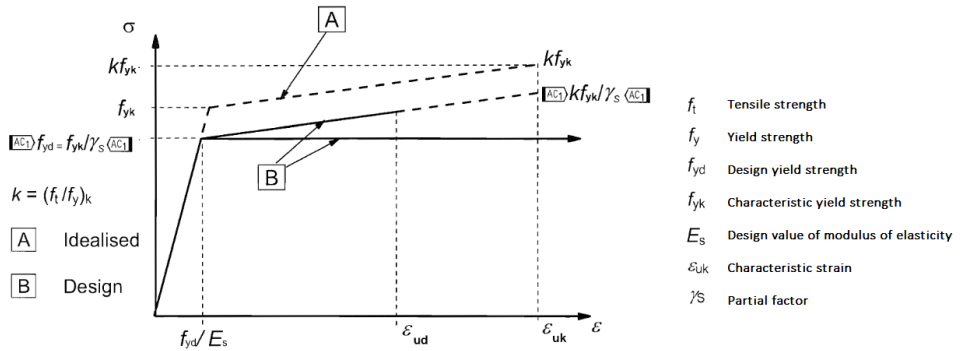
**Figure 2.3** Idealised and design stress-strain diagram for steel according Eurocode 2 [8]

### 2.4.1.3  Poisson's ratio

The Poisson's ratio measures the expansion/contraction of the material in different directions, depending of the load state. It is the ratio between the transverse strain, perpendicular to the load applied, and the axial strain, in the direction of the applied load.

### 2.4.1.4  Thermal degradation of the Young modulus. Stress-strain curve.

When a steel element is exposed to temperature changes its mechanical properties starts degrading as the heat increases. The stress-strain curve is affected by this effect, as well as the Young modulus.

As the temperature is rising the yield strength, the proportional limit and the slope of the linear-elastic range decreases. This variations were determined in Eurocode-3 [9] by establishing different reduction factors. The change of the different reduction factors due to temperature has been plotted in Figure 2.4. In Figure **??** the degradation of the stress-strain curve has been plotted.
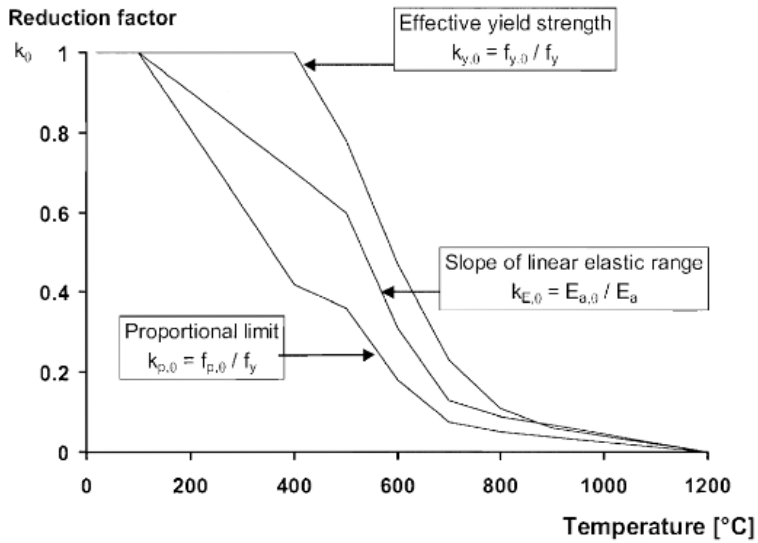
**Figure 2.4** Reduction factors of the stress-strain curve at elevated temperatures, according to Eurocode-3 [9].
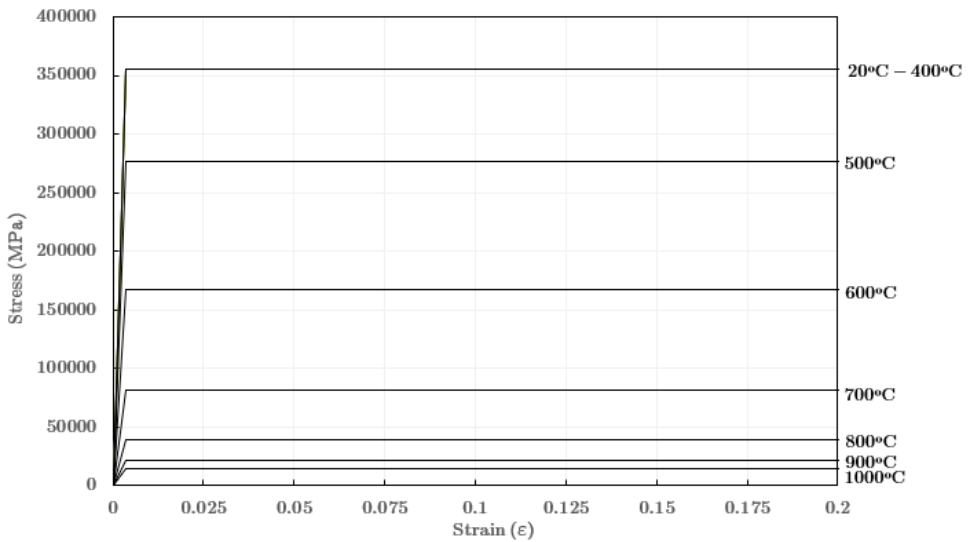


**Figure 2.5** Stress-strain curve degradation due to temperature increase, according to Eurocode-3 [9].

Regarding the Young modulus, in Figure 5.4 it has been plotted its degradation as

the temperature increases. The orange line represent the Eurocode degradation curve and the green and blue represents the Kristian Dahl Hertz curve, extracted from the slides of the course *11023 Structural Fire Safety Design* at DTU [10]. This curve provides a better fit with the experimental data and it is smoother than the Eurocode curve.

It has been calculated using the formulation shown in Equation 2.2 where $T$ is the fire temperature and the rest are parameters that depends on the type of material of the structure analysed. For the type of steel used in this Thesis the parameteres have the values shown in Table 2.1

$$\xi_s(T) = k + \frac{1-k}{1 + \frac{T}{T_1} + \left(\frac{T}{T_2}\right)^2 + \left(\frac{T}{T_s}\right)^8 + \left(\frac{T}{T_{64}}\right)^{64}} \tag{2.2}$$

| k | $T_1$ (°C) | $T_2$ (°C) | $T_8$ (°C) | $T_{64}$ (°C) |
|---|---|---|---|---|
| 0 | 6000 | 620 | 565 | 1100 |

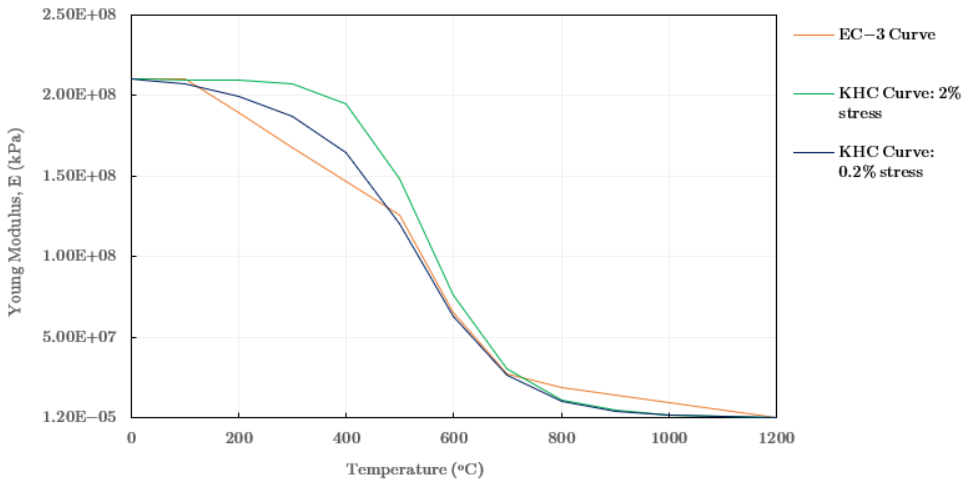**Table 2.1** Values for the KHZ curve for the E-modulus degradation.



**Figure 2.6** Young modulus degradation due to fire exposure of the material.

## 2.4.2   Plasticity

Plasticity is the ability of the material to developed non-reversible deformations due to the action of an applied force. There are different types of plasticity: perfectly plastic or plasticity with hardening. Perfect plasticity is an ideal situation and plasticity with hardening approaches more to a real case.

In a perfectly plastic material, when the yielding load is reached the plastic deformation keeps growing at constant load. The material with plastic hardening need higher loads than the yielding point to its deformation to keep growing.

For this case, it was chosen a perfectly plastic material to keep on the safety side. The yielding point of the steel used is 355 MPA and the stress-strain curve is shown in Figure 2.7, where $\sigma_y$ is the yielding point and $E_s$ is the Young modulus.
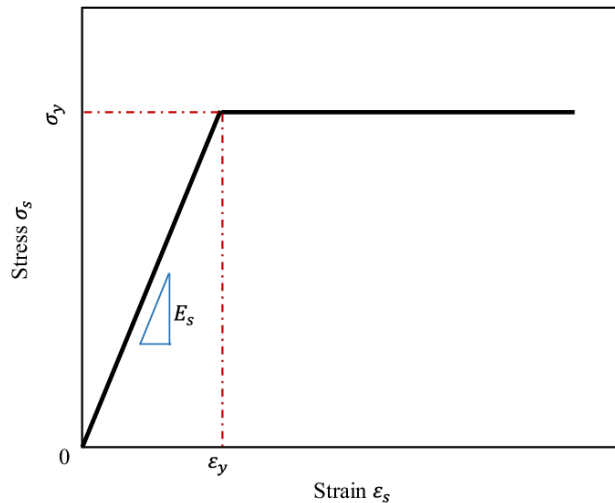


**Figure 2.7** Elastic-perfectly plastic stress-strain curve for steel extracted from [11]

A structure can fail because of plasticity but also due to thermal expansion failure due to plasticity. For this Thesis it is important the second type of failure because it takes place when a thermal field is applied to a structure that cannot expand, then the internal forces grow fast and the structure can fail if they reach the plastic limit.

### 2.4.2.1 Thermal degradation of the material

As it was explained before when the temperature is increased the stiffness of the structures suffers a degradation. The Young modulus is affected by this and consequently the yielding point. As the temperature is increased the value of the yielding point is lower, as it is shown in Figure 2.8, which was presented in the previous section.
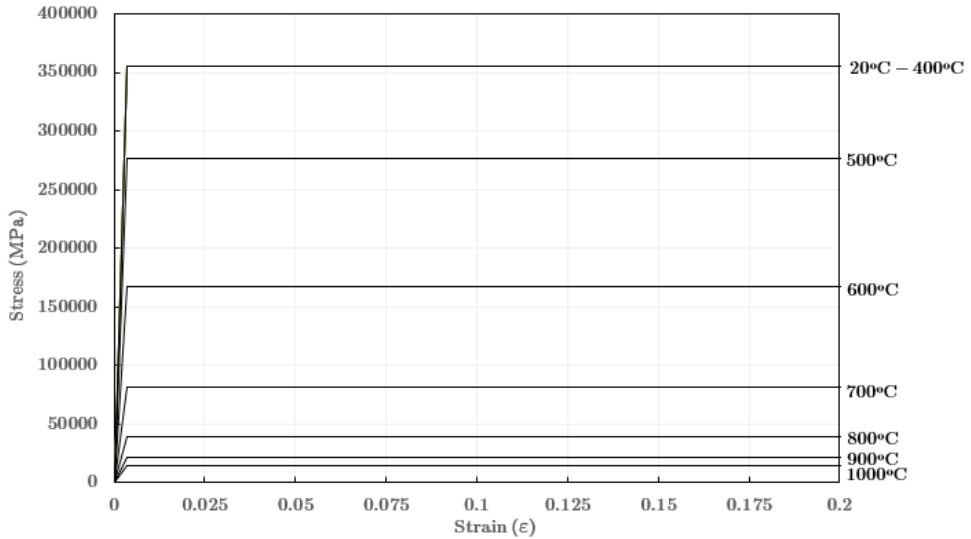


**Figure 2.8** Stress-strain curve degradation due to temperature increase, according to Eurocode-3 [9].

## 2.4.3 Thermal properties

The only thermal property relevant for the study it is going to be developed is the coefficient of thermal expansion of the steel. Regarding the other properties, like the specific heat or the conductivity they are going to be used only for the one way-coupled model. However, this properties will be extracted from the brother project written by Ainara Sofía Fran Vergara [5] which has been developed the thermal study of the door.

### 2.4.3.1 Coefficient of thermal expansion

The coefficient of thermal expansion is a thermal property of the material and it describes how the element expands or contracts due to changes in temperature. The

thermal elongation produce in carbon steel is defined by the Eurocode-3, Part-1-2 [9]. It directly depends on the temperature and it is defined by Equation 2.3, where $l$ is the length at 20ºC, $\Delta l$ is the temperature elongation and $\theta_a$ is the steel temperature (ºC).

$$
\begin{aligned}
&20°\text{C} \leq \theta_a < 750°\text{C}: \\
&\Delta l/l = 1,2 \times 10^{-5}\theta_a + 0,4 \times 10^{-8}\theta_a^2 - 2,416 \times 10^{-4} \\
\\
&750°\text{C} \leq \theta_a \leq 860°\text{C}: \\
&\Delta/l = 1,1 \times 10^{-2} \\
\\
&860°\text{C} < \theta_a \leq 1200°\text{C} \\
&\Delta l/l = 2 \times 10^{-5}\theta_a - 6,2 \times 10^{-3}
\end{aligned}
\tag{2.3}
$$

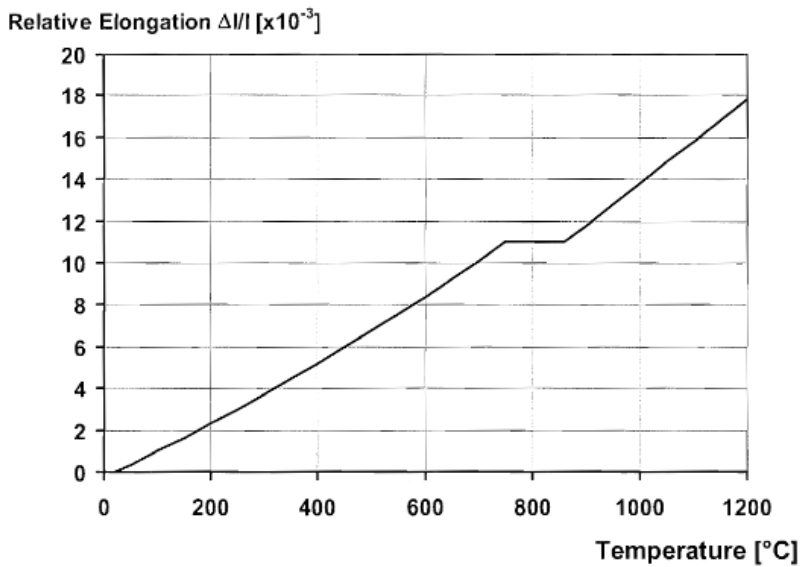**Relative Elongation $\Delta l/l$ [x$10^{-3}$]**



**Figure 2.9** Relative thermal elongation of carbon steel as a function of temperature. Extracted from Eurocode-3 [9]

The coefficient of thermal expansion is related to the slope of this curve and its value vary as a function of temperature, Figure 5.5. The variation is not linear, same as the elongation because it follows the Eurocode formulation.
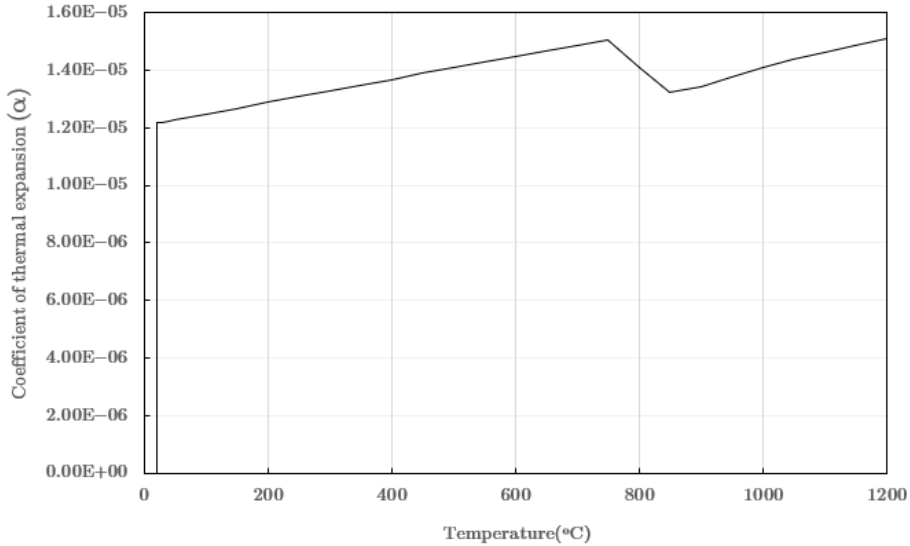
**Figure 2.10** Coefficient of thermal expansion of carbon steel as a function of temperature

For the initial calculations, where there is no temperature dependency on the material's properties, it was used the linear coefficient of thermal expansion for carbon steel given in the Eurocode [9] which does not vary with temperature and has a constant value of $\alpha_l = 12 \times 10^{-6}$per °C.

## 2.5   Non-linear behavior

There are two main types of non-linearity: material and geometrical non linearity. The first one is related to materials that do not have a linear stress-strain curve while in the second one, it is associated to the change of shape in the structure when large deformation appear and non-linear changes in the stiffness appear. Both types affect to the stiffness.

In a linear analysis the stiffness remain constant while in a non-linear analysis the stiffness matrix changes during the deformation process. If these changes in the stiffness are only related to the structure shape the behaviour is classified as geometric non linearity. A clear example of geometric non linearity is buckling.

Regarding buckling and non-linearity, this would be explained in Section 2.7 where the equilibrium state and the effect of this geometric non linearity would be explained.

## 2.6   Plate theory

A plate is a planar element with two dimensions significantly larger than the third one, the thickness. The larger dimensions are in the plane of the plate while the third one is perpendicular to this plane. The plate is loaded on its plane and it only have translation degrees of freedom not rotational ones. They usually work under bending or in-plane loads.
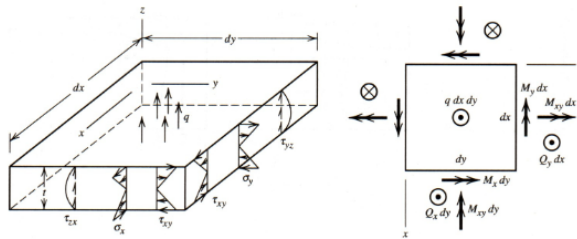


**Figure 2.11** Plate configuration, extracted from [12]

Plates can be classified in two different categories: thin plates or thick plates. This differentiation is important because, depending on its thickness, the theories applied are different. A plate can be considered thin when the thickness-widht ratio is equal or smaller than 1/20. When this ratio is higher than that value the plate can be consider thick.

The theory of Kirchoff is applied to thin plates while the theory of Reissner-Mindlin to thick plates.

### 2.6.1   Kirchhoff plate theory

The thin plate theory assumes out of plane components are negligible and the middle surface remains normal after deformation.

If a thin plate is considered in the x-y plane, with a given thickness $t$ and a dif-

ferential slide of the plate is taken, Figure 2.12, the displacement and the strains can be written as in Equation 2.4 and Equation 2.5.
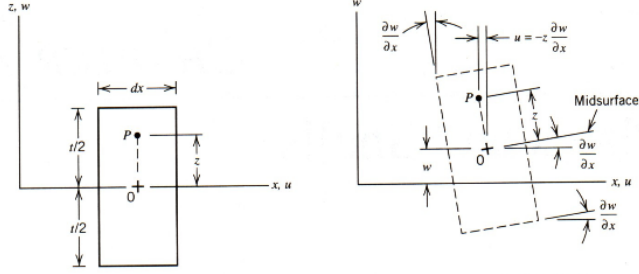


**Figure 2.12** Differential portion of the thin plate, extracted from [12]

$$w = w(x, y)$$

$$u = -z\frac{\partial w}{\partial x} \tag{2.4}$$

$$v = -z\frac{\partial w}{\partial y}$$

$$\varepsilon_x = -z\frac{\partial^2 w}{\partial x^2}$$

$$\varepsilon_y = -z\frac{\partial^2 w}{\partial y^2} \tag{2.5}$$

$$\gamma_{xy} = -2z\frac{\partial^2 w}{\partial x \partial y}$$

$$\gamma_{yz} = \gamma_{zx} = 0$$

If the z-direction stress is considered equal to 0, then the stresses can be written as:

$$\left\{ \begin{array}{c} \sigma_x \\ \sigma_y \end{array} \right\} = -z\frac{E}{1-v^2}\left[ \begin{array}{cc} 1 & v \\ v & 1 \end{array} \right]\left\{ \begin{array}{c} \partial^2 w/\partial x^2 \\ \partial^2 w/\partial y^2 \end{array} \right\} \tag{2.6}$$

$$\tau_{xy} = -2zG\frac{\partial^2 w}{\partial x \partial y} \tag{2.7}$$

The stresses lead to the external bending moments which can be written as:

$$M_x = \int_{-t/2}^{t/2} \sigma_x z\, dz \quad M_y = \int_{-t/2}^{t/2} \sigma_y z\, dz \quad M_{xy} = \int_{-t/2}^{t/2} \tau_{xy} z\, dz \qquad (2.8)$$

Then the stresses can be given as:

$$\sigma_{x,\text{max}} = \frac{6M_x}{t^2}$$

$$\sigma_{y,\text{max}} = \frac{6M_y}{t^2} \qquad (2.9)$$

$$\tau_{xy,\text{max}} = \frac{6M_{xy}}{t^2}$$

This formulation is similar to beam formulation however, the situation is more similar to plain strain due to the wide of the plate.

## 2.6.2 Reissner-Mindlin plate theory

The thick plate theory takes into account the shear deformations and the considers that the middle surface does not remain normal after deformation.

Regarding Midlin formulation, in Figure 2.13 a differential portion of the plate is represented and the deformation and strains obtained are formulated in Equation 2.10 and 2.11.
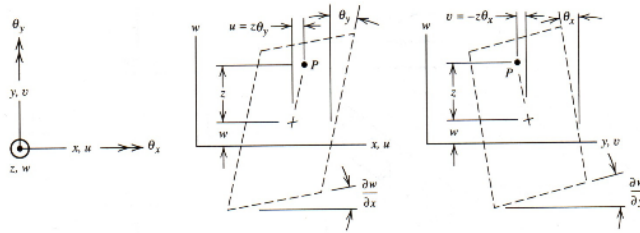


**Figure 2.13** Differential portion of the thick plate, extracted from [12]

$$\begin{aligned} u &= z\theta_y & \varepsilon_x &= z\frac{\partial \theta_y}{\partial x} \\ v &= -z\theta_x & \varepsilon_y &= -z\frac{\partial \theta_x}{\partial y} \end{aligned} \qquad (2.10)$$

$$\gamma_{xy} = z\left(\frac{\partial\theta_y}{\partial y} - \frac{\partial\theta_x}{\partial x}\right)$$

$$\gamma_{yz} = \frac{\partial w}{\partial y} - \theta_x \qquad\qquad (2.11)$$

$$\gamma_{zx} = \frac{\partial w}{\partial x} + \theta_y$$

### 2.6.3   Membrane forces

Plates cannot carry membrane forces, but if the ratio width/thickness of the plate is greater than 0.1 a non linear analysis using shell elements has to be carried for the plate. As a general rule, tensile membrane forces have a stiffening effect while compressive ones decrease the stiffness.

## 2.7   Buckling [13]

In linear mechanics of deformable bodies the displacements are proportional to the loads applied. However, the essence of buckling is the disproportional increment in the displacements under a small increase of load. This phenomenon is considered a non-linear instability phenomenon because its load-displacement trajectory does not follow a linear path.

The buckling load is the load at which the equilibrium state of a structure change suddenly from stable to unstable or from a previous stable configuration to another stable configuration. The stable equilibrium of a structure is characterize by every "small" disturbance create a "small" response. However, a structure is unstable when a "small" disturbance creates a sudden change in deformation or displacement.

### 2.7.1   Linear eigenvalue analysis

The buckling load depends of the geometrical characteristics of the structural element and its configuration, boundary and load conditions. The behaviour of a structure that is buckling is reflected in the shape of its load-displacement curve, called equilibrium path. If the deflection due to buckling is too large the structure fails.

In order to explain the bifurcation path and the load-displacement curve a typical

example of buckling is going to be presented. A slender perfect simply supported elastic column is under axial loading. At first, as the load increases no out-of plane displacement appear,this creates a straight line called primary path which ends when the load reaches the buckling load, on this case the critical Euler load, explained in Section 2.7.5. When this happens the buckling phenomenon takes place without any further load increase and the equilibrium path suffer a bifurcation into two symmetric paths, called secondary paths.
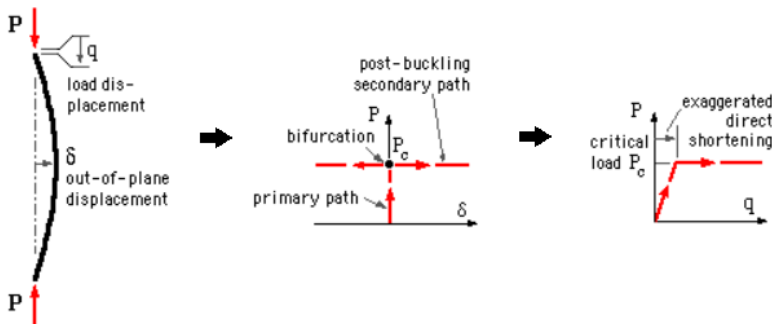


**Figure 2.14** Equilibrium path for a slender perfect simply supported elastic column under axial loading. Image extracted from [14]

By using linear eigenvalue analysis the bifurcation point, the buckling load, can be obtained. In this analysis the eigenvalue is the buckling load, or critical load, and the eigenvector is the buckling mode. With this analysis it is obtained the value for the bifurcation buckling load and the initial shape of the buckling mode. However, this analysis does not go further so the post-buckling behaviour and the buckling deflection is indeterminate. For this reason after the eigenvalue analysis a post-buckling analysis has to be performed.

## 2.7.2  Post-buckling behavior

The post-buckling analysis is non-linear and more information can be extracted from this than from the eigenvalue analysis. The post-buckling behavior is represented in a load-displacement plot where the out of plane displacement is shown, buckling displacement. For perfect structures, without initial imperfection before reaching the buckling load the plot is a straight line. In Figure 2.15 the four types of post-buckling behavior are represented. being $\lambda_B$ the buckling load.
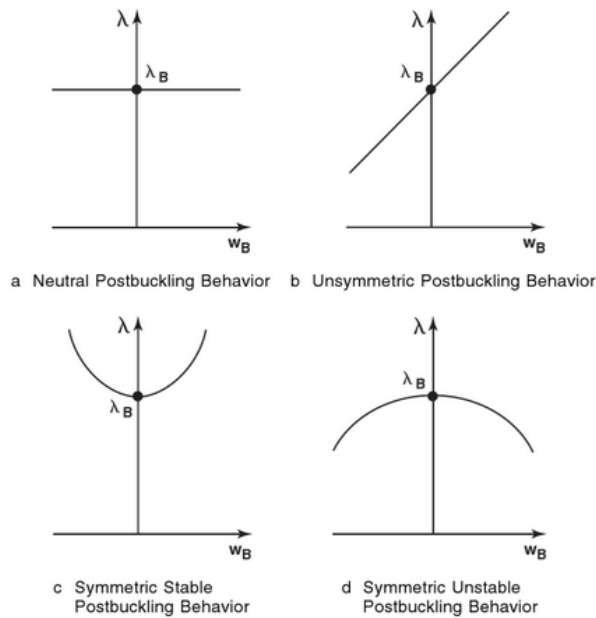
**Figure 2.15** Types of post-buckling behavior for perfect structural elements. Figure extracted from [13]

The symmetric stable behavior shows that the structure that has this type of post-buckling can stand higher loads than the critical load. However, the unstable post-buckling behavior cannot stand higher loads than the critical load after the structure has buckled. On the other hand, the unsymmetric behavior will depend of the boundary conditions and, depending on them, it will stand higher or lower loads than the buckling load.

As an example of post-buckling of different structures, a straight bar axially loaded will have a post-buckling behavior that is both stable and also close to the neutral type. Regarding plates, a flat plate axially loaded in its middle plane will have a symmetric stable post-buckling behavior.

### 2.7.2.1  Initial geometric imperfection and its effects.

In every manufacturing process is inevitable that initial geometric imperfections appear in the structures produced. This imperfections affect the post-buckling curve and, depending of the sensitivity of the structure to imperfections, its effects will be

higher or lower. This effect can be observed in the initial slope and in the initial curvature of the post-buckling plot before the bifurcation point, $\lambda_B$. The degree of the deviation of the post-buckling curve from the perfect structure curve depends on the magnitude and nature of the imperfection.
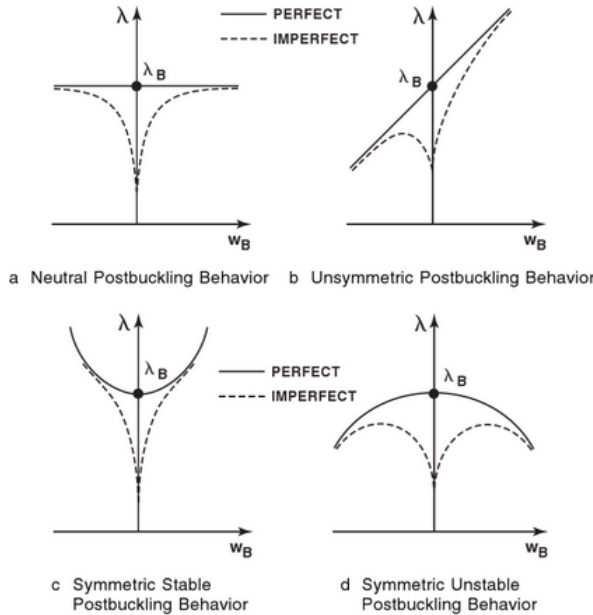


**Figure 2.16** Types of post-buckling behavior for perfect and imperfect structural elements. Figure extracted from [13]

In Figure 2.16 the dashed line represents the behavior of a structure with an initial imperfection and the continuous line the post-buckling curve of a perfect structure.

The effect of imperfection is small if the initial slope is positive or if the initial slope is zero and the curvature positive. However, if the initial slope is negative or the initial slope is zero with an initial negative curvature the effect of imperfections is high. As an example, the right side of Unsymmetric post-buckling behavior, Figure 2.16, has a small susceptibility to imperfections while the left side has a high susceptibility. Another example of small effect of imperfections is the Symmetric stable behavior, and the Symmetric unstable will be an example of high sensitivity to imperfections.

### 2.7.3 Euler buckling theory

Leonhard Euler (1707-1783) obtained the fundamental solution of the bar buckling problem, studying the stability of a flexible column under axial load. This solution is known as the Euler Buckling theory.

To develop this theory Euler studied the behavior of a elastic column of length $L$, and simply supported boundary conditions. At the bottom there was a pinned end and at the top a vertical roller was placed, this allows rotation and vertical movement.
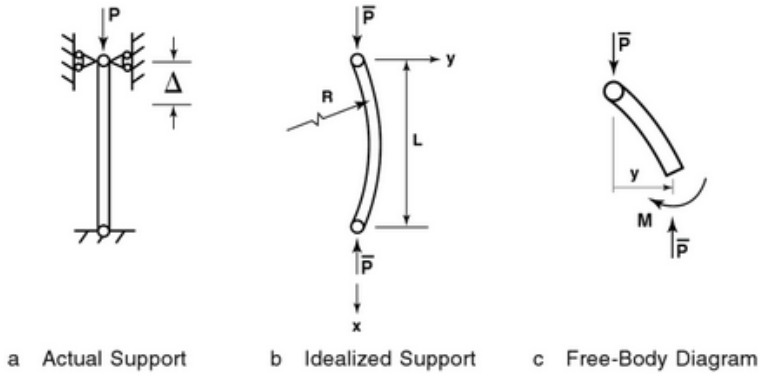


    a   Actual Support        b  Idealized Support      c  Free-Body Diagram

**Figure 2.17** Colummn axially loaded, simply supported, initial straight bar. Extracted from [13]

It was studied the bending of the beam and the internal moment was equalized to the external moment, obtaining the differential Equation 2.12, where $I$ is the second moment of inertia of the column cross-sectional area about the axis that is perpendicular to the buckling plane.

$$Ely'' = -Py \tag{2.12}$$

$$y'' + \frac{P}{EI}y = 0 \tag{2.13}$$

This is an homogeneous differential equation and the general solution is:

$$y = A\sin(\sqrt{\frac{P}{EI}}x) + B\cos(\sqrt{\frac{P}{EI}}x) \tag{2.14}$$

The constants $A$ and $B$ of Equation 2.14 are determined from the boundary conditions of the column, Equation 2.16.

$$
\begin{aligned}
y(0) = 0 &\quad \rightarrow \quad B = 0 \\
y(L) = 0 &\quad \rightarrow \quad A\sin\sqrt{\tfrac{P}{EI}}L = 0
\end{aligned}
\tag{2.15}
$$

This leaves with two possible solution or $A = 0$ or $\sin\sqrt{\tfrac{P}{EI}}L = 0$. However, A cannot be 0 because B already has a 0 value and that will imply that there is not amplitude in the buckling deflection and therefore the bar would not buckle. This is called the trivial solution.

So, the solution to the Equation will be:

$$
\begin{aligned}
&\sin\sqrt{\tfrac{P}{EI}}L = 0 \\
&kL = n\pi \quad n = 1, 2, \ldots
\end{aligned}
\tag{2.16}
$$

So, the eigenvalue equation is Equation 2.13 and the corresponding eigenvalues of the problem are the solutions obtained for different values of $n$.

After solving this equation the buckling load can be obtained, the Euler buckling load, for a simply supported column axially loaded, shown in Equation 2.17 where L is the effective length, which depends on the boundary conditions.

$$
P_{cr} = \frac{\pi^2 EI}{L^2}
\tag{2.17}
$$

And the eigenvector, buckling mode shape, corresponding to the lowest eigenvalue is shown in Equation 2.18 being $A$ the amplitude of the half-sine wave, which is indeterminate but it can be obtained applying large-deflection theory.

$$
y = A\sin\frac{\pi x}{L}
\tag{2.18}
$$

The applicability of Euler's column formulation is limited by the maximum stress at buckling because it must be in the elastic range of the material. So, it is important to have a stress expression for Euler's equation, which is shown in Equation 2.19, where $r$ is the radius of gyration of the cross section, Equation 2.20 where $I$ is the moment

of inertia and $A$ the cross-section area.

$$r = \sqrt{I/A} \tag{2.19}$$

$$\sigma_{\mathrm{E}} = \sigma_{\mathrm{cr}} = \frac{\mathrm{P_{cr}}}{\mathrm{A}} = \frac{\pi^2 \mathrm{E}}{(\mathrm{L/r})^2} \tag{2.20}$$

The buckling stress goes to zero as the slenderness ratio increases, $L/r$, and it increases as the column gets shorter and wider. The problem with a small slenderness ratio is that the Euler formulation is not valid for stresses, $\sigma_E$, higher than the yielding stress of the material, $\sigma_y$ . In Figure 2.18 it can be seen this limit and, when the stress value is higher than the yield stress it means that the column could fail by yielding instead of failing due to buckling.
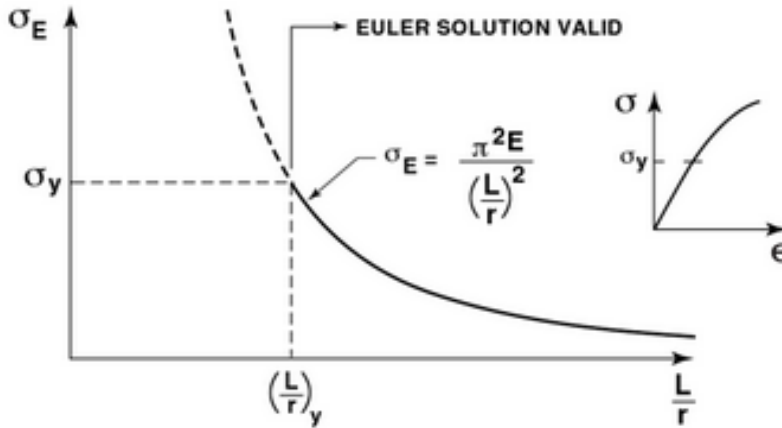


**Figure 2.18** Buckling stress versus slenderness ratio. Extracted from [13]

## 2.7.4   Thermal buckling

In this section it is going to be explained the buckling effects of restraining the thermal expansion in structural elements. When a steel structure is heated the material experience a thermal elongation, which directly depends on the coefficient of thermal expansion (Section 2.4.3). However, when the boundary conditions of the structure does not allow the material to expand, an internal compression force is developed in the element. This force is expressed by Equation 2.23, where $\alpha$ is the coefficient of thermal expansion.

$$P_{cl} = EA \cdot L \cdot \Delta T \cdot \alpha \qquad (2.21)$$

This compression force developed may reach the critical buckling load if the temperatures are high enough. Equalizing the Euler buckling load to this compression load it can be obtained the temperature at which the structure will fail due to buckling. This phenomenon is known as thermal buckling and this maximum temperature is called the critical temperature.

$$P_{cr} = P_{cl}$$

$$(2.22)$$

$$P_{cr} = EA \cdot L \cdot \Delta T_{cr} \cdot \alpha$$

$$\Delta T = \frac{P_{cri}}{AE\alpha} \qquad (2.23)$$

When the critical temperature is reached the element buckles. But, if no material degradation is taken into account and the material is considered elastic, the axial force will remain constant as the thermal strains increase.

### 2.7.5 Buckling of rectangular plates

The objective of this section is to explain the theoretical background behind the buckling of plates. It will be focus specifically on the stability analysis of thin elastic plates which is significantly similar to Euler stability analysis of columns. Classical buckling problems of plates can be formulated using three different methods: the Equilibrium method, the energy method and the dynamic method. On this thesis, it would be explained the Equilibrium method to solve the stability problems on a simply supported plate with axial loading. It is important to bear in mind that going in detail in the derivation of the equations is out of the scope of this Thesis.

#### 2.7.5.1 The Equilibrium method [15]

It is considered an initial state of equilibrium of a plate subjected to an external axial load acting in the plate's middle plane. The corresponding in-plane stress resultants are $N_x$, $N_y$ and $N_{xy}$. Its value can be found from the solution of the plane stress problem for a simply supported plate loaded with an external axial load. The buckling analysis developed in this section considers these characteristics to determined

the stress resultants with no difficulties and directly expressed with the given external forces.

The next assumption is that for certain external forces the plate has buckled slightly. Now, the differential equation of equilibrium can be formulated having into account the conditions explained before. The equilibrium equation of the linear buckling analysis of plates is shown in Equation 2.24 where $N_x$, $N_y$ and $N_{xy}$ are the internal forces acting in the middle plane of the plate.

$$\frac{\partial^4 w}{\partial x^4} + 2\frac{\partial^4 w}{\partial x^2 \partial y^2} + \frac{\partial^4 w}{\partial y^4} = \frac{1}{D}\left(N_x\frac{\partial^2 w}{\partial x^2} + 2N_{xy}\frac{\partial^2 w}{\partial x \partial y} + N_y\frac{\partial^2 w}{\partial y^2}\right) \tag{2.24}$$

It is a homogeneous partial differential equation and it can be solved with the appropriate boundary conditions. This type of problem usually has a trivial solution which corresponds to the initial flat configuration of equilibrium. Nevertheless, the coefficients of the equation depend on the magnitudes of the stress resultants, which are connected to the in-plane external forces. For these loads, the values can be found and then a nontrivial solution can be obtained. The smallest value of these forces is the critical load.

A general formulation of the equilibrium transforms the stability problem into an eigenvalue problem by multiplying the stress resultants ($N_x$, $N_y$, $N_xy$) by a load parameter ($\lambda$). By substituting Equation 2.25 into Equation 2.24 the differential equation for buckling of plates can be found, Equation 2.26.

$$N_x = -\lambda\bar{N}_x \quad N_y = -\lambda\bar{N}_y \quad N_{xy} = -\lambda\bar{N}_{xy} \tag{2.25}$$

$$\nabla^4 w + \frac{\lambda}{D}\left(\overline{N}_x\frac{\partial^2 w}{\partial x^2} + \overline{N}_y\frac{\partial^2 w}{\partial y^2} + 2\overline{N}_{xy}\frac{\partial^2 w}{\partial x \partial y}\right) = 0 \tag{2.26}$$

Solving Equation 2.26 specific values for $\lambda$ can be found and these solutions correspond to the eigenvalues. The smallest of the eigenvalues, non-equal to zero, is the critical buckling load and the corresponding eigenfunction is the buckling mode.

**CASE 1: Buckling of rectangular plate under axial load and simply supported at all the sides [15]**

Now the governing differential equation of plate buckling has been stated, Equation

2.26 or its equivalent Equation 2.24, it is going to be solved for a particular case. This homogeneous, linear partial differential equation with variable coefficients cannot be solved analytically in the general case but for some specific cases a exact solution can be found. Now, this solution is going to be obtained for a rectangular simply supported plateb on all the sides subjected to a uniform distributed compressive load ($q_x$) acting at the edge in the x-direction, Figure 2.19. For this task is going to be used the equilibrium method, as it was mentioned before.
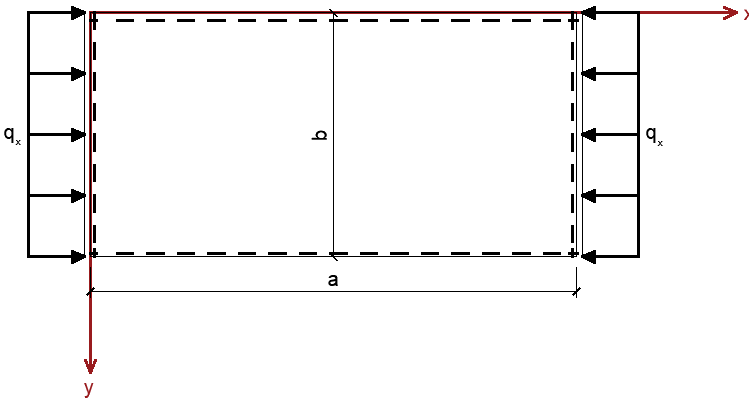


**Figure 2.19** Rectangular plate simply supported on all sides and axially loaded.

For this case there is only one in plane stress that is not equal to zero, $N_x$. So, Equation 2.24 can be rewritten as Equation 2.28 having into account the stress conditions, Equation 2.27.

$$N_x = -q_x \quad N_y = N_{xy} = 0 \tag{2.27}$$

$$D\nabla^2\nabla^2 w + N_x \frac{\partial^2 w}{\partial x^2} = 0 \tag{2.28}$$

The solution seek for this equation will have the form of Equation 2.29, which is the solution of the deflection surface $\omega(x,y)$ in the form of an infinite Fourier series. This Equation refers to the bending of simply supported rectangular plates subjected to bending.

$$w(x,y) = \sum_{m=1}^{\infty}\sum_{n=1}^{\infty} w_{mn} \sin\frac{m\pi x}{a}\sin\frac{n\pi y}{b} \tag{2.29}$$

After introducing Equation 2.29 into Equation 2.24 the following is obtained:

$$\sum_{m=1}^{\infty} \sum_{n=1}^{\infty} \left[ D\pi^4 \left( \frac{m^2}{a^2} + \frac{n^2}{b^2} \right)^2 - q_x \pi^2 \frac{m^2}{a^2} \right] w_{mn} \sin \frac{m\pi x}{a} \sin \frac{n\pi y}{b} = 0 \qquad (2.30)$$

The trivial solution will corresponds to $\omega_{nm}$ equal to 0 but this is related to the un-buckled equilibrium of the plate and this is not what we are looking for. The other solution that can be determined is obtained by setting the element between brackets equal to zero, Equation 2.31, which implies that $q_x$ should have the value expressed in Equation 2.32.

$$D\pi^4 \left( \frac{m^2}{a^2} + \frac{n^2}{b^2} \right)^2 - q_x \pi^2 \frac{m^2}{a^2} = 0 \qquad (2.31)$$

$$q_x = \frac{\pi^2 D}{b^2} \left( \frac{mb}{a} + \frac{n^2 a}{mb} \right)^2 \qquad (2.32)$$

Equation 2.32 gives the results of $q_x$ for m = 1, 2, 3...; and n = 1, 2, 3... as possible forms of the deflected surface using Equation 2.29. The smallest value obtained as a result, which corresponds to n=1, is the critical value. So, the formulation can be written as in Equation 2.33 or in its equivalent form 2.34 where K is the buckling load parameter and its value is given by Equation 2.35, being $m$ the number of half-sine waves in the longitudinal direction.

$$N_x = \frac{\pi^2 D}{b^2} \left( \frac{mb}{a} + \frac{a}{mb} \right)^2 \qquad (2.33)$$

$$q_x = K \frac{\pi^2 D}{b^2} \qquad (2.34)$$

$$K = \left( \frac{mb}{a} + \frac{a}{mb} \right)^2 \qquad (2.35)$$

The parameter $D$ used in Equation 2.34 is known as the flexural stiffness of the plate, its equivalent to $EI$ for beams, and its value is given by Equation 2.36 where $t$ is the thickness of the plate, $E$ the Young modulus and $v$ is the Poisson's ratio.

$$D = \frac{Et^3}{12 \left(1 - v^2\right)} \qquad (2.36)$$

For a given value of $m$ the buckling load parameter, $K$, only depends on the aspect ratio of the plate, $a/b$. So, for a given aspect ratio the critical load is calculated by selecting a value of $m$ that makes $q_x$ minimum. So, knowing that only $K$ depends of $m$:

$$\frac{\mathrm{d}K}{\mathrm{d}m} = 2\left(\frac{mb}{a} + \frac{a}{mb}\right)\left(\frac{b}{a} - \frac{a}{m^2b}\right) = 0 \tag{2.37}$$

$$m = \frac{a}{b} \tag{2.38}$$

Then, the value of the critical load can be expressed as Equation 2.39 where $K$ is equal to 4. The corresponding critical stress is expressed in Equation 2.40.

$$\min q_x = q_{x,cri} = \frac{4\pi^2 D}{b^2} \tag{2.39}$$

$$\sigma_{x,cr} = \frac{N_{x,cr}}{t} = \frac{q_{x,cr}}{t} = \frac{4\pi^2 D}{b^2 h} = \frac{\pi^2 E}{3\left(1 - v^2\right)}\left(\frac{t}{b}\right)^2 \tag{2.40}$$

The variation of the buckling load parameter, $K$, as a function of the aspect ratio, $a/b$, can be found using Figure 2.20. In this Figure the number of half-waves, $m$, in the direction of the applied compressive loads for any value of the aspect ratio can also be found.
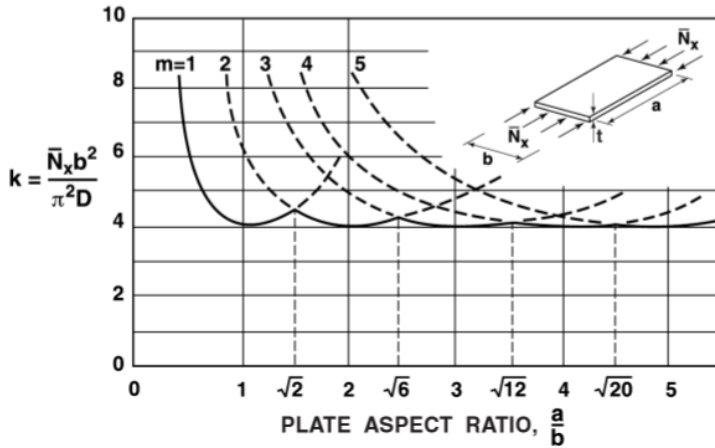


**Figure 2.20** Bukling load parameter, $K$, as a function of the aspect ratio $a/b$. Extracted from [13].

**CASE 2: Buckling of a rectangular plate under axial load and simply supported at the top and bottom [16]**

Now, the solution for a simply supported plate on two sides and free on the other two is going to be exposed. The characteristics of this particular case are shown in Figure 2.21, the calculations and theory followed to get to the solution are analogue as the previous Sections. For further information regarding the demonstration of the solution it can be check in the book "Mechanics of optimal structural design: Minimum Weight Structures" by David W.A.Rees at "Appendix B: Plate buckling under uniaxial compression" [16].
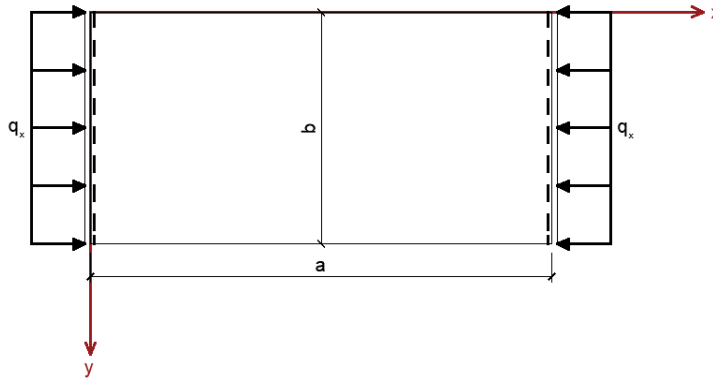


**Figure 2.21** Rectangular plate, simply supported on two sides and free on the others, and axially loaded.

The buckling load at which the plate starts buckling is shown in Equation 2.41 and its corresponding critical stress in Equation 2.42. In this Equation D is the flexural stiffness of the plate and its value is given by Equation 2.36, being $t$ the thickness of the plate.

$$q_{x,cri} = \frac{\pi^2 EI}{(1 - v^2)\, a^2} = \frac{\pi^2 Db}{a^2} \tag{2.41}$$

$$\sigma_{x,cr} = \frac{q_{x,cri}}{t} = \frac{\pi^2 Db}{ta^2} = \frac{\pi^2 Eb}{12(1 - v^2)} \left(\frac{t}{a}\right)^2 \tag{2.42}$$

# Numerical benchmark

In this chapter it is going to be explained the different elements and types of analysis used in Abaqus, a finite element software (FEM), used during the development of this Thesis. It would be explained briefly the theory behind them.

## 3.1 Type of analysis [17][18]

Four different types of analysis have been used along this Thesis. One of them, Eigenvalue analysis, was used to study the buckling behaviour, the Statically incremental and Riks analysis were used to analysed the post-buckling and the coupled analysis was used to to study the behaviour of elements that have displacement, rotation and temperature as degrees of freedom.

### 3.1.1 Eigennvalue analysis

This analysis is used to estimate the critical load in stiff structures. It is a linear perturbation procedure and it can also be employ in the investigation of the imperfection sensitivity of a structure.

The Eigenvalue buckling problem appears when the model stiffness matrix becomes singular, Equation 3.1, and has non-trivial solutions.

$$K^{MN}v^M = 0 \tag{3.1}$$

The tangent stiffness matrix when the loads are applied is represented by $K^{MN}$ and the non-trivial displacement solutions are $v^M$.

This analysis is used to estimate the critical buckling load of structures and its buckling mode shapes. Stiff elements carry their design loads by axial or membrane

action better than with bending action. The behaviour of a structure before buckling is characterized by small deformations but, when the critical load is reached it bends suddenly with lower stiffness.

So, the eigenvalue problem is shown in Equation 3.2 where an incremental loading pattern, $Q^N$ is add to the eigenvalue prediction step. The value of this load is not relevant because it will be scaled by the load multipliers $\lambda_i$.

$$\left(K_0^{NM} + \lambda_i K_\Delta^{NM}\right) v_i^M = 0 \tag{3.2}$$

The load multipliers, $\lambda_i$, are the eigenvalues, the stiffness matrix of the base state is $K_0^{NM}$ and includes the pre-loads effect $P^N$. The initial stress and load stiffness matrix is characterized by $K_\Delta^{NM}$ and it is related to the incremental loading pattern $Q^N$. The buckling mode shapes, eigenvectors, are $v_i^M$. The critical buckling loads are: $P^N + \lambda_i Q^N$.

#### 3.1.1.1 Loads and predefined fields

In an eigenvalue analysis different types of load can be applied, from concentrated nodal forces till predefined temperature fields. It is even possible to apply pre-loads but it should not surpass the critical load. Regarding the predefined fields, nodal temperatures can be specified. The temperatures will cause thermal strain and, if a thermal expansion coefficient has been defined for the material, incremental stresses will be generated. So, the structure would buckle due to thermal stress.

### 3.1.2 Statically incremental analysis

A static stress is used when the inertia effects can be neglected, it can be a linear analysis or non-linear. It does not take into account time-dependent material effect like creep, but it takes the plasticity behavior into account. During this analysis it is necessary to assign a time period to the analysis and adjust the time step, this is directly related with the amplitude options, which can be used to determine the variation of loads and temperature fields during time.

In a linear static analysis the definition of load cases and appropriate boundary conditions is fundamental. This analysis can reduce computational cost in large analyses where all or part of the problem has linear response. Regarding the non-linear

static analysis, it takes into account the large-displacement effects and material non-linearitities. The large displacement formulation is used.

The degrees of freedom in this type of analysis are six, related to displacement and rotation. It is also possible to have warping DOF in open-section beam elements and fluid pressure DOF if hydro-static fluid elements are added to the model.

Even though this analysis does not consider temperature DOF, a temperature field can be added to the analysis. Nodal temperatures can be added to the structure. If a thermal expansion coefficient is defined for the material used, any difference between the applied temperature and the initial temperature will cause thermal strain.

### 3.1.3   Riks analysis

This type of analysis is commonly used to predict unstable and geometrically non-linear collapse of a structure. It can be used to study the post-buckling behaviour of a structure.

Geometrically non-linear static problems could involve buckling or collapse behavior, where the load-displacement response have a negative stiffness and the structure have to release strain energy to keep in equilibrium. There are different ways of modelling this behaviour and Riks analysis applied the known as *"modified Riks method"* to achieve that. This method can be used when the load case is proportional, the load magnitude has to be ruled by a single scalar parameter.
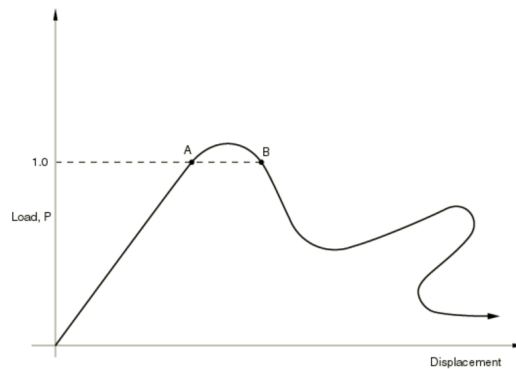


**Figure 3.1** Proportional loading with unstable response, extracted from [17].

This method uses the load as an additional unknown, solving at the same time loads and displacements. For this reason, another quantity has to be used to measure the progress of the analysis, it is the variable called *arc length, l*. This parameter is used along the static equilibrium path in the load-displacement space. The solution would be provide regardless the response is stable or unstable.

All the loads defined before the Riks analysis are treated as dead load and the ones added in this step are consider as a reference load. The loading during this anlaysis is always proportional and it can defined by Equation **??**, where $P_0$ is the dead load, $P_{ref}$ is the reference load vector and  is the load proportionality factor.

$$P_{\text{total}} = P_0 + \lambda \left(P_{\text{ref}} - P_0\right) \tag{3.3}$$

Regarding the incrementation, Riks only uses 1% of extrapolation of the strain increment. An initial increment in arc length, $\Delta l_{in}$, is defined at the beginning of the analysis when the step is defined. Then the initial load proportionality factor is obtained using Equation 3.4, where $l_{period}$ is the arc length scale factor specified (usually is equal to 1).

$$\Delta \lambda_{in} = \frac{\Delta l_{in}}{l_{period}} \tag{3.4}$$

The initial proportionality factor, , $\Delta l_{in}$, is used at the first iteration but for the next ones the value of $\lambda$ is computed automatically so there is no user control over the load magnitude.

Lastly, Riks analysis works well in problems in which the equilibrium path in load-displacement is smooth and does not branch. For this reason, in the post-buckling problems it is important to introduce an initial imperfection to the geometry to turned the problem into a problem with continuous response instead of bifurcation.

### 3.1.4   Coupled analysis

A fully coupled thermal-stress analysis is needed when the stress analysis is dependent on the temperature distribution and the temperature distribution depends on the stress. For this Thesis a one-way coupled analysis was studied because only the influence of the temperature to the stress analysis will be considered.

Abaqus has the option of using a thermal-stress analysis and this requires elements with both temperature and displacement degrees of freedom. It combines the thermal

analysis with a stress analysis.

The coupled elements use linear or parabolic interpolation for geometry and displacements, while the temperature is always interpolated linearly. The temperature of the inside nodes is determined by linear interpolation from the corners nodes.

## 3.2 Type of elements [17][18]

Abaqus has an extend library of elements which make it able to solve many different problems. Depending of the geometric characteristics, the loading condition and other general characteristics of the case analysed the element type has to be chosen. In order to find the most accurate results a brief analysis of the different elements has to be performed in order to choose the proper one, the one that fits best for the problem studied.

There are five properties that characterizes the element behavior: family, degrees of freedom (DOFs), number of nodes, formulation and integration. This attributes are reflected in the name of the element, identifying it. The families used along this document are reflected in Figure 3.2.



Shell elements

Continuum (solid and fluid) elements

Membrane elements
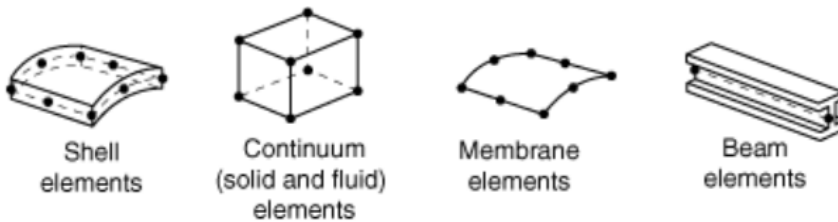
Beam elements

**Figure 3.2** Families of Abaqus elements that are going to be used in this Thesis [17].

### 3.2.1 Beam elements

Beam elements are a one dimensional line element that can be modelled in a 2D space or a 3D space. The theory behind this Abaqus type of element is the beam theory. Abaqus has different types of beam elements in its library, like Euler-Bernoully beams, B23, or Timoshenko beams, B22.

Euler-Bernoulli beams. B23, does not allow transverse shear deformation and the sections remain plane and perpendicular to the beam's axis. They are used to model slender beams and the cross-section measures should be less than 1/15 of the the span in order to consider shear flexibility negligible.

Regarding Timoshenko beams, B21 or B22, they are characterized by allowing the transverse shear deformation. Its use is recommended for thick beams but they can also be employed for modelling slender beams. Abaqus assumes that the transverse shear behavior of these beams is linear elastic with a fixed modulus.

### 3.2.2 Shell elements

Shell elements are a type of structural element in which one dimension, in this case the thickness, is significantly smaller than the rest of them. The elements available in Abaqus can be divided in conventional shells and continuum shells. The first one discretize a structure by defining a reference surface while the continuum shell discretize the entire 3D structure.

The conventional element has displacement and rotational degrees of freedom while the continuum element only have displacement degrees of freedom, no rotations.
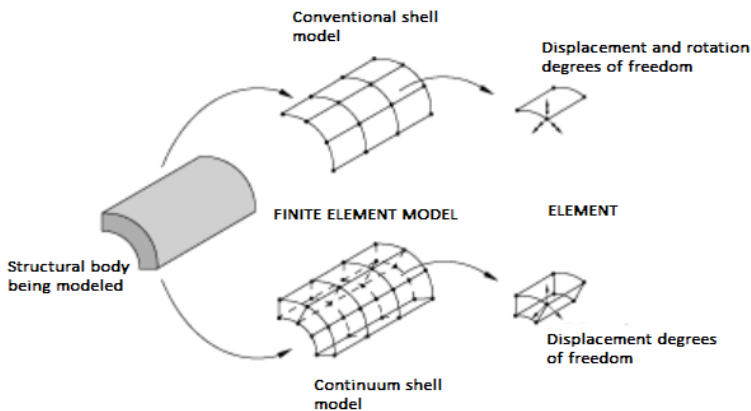


**Figure 3.3** Conventional versus continuum shell elements in Abaqus [17].

Abaqus library for shell elements can be divided in three categories: general purpose shells, thin shells and thick shells. Each one of these options follows a different shell

theory and the type of element chosen directly depends on the case that it is being analysed.

General purpose shells are three dimensional elements which provides accurate solutions for both, thin and thick shells. They do not experiment shear locking or unconstrained hourglass modes. The hourglass control is not required in bending and membrane response of the fully integrated shell element.

Thin shell elements in Abaqus follows the Kirchhoff theory while thick elements follows Reisner-Midlin theory. The first one does not consider the shear deformation while Mindlin theory does, shear flexible element.

### 3.2.2.1   General-purpose conventional shell elements

This type of elements provide accurate solutions to most applications but in some specific cases it is necessary to use thin/thick elements instead of the general-purpose one. It allows transverse shear deformation and it uses thick shell theory or thin shell theory depending of the thickness of the plate. That is the main reason why this type of element is recommended to use in most of cases. It is also important to consider that the shear deformation decreases as the thickness does.

Element types S3/S3R, S3RS, S3RT, S4, S4R, S4RS, S4RSW, S4RT, SAX1, SAX2, SAX2T, SC6R, and SC8R are general-purpose shells. Thick conventional shell elements A shell is considered thick when the thickness is bigger the 1/15 of the characteristic length of the shell, as it can be the distance between supports in a static case. This kind of element is specially relevant when the transverse shear flexibility is important and second order interpolation needed.

Element types S8R and S8RT are thick shell elements in Abaqus. Thin conventional shell elements It is used when the tickness is smaller than 1/15 of the characteristic length. The Kirchhoff constraint must be fulfilled because the transverse shear flexibility is negligible. However, the thickness can be larger than this value because Abaqus has two different types of thin shell elements, one that solve thin shell theory (Kirchhoff requirement) and one that converge to thin shell theory as thickness decreases. This last type is the one that allows a bigger thickness.

The first type of thin elements solves thin shell theory and has six degrees of freedom

on each node. If this element is applied to a thick shell the prediction will always give a thin shell solution.

The second type, impose Kirchhoff constraint numerically and it should not be used for structures where the shear deformation is important, that could give inaccurate results.

It is used element STRI3 for the first type and elements S4R5, STRI65, S8R5, S9R5, SAXA1n, and SAXA2n for the second one.

### 3.2.3 Solid (continuum) elements

#### 3.2.3.1 Continuum shell elements

The main difference between continuum shell elements and shell elements is that the continuum ones discretize a 3D structure while the conventional shell discretize a reference surface.

This element only have displacement degrees of freedom and allows large rotations and finite membrane deformation so they are appropriate for nonlinear analysis. The transverse shear deformation is also considered in this element. One of its advantage comparing to the conventional shell is that it provides a more refined through thickness response, obtaining better force predictions.

It is also important to take care of the verification of the overall deformation, being fundamental to check if it is consistent with the plane stress assumption. If the response is bending dominated no significant thickness change will be observed.

For models of thin structures that require a three-dimensional constitutive material behavior, the continuum solid shell (CSS8) element is recommended

### 3.2.4 Coupled-temperature-displacement elements

This type of element is employed when a coupled-temperature-displacement analysis is performed. A coupled temperature-displacement analysis is characterize by the dependence between the stress analysis and the temperature solution, and the dependence between the thermal analysis and the the displacement solution.

This elements have both temperature and displacement degrees of freedom. In modified triangle and tetrahedron elements the temperature degrees of freedom are active in all the nodes while in second order elements it is only active at the corner nodes. The interpolation used is linear or parabolic for displacements and the temperature is always interpolated linearly.

The elements available in Abaqus library for coupled temperature-displacement analysis are part of other element families. The families that are going to be relevant for this Thesis are: Solid (continuum) elements and Shell elements. The elements available are the same as the ones described before in Section 3.2.2 and 3.2.3, but they include in its name description the letter T, which marks them as coupled temperature-displacement elements.

As an example of the type of elements applicable S3T is a 3-node thermally coupled triangular general-purpose shell with finite membrane strains; S4T is a 4-node thermally coupled doubly curved general-purpose shell with finite membrane strains; C3D8T is an 8-node thermally coupled brick with tri-linear displacement and temperature.

## 3.3   Connector elements [17][18]

Connector elements in Abaqus are useful when it is necessary to connect two different parts of the model between them. Sometimes the connection are easy, like a weld connection between steel panels or a door connected to a frame by a hinge. However, there are more complex connections like connections with kinematic constraints. But, for the purpose of this thesis the connection used are not that complex.

There are different types of connectors available in Abaqus library which can be resume in four different groups:

- Translational basic connection components, which affect translational DOFs at both nodes and may affect rotational DOFs at the first node of the connector element.

- Rotational basicconnection components, which affect only rotational DOFs at both nodes of the connector element.

- Assembled connections, which are a predefined combination of translational and rotational basic connection components.

- Specialize rotational basic connection components, which besides the roational DOFs they affect to other degrees of freedom.

- Complex connections, which affect a combination of degrees of freedom at the nodes.

The type of connectors relevant for this Thesis are weld connections and link connectors.

The weld connection impose kinematic constraints and combines two connections types: JOIN + ALIGN. Its characteristics are shown in Figure 3.4 and Figure 3.5.
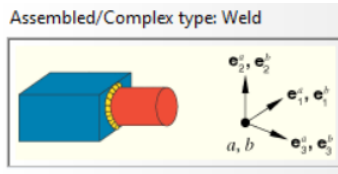


**Figure 3.4** Diagram of the weld connector type.



**Figure 3.5** Characteristics of the weld connector type.

Regarding link connectors, it maintains a constant distance between two nodes. Its rotational degrees of freedom are not affected at either node. Its characteristics are shown in Figure 3.6 and Figure 3.7.

**Figure 3.6** Diagram of the link connector type.



**LINK**

| | |
|---|---|
| Basic, assembled, or complex: | Basic |
| Kinematic constraints: | $l = constant$ |
| Constraint force output: | $f_1$ |
| Available components: | None |
| Kinetic force output: | None |
| Orientation at $a$: | Ignored |
| Orientation at $b$: | Ignored |
| Connector stops: | None |
| Constitutive reference lengths: | None |
| Predefined friction parameters: | None |
| Contact force for predefined friction: | None |

**Figure 3.7** Characteristics of the link connector type.

CHAPTER 4

# Numerical modelling

The objective of this chapter is to explained the process followed to model the Final Door Model. It will developed from the simplest model performed until the more complex one. However, it would not include the validation of a single plate and the study of the different type of mesh elements available in Abaqus, Appendix D and Appendix E. The type of element chosen to model the plates that form the door is a general shell element with full integration, S4, and it is going to be used in almost all the models developed in this Chapter. Regarding the meshing, it will depend on the type of analysis ran and the level of discretization needed.

| Model | Description | Working space | Type of element | | Connectors | Nº Mesh elements |
|-------|-------------|---------------|-----------------|---|------------|------------------|
| **Model 1** | Cross-section | 2D | 1D | B23 | No | 28 |
| **Model 2** | 1 plate | 3D | 2D | S4 | No | 56x56 |
| **Model 3** | 2 plates | 3D | 2D | S4 | CONN3D2 | 56x56 both |
| **Model 4** | Door model | 3D | 2D | S4 | No | Variable |

**Table 4.1** Models developed during this chapter.

The aim of this different models is to study its buckling and post-buckling behavior to understand how it works and how this affects to the Door model. Two load cases will be applied to all the models, first a mechanical load and secondly a temperature field that follows the Standard fire curve. It also will be performed two types of analysis: Eigenvalue analysis to find the buckling mode shapes and the critical buckling load, and the Post-buckling analysis, to analysed the behavior of the models after buckling.

Model 1 will be a 2D model with a hollow cross-section, it will used a beam element, being the only Model that does not use shell elements. Its buckling will follow the Euler theory for buckling of columns and its geometry is equivalent of the steel Door without the top and bottom plates.
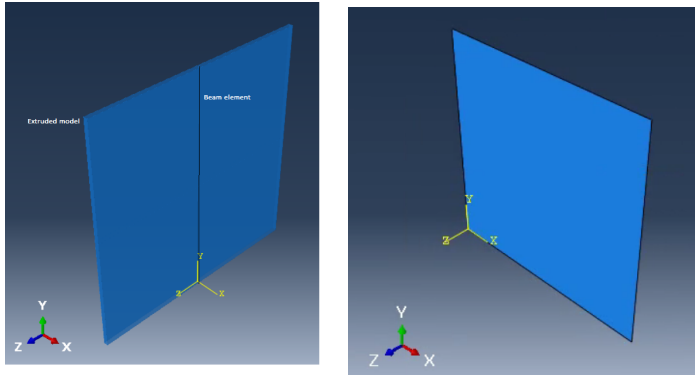
**Figure 4.1** Left: Model 1, cross section model. Right: Model 2, single steel plate

Model 2 will be a simply supported single steel plate with the width and height of the door and 1 mm of thickness. Model 3 consist in two steel plates, equal geometric characteristics to Model 2, connected between them on the sides. One of the plates will be simply supported and the load case will be applied to it.

Lastly, a Door model is performed, Model 4, and it is made of six connected steel plates. The boundary conditions and the load case would only be applied to one of the plates.
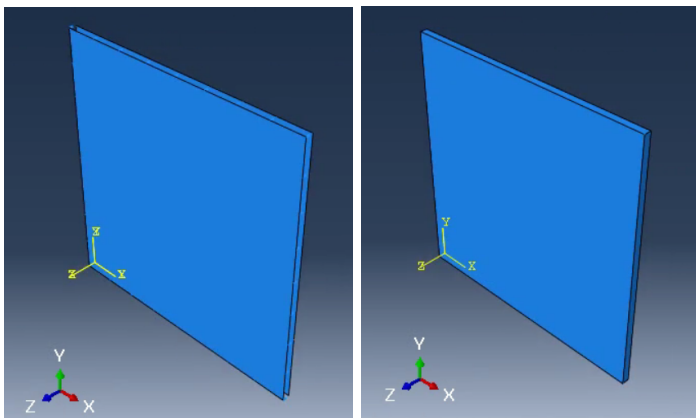


**Figure 4.2** Left: Model 3, two connected plates. Right: Model 4, door model

The reason why in Model 3 and 4 the boundary conditions are only applied to one of the plates is because the door that is going to be modelled is a sliding door so it is

only going to be connected to the sliding mechanism by one of the sides.

The last sections of this Chapter will focus on the influence of the boundary conditions on the model and in the coupled analysis of a single steel plate.

## 4.1 Model 1: Beam analysis

### 4.1.1 Model approach

This analysis has been performed using beam elements with a hollow cross-section. The geometry of the cross section is the same as the one plotted in Figure 4.3. The element type used is B23 and first it was ran an eigenvalue analysis to find the buckling modes and then a statically incremental analysis, to analyse the post-buckling behaviour.

The column is simply supported and the temperature field used follows the Standard fire curve
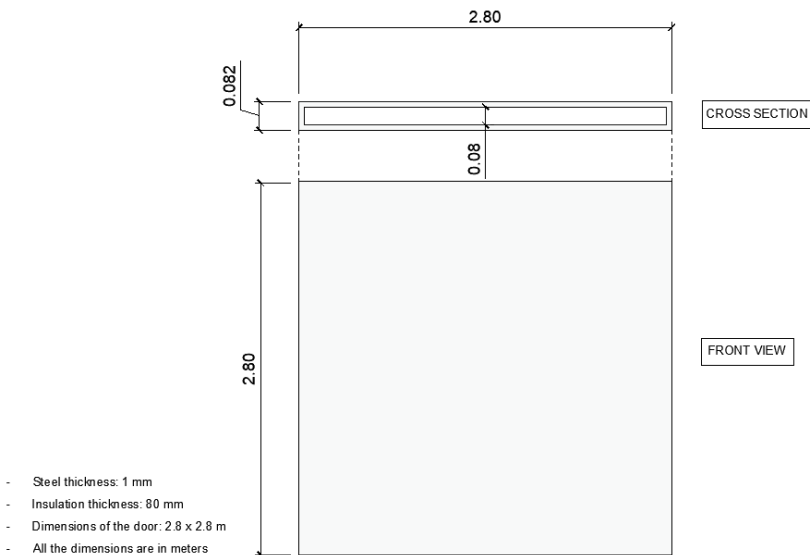


**Figure 4.3** Geometrical properties of the beam cross section and frontal view..

## 4.1.2  Analytical solution

First, the analytical solution for this model is going to be calculated. The calculation are based in Euler buckling theory, explained in Section 2.7.3. The formulation used is shown in Equation 4.1 and the results obtained are shown in Table 4.2, where $I$ is the inertia of the cross-section and $L_{ef}$ is the equivalent length of the column, which depends on the boundary conditions. For this case, simply supported column, the equivalent length is equal to the total length of the column.

$$P_{cr} = \frac{\pi^2 E I}{L_{ef}^2} \tag{4.1}$$

| E (KPa) | I $(m^4)$ | $L_{ef}$ (m) | A $(m^2)$ | $P_{cri}$ (KN) | $\Delta$T (ºC) | $T_F$ (ºC) |
|---|---|---|---|---|---|---|
| $210 \cdot 10^6$ | $9.2712 \cdot 10^{-6}$ | 2.8 | 0.00576 | 2450.65 | 168.8 | 188.83 |

**Table 4.2** Anlytical solution for the buckling load and the critical buckling temperature of a 2.8 meters length column with a hollow cross-section.

The critical temperature at which the system starts buckling can be estimated using Equation 4.4, which is explained in Section 2.7.4. The coefficient of thermal expansion, $\alpha$, is equal to $12.2 \cdot 10^{-6}$ $^oC^{-1}$. The initial temperature of the column is equal to 20ºC.

$$\Delta T = T_F - T_0 = \frac{P_{cri}}{A E \alpha} \tag{4.2}$$

## 4.1.3  Eigenvalue analysis

Now the Eigenvalue analysis is going to be performed for two different load cases, one with a vertical load acting at top of the column and the other is a temperature field acting along the whole length of the column.

The results obtained for the mechanical load case are shown in Figure 4.4 and in Figure 4.5 the results for the case with the temperature field acting are displayed. As it can be observed, the buckling modes have the same shape for both cases and the results obtained with Abaqus are practically equal to the ones calculated analytically.

The comparison between the results obtained in Abaqus and the analytical solution are shown in Table 4.3.
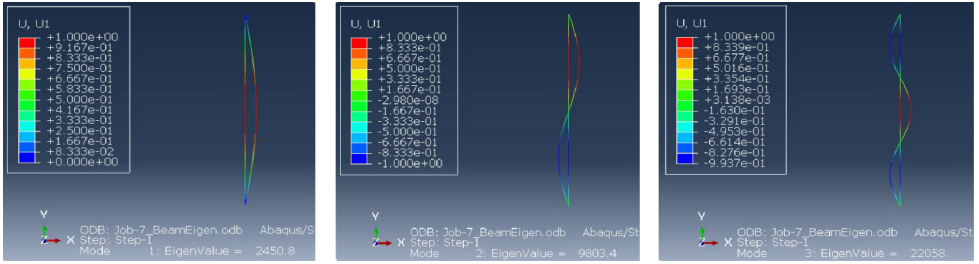
**Figure 4.4** Eigenvalue analysis results for the simply supported column under mechanical load.
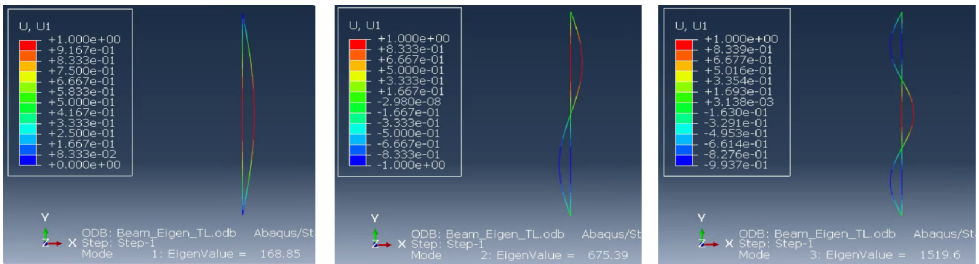


**Figure 4.5** Eigenvalue analysis results for the simply supported column under thermal load.

|  | **Analytical solution** | **Abaqus results** |  |
|---|---|---|---|
| $P_{cr}$ | 2450.65 | 2450.80 | KN |
| $\Delta T_{cr}$ | 168.80 | 168.85 | ºC |
| $T_F$ | 188.80 | 188.85 | ºC |

**Table 4.3** Comparison between the analytical results and Abaqus results for the Eigenvalue analysis 2.8 length column with a hollow cross-section.

### 4.1.4  Post-buckling analysis

Then the post-buckling behaviour is studied with the statically incremental analysis. First, an initial imperfection has to be introduced into the model so, an initial load is applied at the middle of the beam. The load has to be small enough to produce only a small displacement. For this case it was chosen 3 KN which produces 1 mm maximum initial displacement at the middle.

First the load case with the punctual load applied at top is ran and them the temper-

ature field case. The results of both models have been compared in Figure 4.6, where the load versus the out of plane displacement is plotted. The load used in this plot for the temperature field case is the load produce at the supports when the beam is trying to expand due to temperature increment.
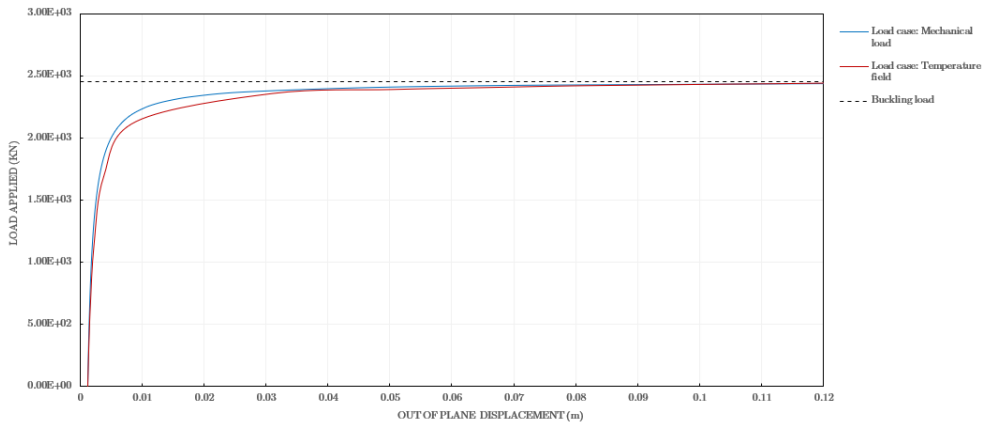


**Figure 4.6** Out of plane displacement versus load applied for both load cases.

Then, the temperature versus out of plane displacement has been plotted for the temperature field case, Figure 4.7.
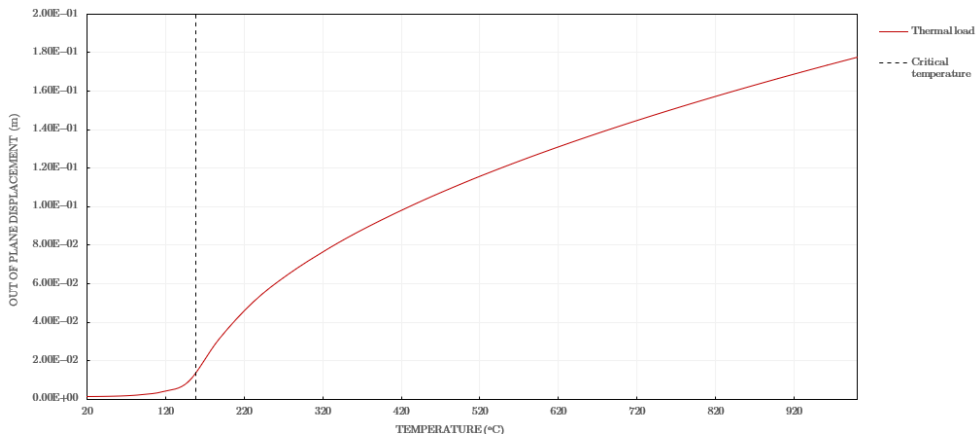


**Figure 4.7** Temperature versus out of plane displacement.

## 4.2   Model 2: Single steel plate

### 4.2.1   Model approach

This model consist on a single steel plate with the same width and height of the door and a thickness of 1 mm and 10 mm.
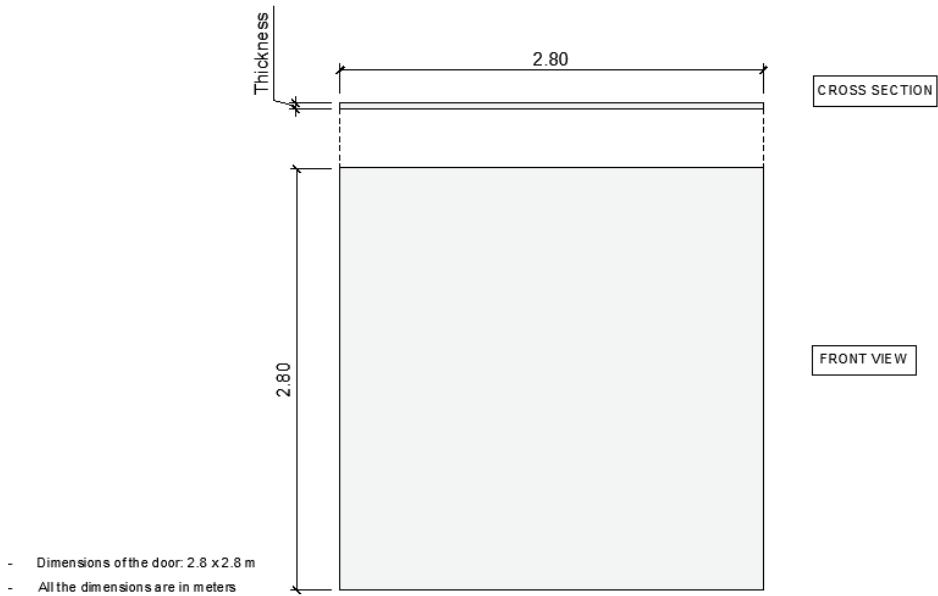


**Figure 4.8** Geometrical characteristics of Model 2: Single steel plate

The structure is simply supported on two sides, top and bottom, and free on the other two sides. It will be subjected to two types of loading: thermal load and mechanical load. The mechanical load will be applied as a distributed load along the top edge of the shell and the thermal load will be applied to the whole panel. When temperature is applied to the system, the vertical displacement at the top of the shell is going to be restricted to limit the thermal expansion.

### 4.2.2   Analytical solution

First, it is going to be calculated analytically the critical load at which the panel starts buckling, $P_{cri}$, for the two different thickness. Then, the critical temperature

at which buckles can be determined.

The theory behind these formulations has been explained earlier at Section 2.7 and the buckling and post-buckling behavior of a single plate model has been validated and calibrated in Appendix D.

To calculate the buckling load of a simply supported plate Equation 4.3 is used. This formulation comes from the Euler buckling theory and its equation for calculating the critical buckling load in beams. The formula used is a variation that allows to calculate buckling in plates and shells [19].

$$P_{cri} = \frac{\pi^2 EI}{(1 - v^2) a_{ef}^2} = \frac{\pi^2 Db}{a_{ef}^2} \tag{4.3}$$

Having into account that the plate is simply supported its effective side length $a_{ef}$ is equal to the total length of the side, which for this case is equal to the height of the panel, 2.8 meters. The value for $b$, which is the width of the panel is the same for both cases, 2.8 meters. The results for the two different thickness are shown in Table 4.4.

| Thickness (mm) | E (KPa) | I $(m^4)$ | $a_{ef}$ (m) | $v$ | $P_{cri}$ (KN) |
|---|---|---|---|---|---|
| 1 | $210 \cdot 10^6$ | $233.3 \cdot 10^{-12}$ | 2.8 | 0.3 | **0.0678** |

**Table 4.4** Analytical solution for the buckling load for a plate with 1 mm and 10 mm thickness.

Now, the critical temperature at which the system starts buckling can be estimated using Equation 4.4, which is explained in Section 2.7.4.

$$\Delta T = T_F - T_0 = \frac{P_{cri}}{AE\alpha} \tag{4.4}$$

The value of the coefficient of thermal expansion, $\alpha$, is the one given in the Eurocode [9] for carbon steel and its value is equal to $12 \cdot 10^{-6} \ C^{-1}$ which is not temperature dependent and only valid for temperatures higher than 20ºC. The initial temperature of the system, $T_0$, is 20ºC and the solution obtained is shown in Table 4.5.

| Thickness (mm) | E (KPa) | A ($m^2$) | $\alpha$ ($C^{-1}$) | $P_{cri}$ (KN) | $\Delta T_{cr}$ (ºC) | $T_F$ (ºC) |
|---|---|---|---|---|---|---|
| 1 | $210 \cdot 10^6$ | 0.0028 | $12 \cdot 10^{-6}$ | 0.0678 | **0.0096** | **20.0096** |

**Table 4.5** Analytical solution for the critical buckling temperature for a plate wiith 1 mm and 10 mm thickness.

### 4.2.3 Eigenvalue analysis

Now, the Eigenvalue analysis is going to be performed in order to obtained the critical load at which the steel panel starts buckling. Two load conditions are going to be applied, the first one is distributed mechanical load along the top edge of the plate. The second load condition consist in a thermal field applied to the whole structure and, in order to limit the vertical expansion due to temperature and allow buckling, the vertical degree of freedom at top and bottom will be restricted.

The meshing used is made of 56x56 quadrilateral elements with a side length of 0.05 meters. The numerical values obtained are lower than the analytical solution because the Analytical formulation is more conservative than Abaqus. However, the error between this solutions is less than 5% which is considered as acceptable.

The mode shapes obtained for the three first eigenvalues match perfectly with the results expected in both load conditions, Figure 4.9 and 4.10.
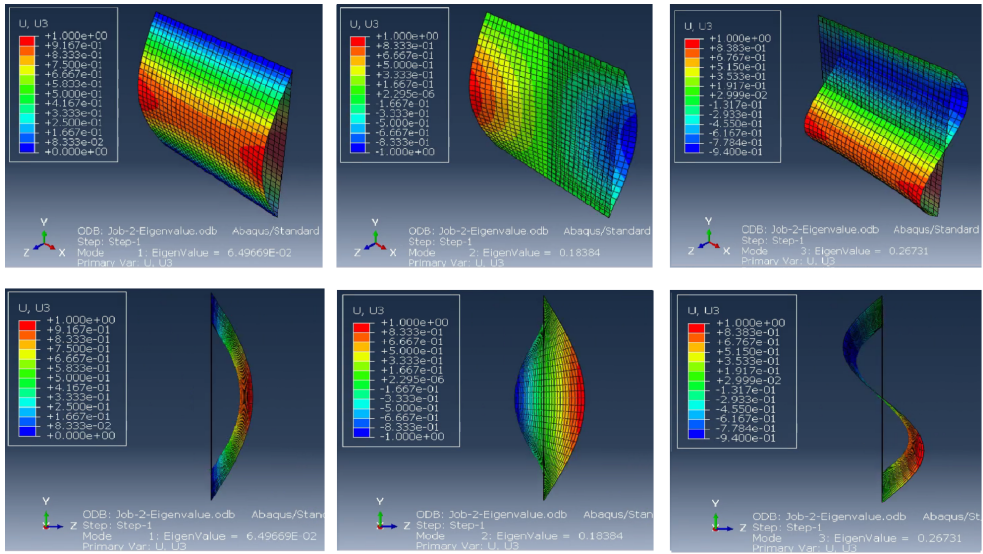
**Figure 4.9** Eigenvalue analysis results for 1 mm thickness plate under mechanical load.
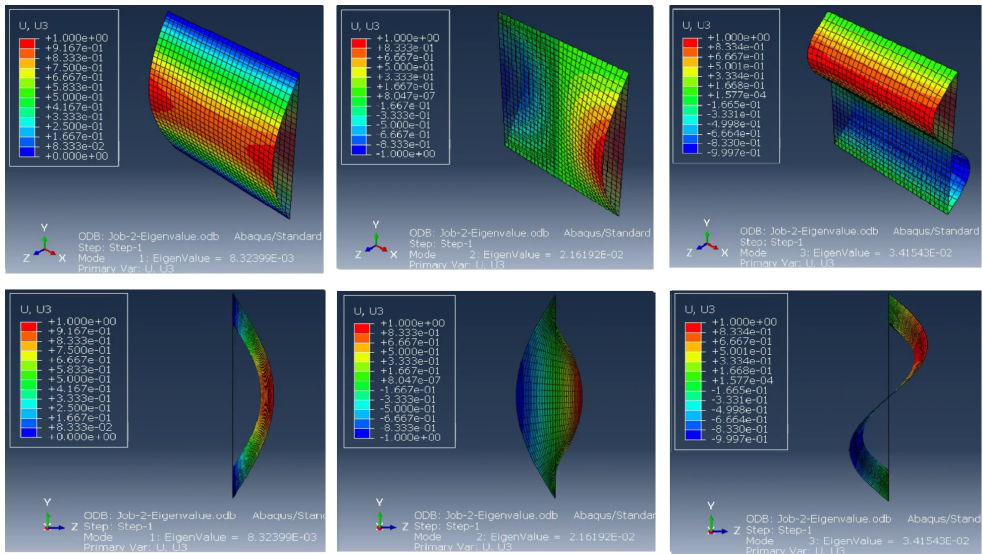


**Figure 4.10** Eigenvalue analysis results for 1 mm thickness plate under thermal load.

Regarding the numerical results obtained for the mechanical load, the Abaqus results are a sligthly lower than the analytical values, less than 5% of difference. The main

reason is that the analytical formulation are more conservative than Abaqus theory behind the Eigenvalue analysis, this was explained in Section 3.1.1. Regarding the critical temperature this difference is higher than in the previous case.

| | Analytical solution | Abaqus results | |
|---|---|---|---|
| $P_{cr}$ | 0.0678 | 0.0649 | kN |
| $\Delta T_{cr}$ | 0.0096 | 0.00832 | ºC |
| $T_F$ | 20.0096 | 20.00832 | ºC |

**Table 4.6** Comparison between the analytical results and Abaqus results for the Eigenvalue analysis of 1 mm thick plate.

### 4.2.4 Post-buckling analysis

Now the post-bucklin is going to be studied. For the load case where a temperature field is applied it has been used the Standard fire curve distribution, developed in Section 2.3.

The initial imperfection add to the system has been introduced by adding a distributed load at the middle section of the plate. The load has to be small enough to produce only a small imperfection. For this case the load introduce an initial imperfection with the maximum value of 0.4 mm at the middle of the plate.
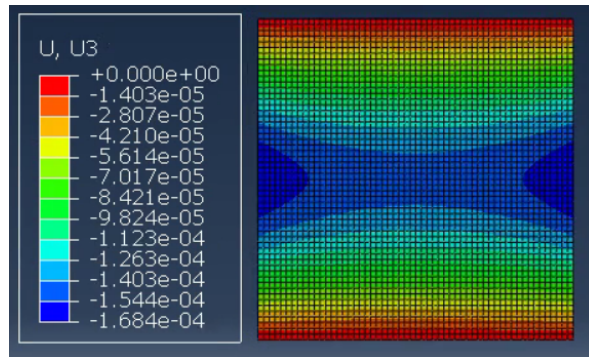


**Figure 4.11** Initial imperfection of the plate.

First, the mechanical load case is studied. In Figure 4.12 the Load-displacement curve has been plotted, where the out of plane displacement as a function of the applied load is shown. The load shown represents the total force applied to the system.

As it was expected the post buckling behavior approaches to a symmetric stable behavior, as it was explained in Section 2.7 and its validation with the analytical solution is shown in Appendix D.
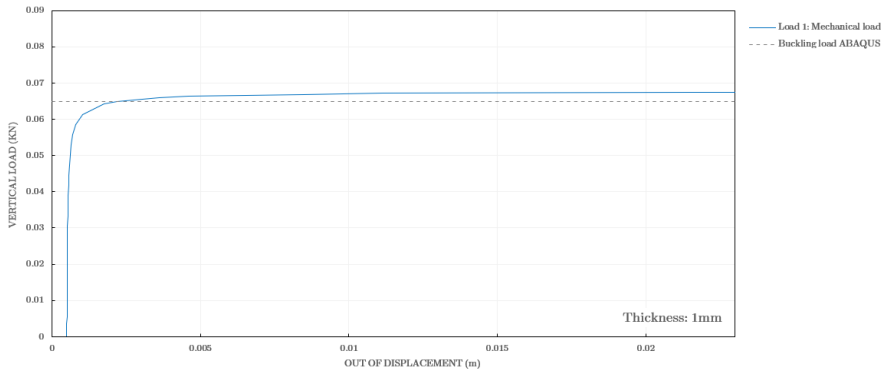


**Figure 4.12** Out of plane displacement (U3) versus mechanical load applied for 1 mm thickness plate under mechanical load.

In Figure 4.13 the out of plane displacement and the vertical stress is shown for mechanical distributed load.
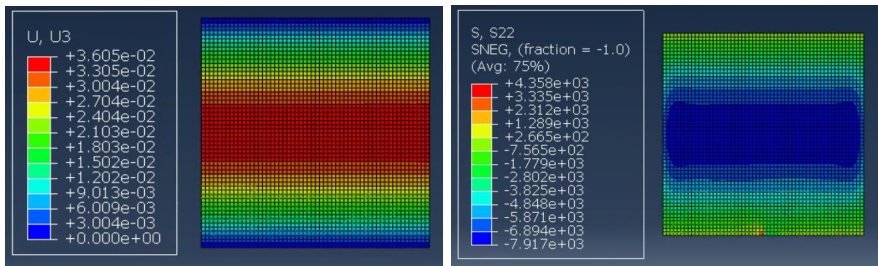


**Figure 4.13** Left: Out of plane displacement for 1 mm thickness plate under mechanical load of 0.0847 KN. Right: Vertical stress (S22) for 1 mm thickness plate under mechanical load of 0.0847 KN.

Afterwards, the thermal load case is going to be studied. It was observed that, when the buckling load is surpassed some problems in the analysis appear and the buckling shape changes. At first, the buckling mode shape is the same as the one obtained for the first buckling mode, but as the temperature increase this shape changes, Figure 4.14.
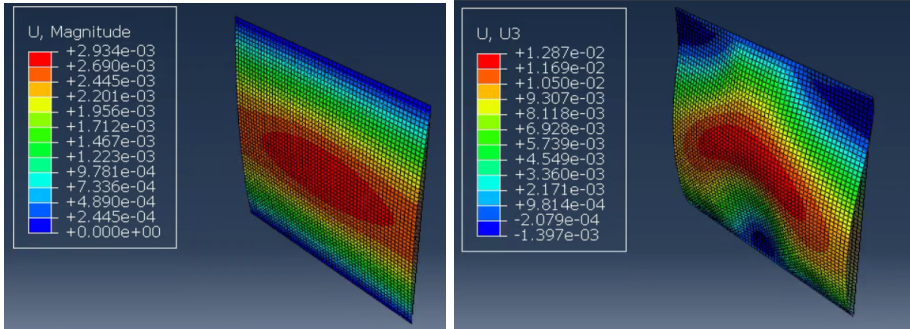
**Figure 4.14** Left: Out of plane displacement at 20.21º for 1 mm thickness plate under thermal load. Right: Out of plane displacement at 24.16º for 1 mm thickness plate under thermal load.
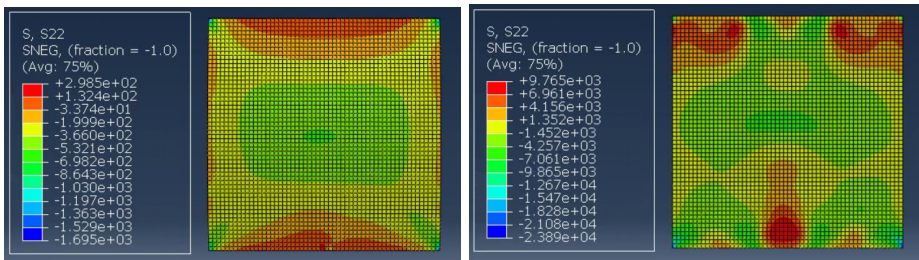


**Figure 4.15** Left: Vertical stress (S22) at 20.21ºC for 1 mm thickness plate under thermal load. Right: Vertical stress (S22) at 24.16ºC for 1 mm thickness plate under thermal load.

Then, the Temperature-displacement curve is plotted, Figure 4.16, and the Stress-temperature curve, Figure 4.17. At the Stress-temperature curve it can be seen the point where buckling shape starts to change, around 20.75ºC.
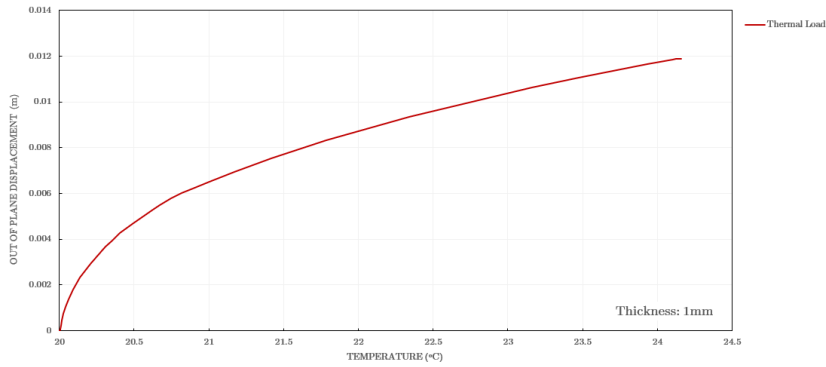
**Figure 4.16** Temperature versus out of plane displacement for 1 mm thickness plate under thermal load. Point studied: middle point of the plate.
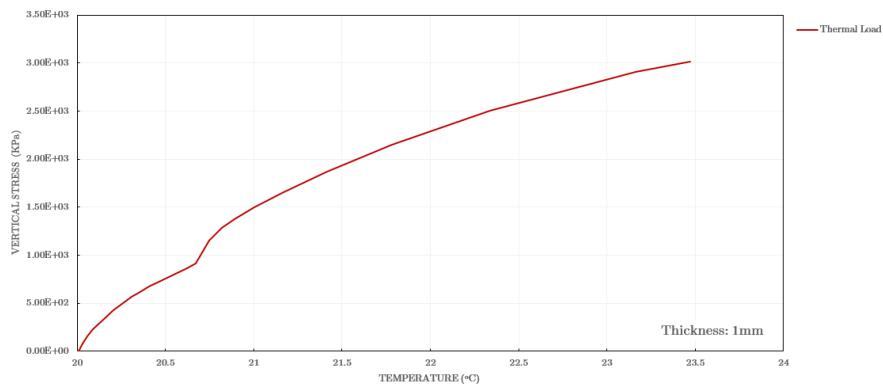


**Figure 4.17** Temperature versus vertical stress for 1 mm thickness plate under thermal load. Point studied: middle point of the plate.

## 4.3   Model 3: Connected Plates

### 4.3.1   Model approach

This model is compound of two steel plates connected on all its sides by axial connectors. The geometric characteristics of the plate are the same as the one used in Model 2. In Figure 4.18 the geometry of one of the plates is shown and in Figure 4.19 the disposition of the whole Model is presented, the separation between the plates is equal to 80 mm.

The gap between the two plates represent the space where the insulation would be placed in a real fire resistance door. The link connectors connect the movement of two nodes in one direction, for this case they are connectors of the x-axis displacement.
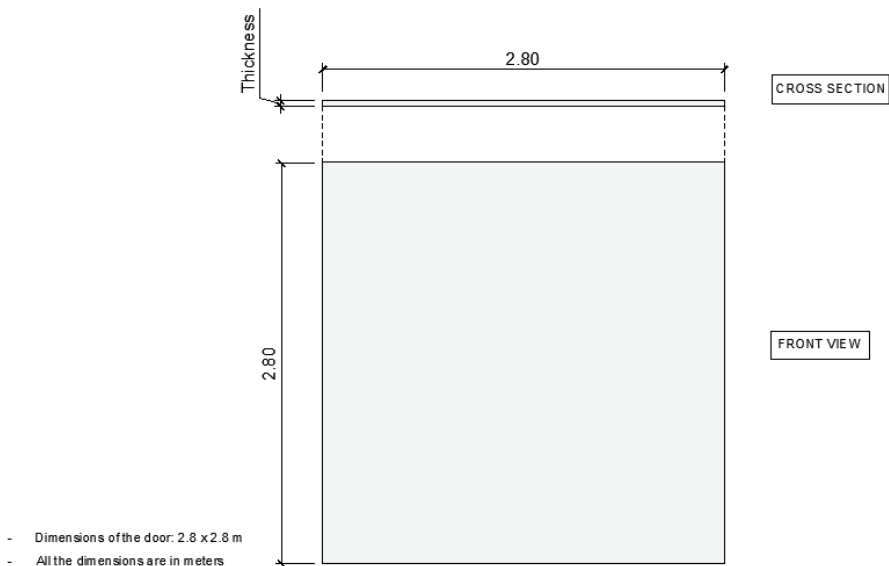


**Figure 4.18** Geometrical characteristics of one of the steel plates of the model. Thickness equal to 1 mm.

The boundary conditions of the system will be simply supported at top and bottom and free on the sides. This boundary conditions will only be applied to one plate. The load will be applied only to the plate with the assigned boundary conditions and it

will be first a mechanical load distributed along the top edge and then a temperature field applied to all its surface. This temperature field will follow the Standard fire curve, Section 2.3.
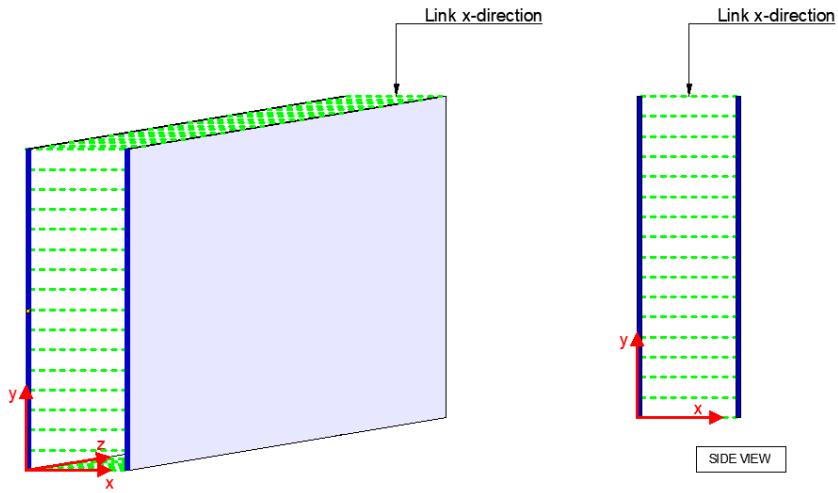


**Figure 4.19** Left: 3D of the Model. Right: Side view of the Model.
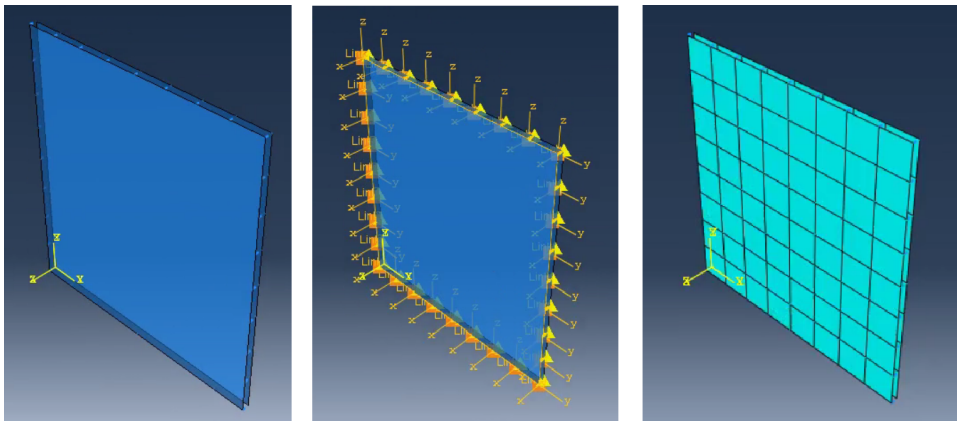


**Figure 4.20** Model configuration and connectors.

The mesh used for this model is of 56x56 elements of 0.05 m of length. The type of element is convenctional shell element, S4, with full integration.

## 4.3.2 Eigenvalue analysis

Two different load conditions are going to be applied, the first one is a mechanical distributed load applied along one of the plate edges and the second one will be a temperature field acting in the whole surface of one of the plates. The plate where the loads are going to be applied is the one that have the simply supported boundary conditions.

For the mechanical load, the results of the Eigenvalue analysis is shown in Figure 4.21 and, for the thermal load is shown in Figure 4.22. The eigenmodes of both load cases are the same and the shape is equal to the buckling modes of a single steel plate.
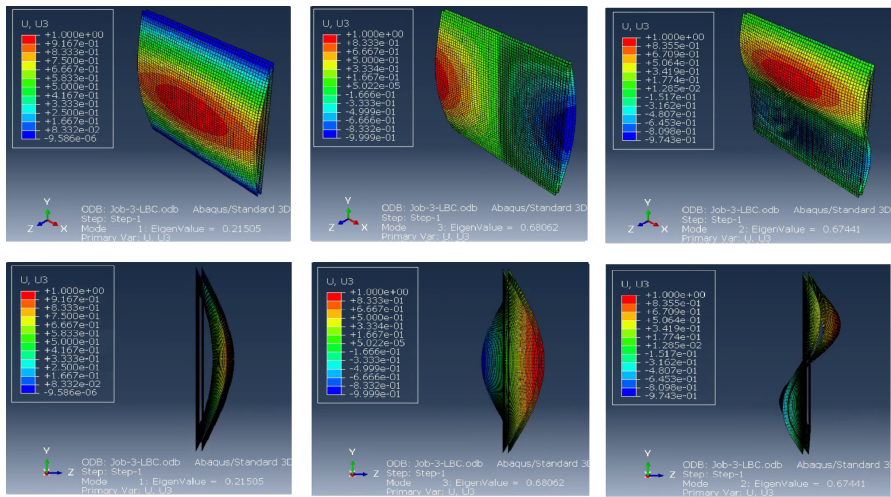


**Figure 4.21** Eigenvalue analysis results of the connected plates under mechanical load.
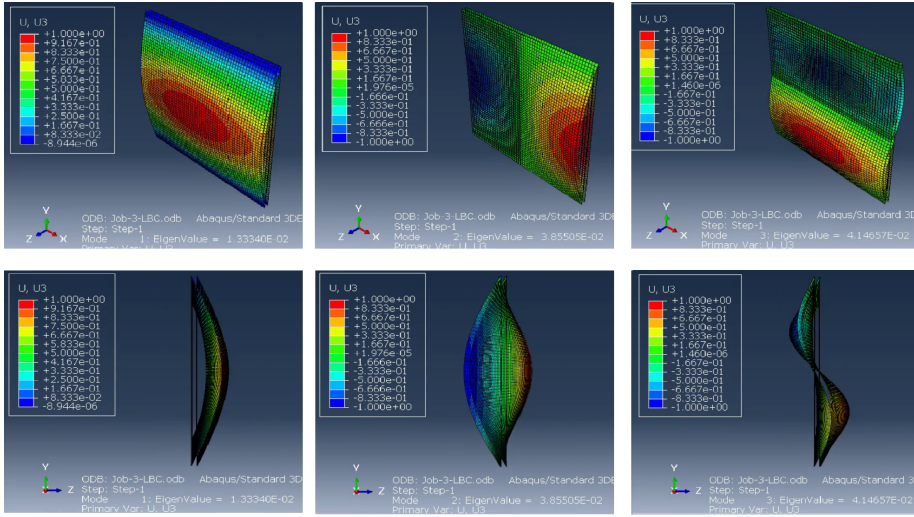
**Figure 4.22** Eigenvalue analysis results of the connected plates under thermal load.

| Abaqus results | Eigenvalue 1 | Eigenvalue 2 | Eigenvalue 3 | |
|---|---|---|---|---|
| $P_{cr}$ | 0.215 | 0.674 | 0.680 | kN |
| $\Delta T_{cr}$ | 0.013 | 0.038 | 0.041 | ºC |
| $T_F$ | 20.013 | 20.038 | 20.041 | ºC |

**Table 4.7** Results obtained in Abaqus for the Eigenvalue analysis of the connected plates.

The values for the critical temperature and the buckling load are displayed in Table 4.7 and, comparing to the single plate case, its values are higher for both, the critical load and the critical temperature. The main reason is that, even though the connectors does not provide stiffness to the system, it connects two steel plates leaving a distance between them. This connection connect the horizontal displacement of the loaded plate to the other so, when one plate moves the other has to move to. This two plates connected are stiffer than one single plate and the inertia of the set is higher than a single plate, for this reason the buckling load is higher.

## 4.3.3 Post-buckling analysis

Then the post-buckling analysis of the model is performed. The first step is to add an initial imperfection this have been done by adding a distributed load along the middle of the master surface, the initial imperfection is shown in Figure 4.23.
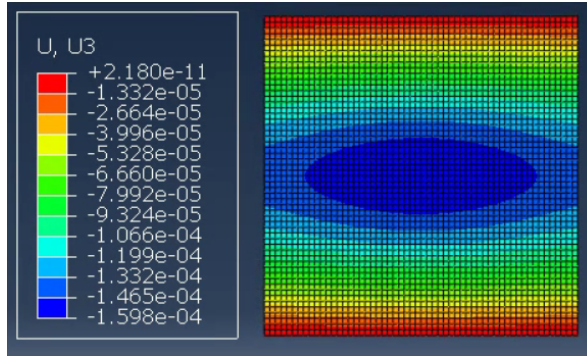
**Figure 4.23** Initial imperfection of the model, master surface.

The first load case studied is the distributed mechanical load, obtaining the load-displacement curve, Figure 4.24. A zoom at the beginning of the curve has been developed to appreciate better the behaviour of the plates, Figure 4.25. In Figure 4.26 the out of plane displacement for both plates is shown for 2.42 kN and in Figure 4.27 for 3.6 kN.
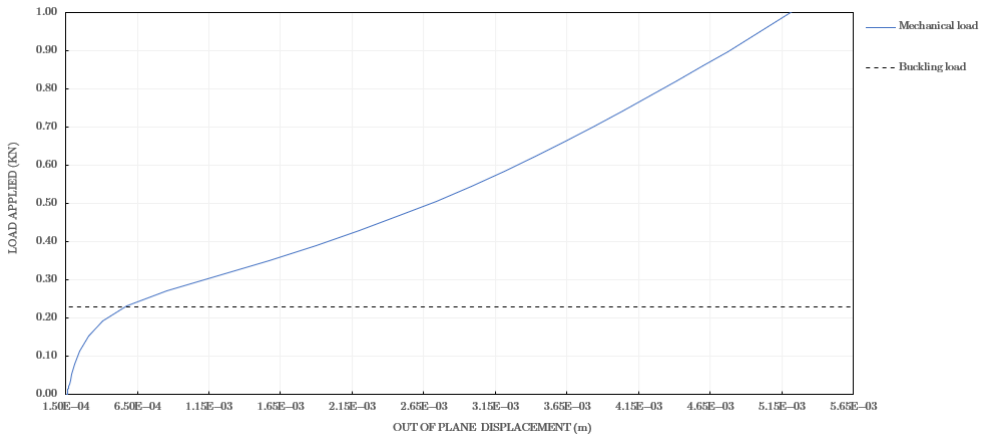


**Figure 4.24** Out of plane displacement versus mechanical load applied.
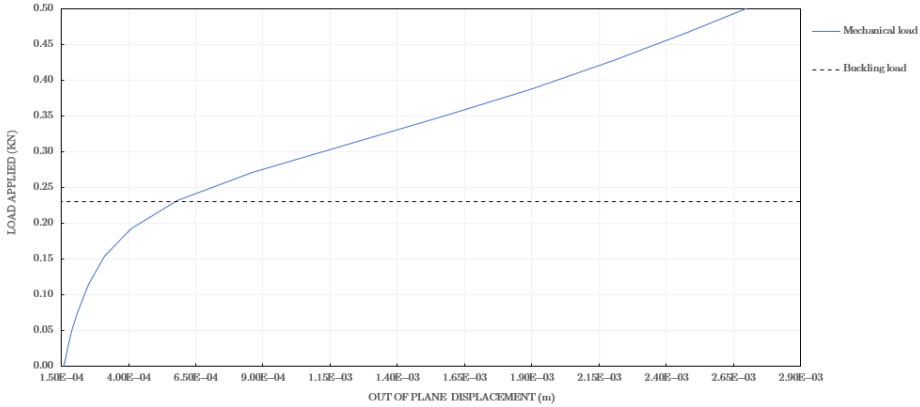
**Figure 4.25** Zoom at the beginning of the load-displacement curve.
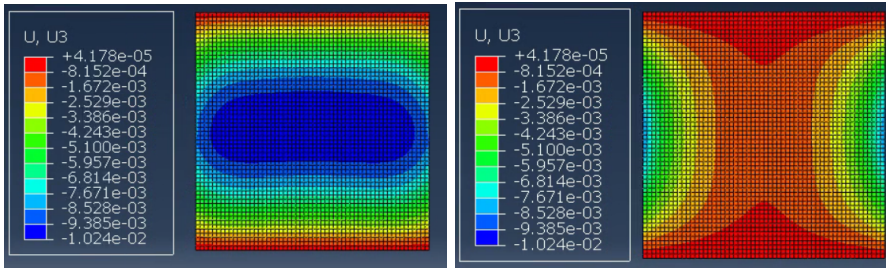


**Figure 4.26** Left: Out of plane displacement of the master surface at 2.42 kN. Right: Out of plane displacement of the slave surface at 2.42 kN.
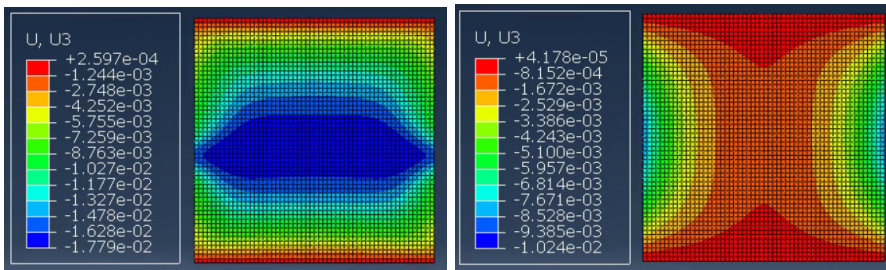


**Figure 4.27** Left: Out of plane displacement of the master surface at 3.6 kN. Right: Out of plane displacement of the slave surface at 3.6 kN.

Now, the case with the temperature field that follows the Standard fire curve is processed. In Figure 4.28 it is shown the out of plane displacement obtained for

20.8ºC. Then, after surpassing certain temperature the out of plane displacement stop following the buckling shape of the first buckling mode, this is shown in Figure 4.29.
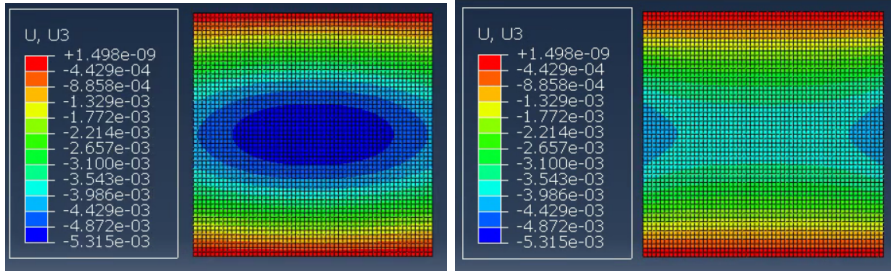


**Figure 4.28** Left: Out of plane displacement of the master surface at 20.8ºC. Right: Out of plane displacement of the slave surface at 20.8ºC.
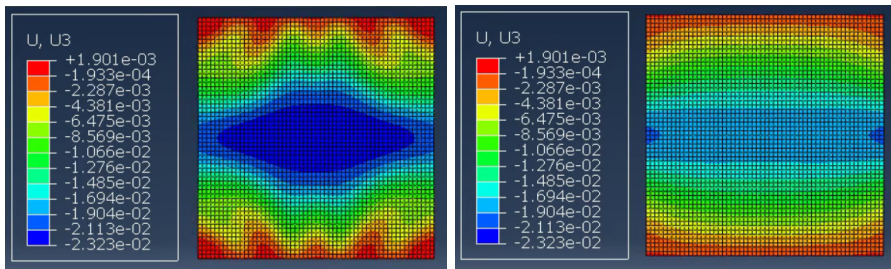


**Figure 4.29** Left: Out of plane displacement of the master surface at 32.6ºC. Right: Out of plane displacement of the slave surface at 32.6ºC.

Then, the temperature-displacement curve, Figure 4.30, has been plotted. In Figure 4.31 an augmented part of the previous graph has been represented, showing the different behaviour of the curve before and after buckling.
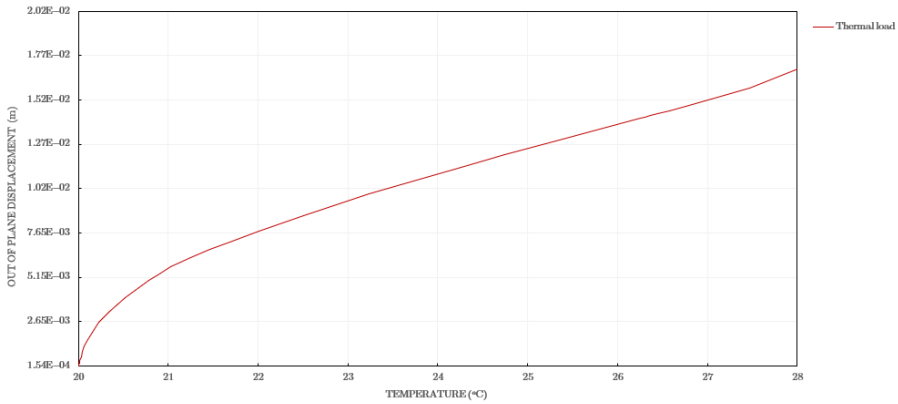


**Figure 4.30** Temperature versus out of plane displacement.
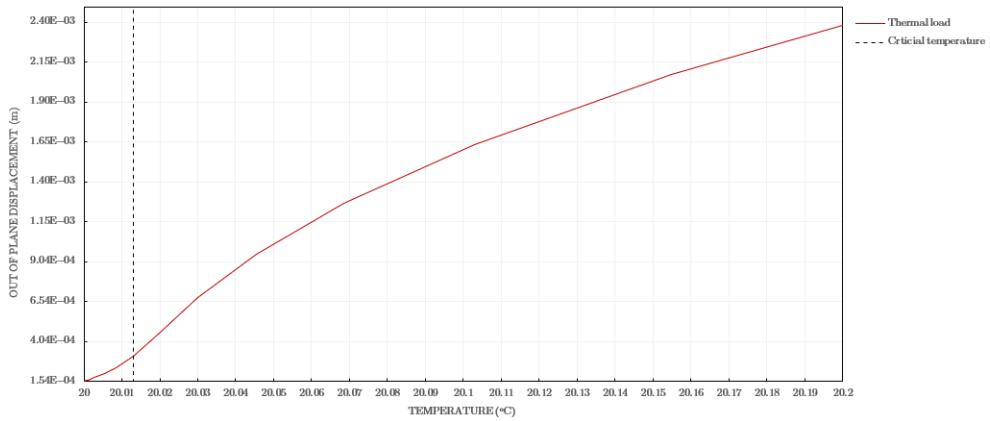


**Figure 4.31** Augmented graph of the temperature-displacement curve.

## 4.4   Model 4: Door model

After analysing a single steel plate and two plates connected it is going to be developed the Door model, which is compose by 6 steel plates. The plates are connected between them and its disposition resembles to a close steel box. There are two main plates at the front, two at the sides, one at top and one at the bottom. Its geometric characteristics are shown in Figure 5.2 and the 3D view of the Door is shown in Figure 5.1.
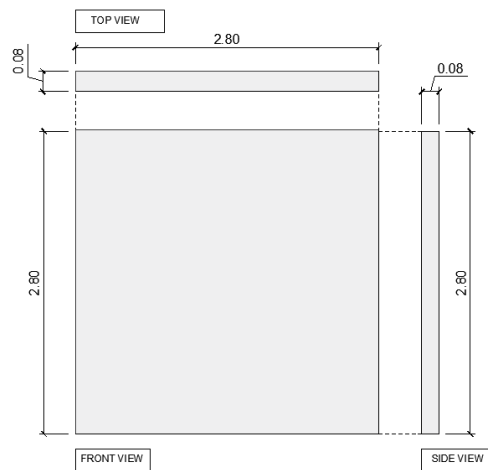


**Figure 4.32** Geometric characteristics of the Door model, all the measures are in meters. Thickness of the plates equal to 1 mm.
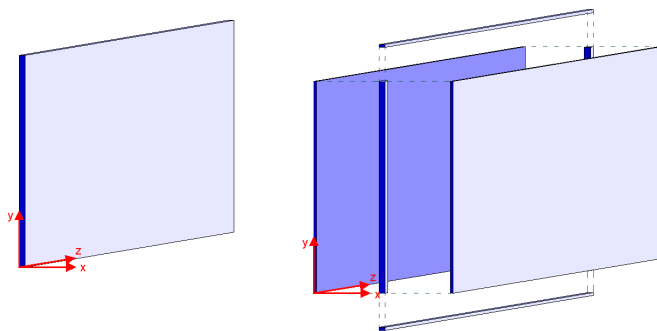


**Figure 4.33** Left: 3D of the Door model. Rigth: 3D of the components of the door model.

In reality, the steel plates that made the Door model are welded between them. For this reason the model developed in this section will have fix joints between the plates, to reproduce the behavior of a weld connection. This was modelled using the extrusion tool in the Part module of Abaqus, which allows to add plates to an existing plate by connecting one of their edges. This connection fully connects the degrees of freedom of one edge to the other and does not allow rotation between the plates.

### 4.4.1 Eigenvalue analysis

The Eigenvalue analysis to obtain the critical load and the critical temperature is performed. First it is going to be analysed the mechanical load case. A distributed mechanical load is going to be applied along one of the edges of the main plate. The boundary conditions will only be applied to one of the main plates in a way that it is simply supported. In Figure 4.34 the buckling modes are shown.
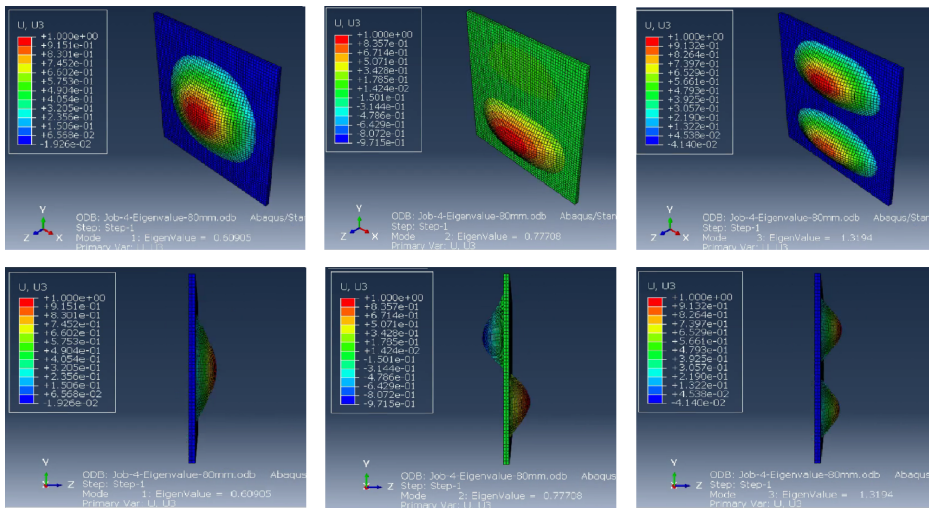


**Figure 4.34** Model 1: Eigenvalue analysis results of the door under mechanical load.

For the thermal load case the same boundary conditions will be applied to one of the main plates and the temperature field will be acting in the same plate. The distribution of temperatures will follow the Standard fire curve. The Eigenmodes are shown in Figure 4.35.
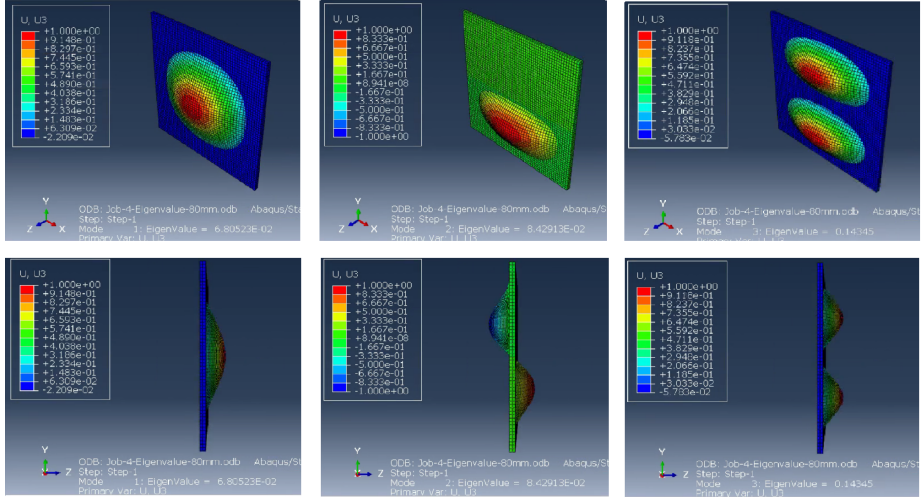
**Figure 4.35** Model 1: Eigenvalue analysis results of the door under thermal load.

The buckling load and the critical temperature results have been registered in Table 4.8.

| Abaqus results | Eigenvalue 1 | Eigenvalue 2 | Eigenvalue 3 | |
|---|---|---|---|---|
| $P_{cr}$ | 0.509 | 0.777 | 1.319 | kN |
| $\Delta T_{cr}$ | 0.068 | 0.084 | 0.143 | ºC |
| $T_F$ | 20.068 | 20.084 | 20.143 | ºC |

**Table 4.8** Results obtained in Abaqus for the Eigenvalue analysis of the door, Model 1.

## 4.4.2  Post-buckling analysis

After analysing the buckling modes of the door a post-buckling analysis is performed. Two load states will be applied, as before, the first one will be a distributed mechanical load along one of the edges of the plate and the other one a temperature field applied to the surface of one of the main plates. The temperature field will follow the Standard fire curve.

Analysing the behavior of the door under the action of a mechanical load along one of its edges, it has been plotted the temperature-displacement curve, Figure 4.36.
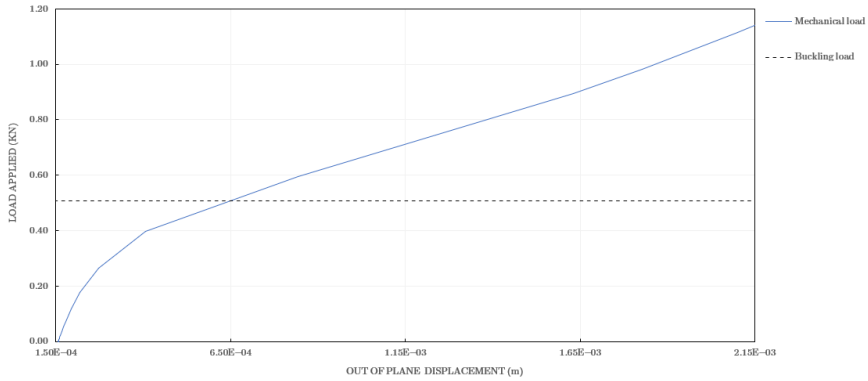
**Figure 4.36** Out of plane displacement versus mechanical load applied at the door model.

In Figure 4.37 the out of plane displacement is shown.
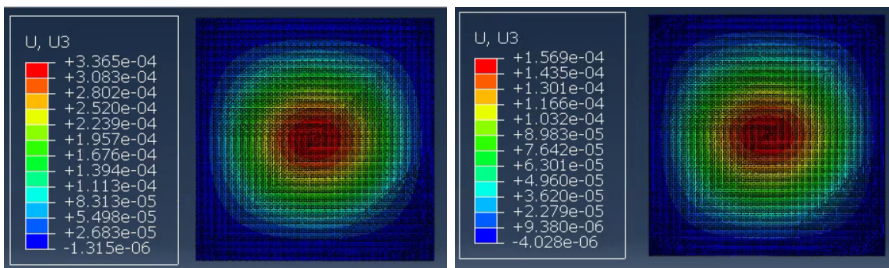


**Figure 4.37** From left to right: Out of plane displacement at 0.12 kN and at 0.43 kN.

Now, the temperature field is applied to the door to study its post-buckling behavior.
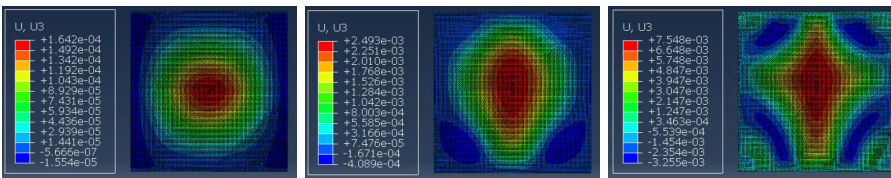


**Figure 4.38** From left to right: Out of plane displacement at 20.05º, at 20.01ºC and 20.6ºC

The temperature-displacement curve for the middle point of the plate has been plotted in Figure 4.39.
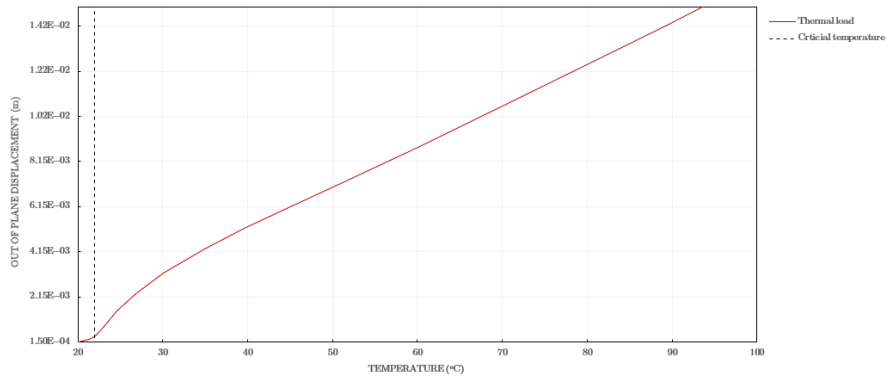
**Figure 4.39** Temperature versus out of plane displacement of Model 1 under thermal load

## 4.5 Influence of boundary conditions

The expected mechanical behavior of a fire-resistance door was similar to the one observed in Section 4.3, but this is not accurate because the sides and the top and bottom plates that conform a real door are missing and, consequently, the stiffness that they add to the Door model. However, when these plates are add to the model the behavior changes from a simply supported plate at top and bottom to a clamped plate on all sides, the reason is that the rigidity of the side plates is too big. So, when the temperature field is add to the door the deformation and behavior is similar to a clamped plate, this can be observed comparing the Eigenvalue analysis of both models. In Figure 4.40 the Eigenmodes of a clamped plate are shown.
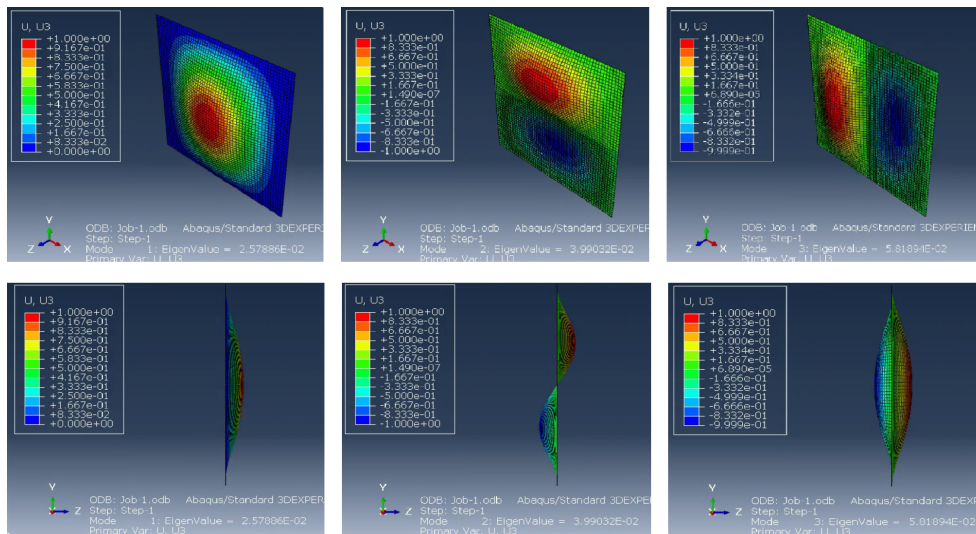


**Figure 4.40** Eigenvalue analysis of a clamped plate on all its sides under thermal loading and the geometric characteristics of the door.

As it can be observed the first two eigenmodes have the same shape as in the Door model, Figure 4.35, but in the third one it changes. This could be due to the rigidity effect of the sides and the rigidity that the second plate provides to the Door model.

In order to check if the behavior of the door was correct and close to reality its deformation was compared to the results from another investigation. In Figure 4.41 is shown the deformation of a pedestrian fire-resistance door under thermal load, extracted from *"Diseño y simulación de una puerta cortafuego peatonal batiente de*

*simple hoja"* [20]. The deformation shape is similar to the one obtained in the post-buckling analysis of Door model. The out of plane displacement pattern resembles circular like in the clamped plate case. In addition, if we compare this deformation pattern with the simply supported plate, the deformation is different because in the simply supported is horizontal not circular.
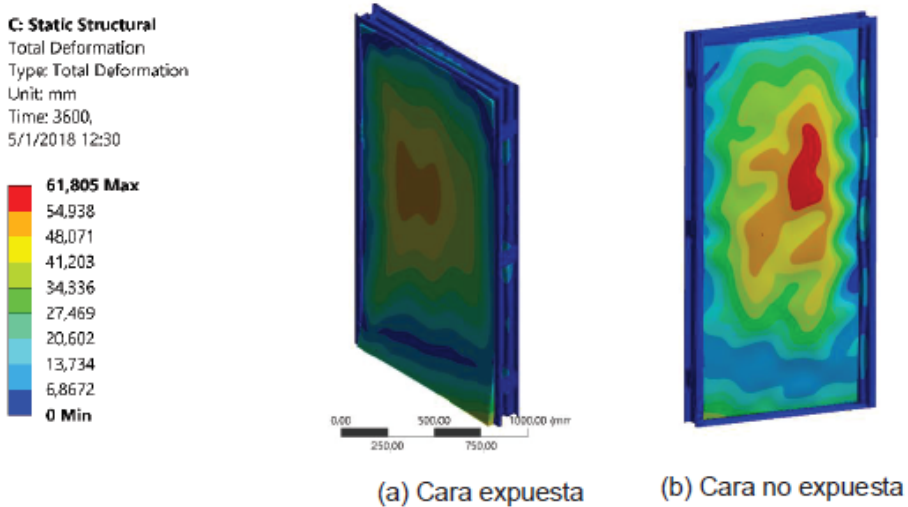


(a) Cara expuesta            (b) Cara no expuesta

**Figure 4.41** Deformation of a pedestrian fire-resistance door after 3600 seconds, on the left the expose side to fire and on the right the unexpose side. Extracted from *"Diseño y simulación de una puerta cortafuego peatonal batiente de simple hoja"*, [20].

In the Door model developed before its also been affected by the rigidity of the weld connections, because for Abaqus it is a perfect weld connection that does not allow relative rotation between the joint plates. This could be far from reality because this type of connection are not perfect and allow some relative rotation between the plates. This could affect to the behavior of the model.

## 4.6   Coupled model

Now the coupled analysis will be studied. It will be performed two types of analysis, the first one will be a statically incremental analysis with a temperature field obtained from the thermal analysis performed in the brother-project [5]. The second analysis will be a coupled analysis with the mechanical boundary conditions and the

thermal boundary conditions all together, the fire curve will be the standard fire curve.

A single steel plate will be studied with a thickness of 10 mm and the same dimensions of the door, 2.8x2.8 meters. The objective of this section is to check that using thermal data in a mechanical analysis and performing a coupled analysis would give the same results. For this reason it was chosen a thicker plate, to ensure that the analysis is run perfectly and it does not abort. This is possible because the thermal data of this plate is available.

It has been performed the coupled analysis and the mechanical analysis with the thermal model fire curves and the results obtained are shown in Figure 4.42 and Figure 4.43.

It can be observed that both models are analogue and the results are practically the same. So, it can be conclude that instead of performing two types of analysis, first a thermal analysis and then a mechanical analysis, a single one way coupled model can be used.
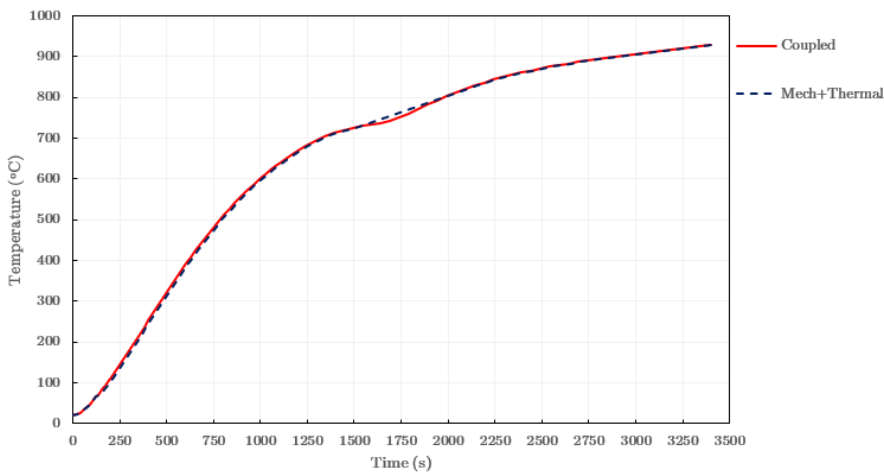


**Figure 4.42** Temperature versus time.
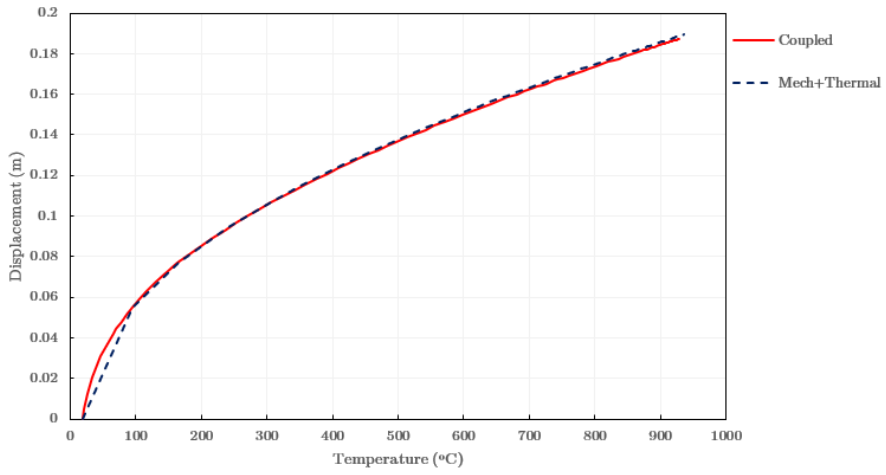
**Figure 4.43** Displacement versus time Model with 10mm of thickness.

CHAPTER 5

# Final Model

In this Chapter the Final Model of the door is going to be explained and analysed, justifying all the decisions and assumptions made to reach this solution.

## 5.1 Model description

The start point of the final model is the door model described in Chapter 4, which represents the external structure of a fire-resistance steel door. In this Thesis, no connectors will be modelled so the mechanical resistance of the structure will be provided by the external structure. As it was explained before, this implies a low buckling load and a low critical temperature due to the small thickness of the plates that conform the door and the lack of middle connections between the two frontal plates.
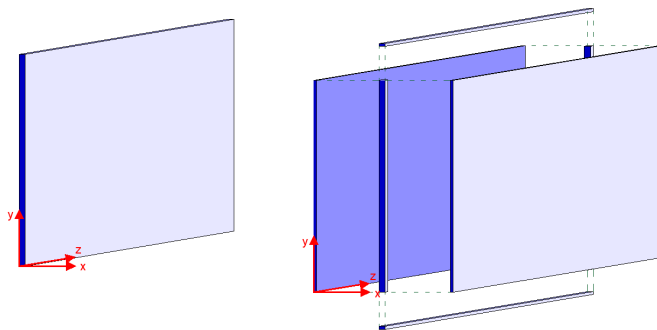


**Figure 5.1** Left: 3D of the Door model. Rigth: 3D of the components of the Door model.

In both models plasticity will be implemented and all the material properties will be time dependent, affecting to the Young modulus, the yield limit and the coefficient of thermal expansion. However, due to the small load at which the instability starts this time dependency would not affect to the system.
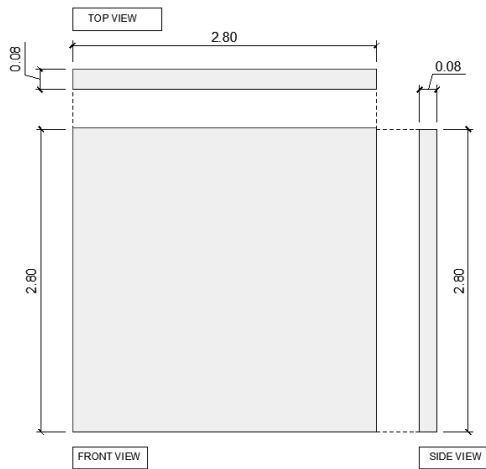
**Figure 5.2** Geometric characteristics of the Door model used in Chapter 4, all the measures are in meters. Thickness of the plates equal to 1 mm.

Two cases will be studied with different boundary conditions. First, a brief description of the door functionality will be given. It is a sliding door with rails, located at top and bottom, in only one of the sides. When the door is closed one of the sides is in direct contact with the side frame and the rest of the door is in contact with the walls. When the door is open it rolls through the rails sliding behind a wall, that is located really close to one of the front door plates but without touching it. So, the first case will consider a steel door simply supported at top and bottom due to the action of the rials. The second case will assume that the door is close and the sides are restricted by the frame and the walls, so it would be simply supported at top and bottom and restrained on the sides.

Lastly, a simplify model with connectors would be modelled in order to compare the results obtained on the other two models. However, this model would be really simple and no further investigation would be developed being one of the reasons the fact that there is not a Thermal model of this components. The purpose of this model is to observed the increase on the stiffness of the door when the two front plates are connected along its surface.

### 5.1.1   Material properties

The properties of the material used were explained before in Chapter 2, Section 2.4. All the properties would be time-dependent and the plasticity curve followed will be perfectly plastic, as it was explained before.
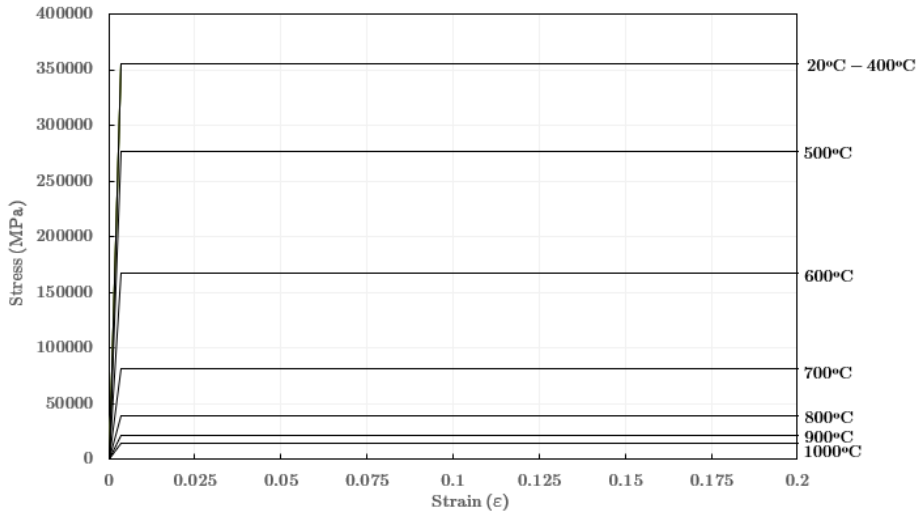


**Figure 5.3** Stress-strain curve degradation due to temperature increase, according to Eurocode-3 [9].

Regarding the Young modulus degradation it would be used the Kristian Dahl Hertz curve related to the 0.2% stress degradation, explained in the course *11023 Structural Fire Safety Design* at DTU, Technical University of Denmark. This curve is similar to the degradation curve shown in Eurocode-3, [9], but this one follows a smoother path.
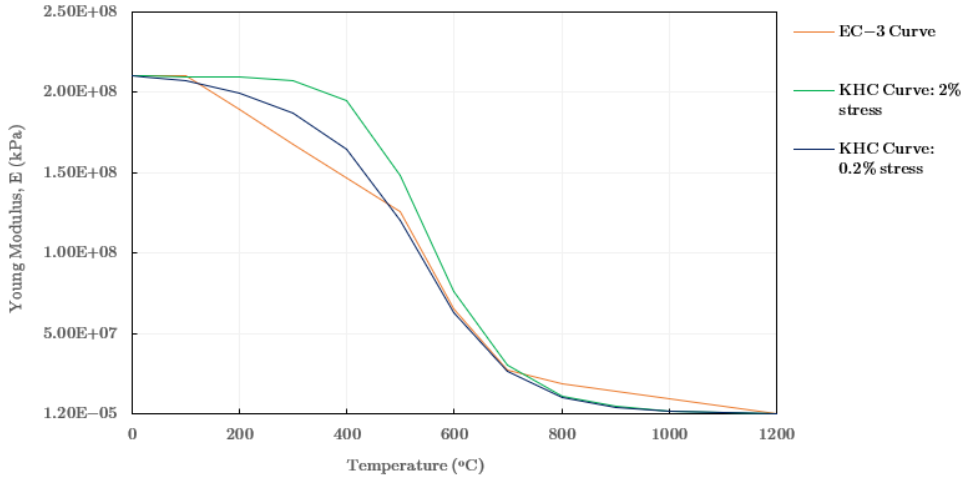
**Figure 5.4** Young modulus degradation due to fire exposure of the material.

The Poisson's ratio will remain the same for all temperatures, 0.3, and the coefficient of thermal expansion will follow the temperature variation given by Eurcode-3, [9].
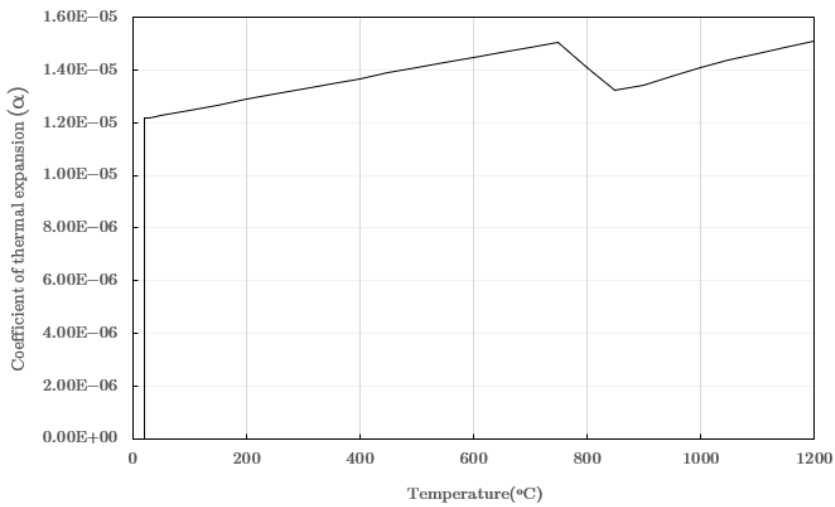


**Figure 5.5** Coefficient of thermal expansion of carbon steel as a function of temperature

## 5.2 Analysis

The analysis of the final model can be divided in two cases, as it was explained before. In the first one the top and bottom of one of the front plates will be simply supported, as a representation of the open door supported by the rails, and the second model will be simply supported at top and bottom of one of the plates and restricted on the sides, to represent the effect of the side walls when the door is close.

Two types of analysis could be performed, a coupled analysis or a statically incremental analysis using as an input the temperature distribution obtained with the processing of a thermal model. In this case this model was ran by Ainara Sofía Franco Vergara in her Thesis, *Numerical model of the thermal behaviour of steel doors in fire.* In Chapter 4 it was compared both type of analysis and it was conclude that they are analogue and it was equivalent to use the coupled analysis or the statically incremental analysis with the thermal analysis results. For this reason, it was decided to use the second option and the statically incremental analysis was used with the thermal model results.
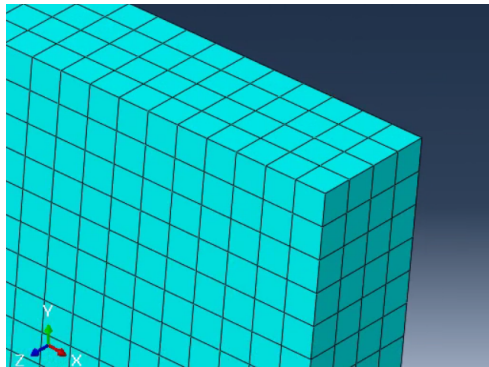


**Figure 5.6** Detail of the mesh in the cross section of the door.

The temperature distributions used have been extracted from five points of the Thermal model. Two of them are located one in the expose surface and one in the unexposed. The other three are based in the cross section. For this reason the mesh has to be thin enough to provide two points in the cross section. For this reason, in both cases the mesh is compose by quad elements of 0.02 meters length. The whole door has the same mesh even though it could be a wider mesh in the front panel and a thinner mesh on the sides. The main reason is that square elements provides better

solution than rectangular elements in FEM modelling. The mesh will have 140x140 elements on the front panels and 4x140 on the sides. The type of element used is the same as in Chapter 4, conventional shell element with full integration, S4.

The temperature distributions used are shown in Figure 5.7 for the exposed side, Figure 5.8 for the unexposed side and Figure 5.9 for the cross-section points.
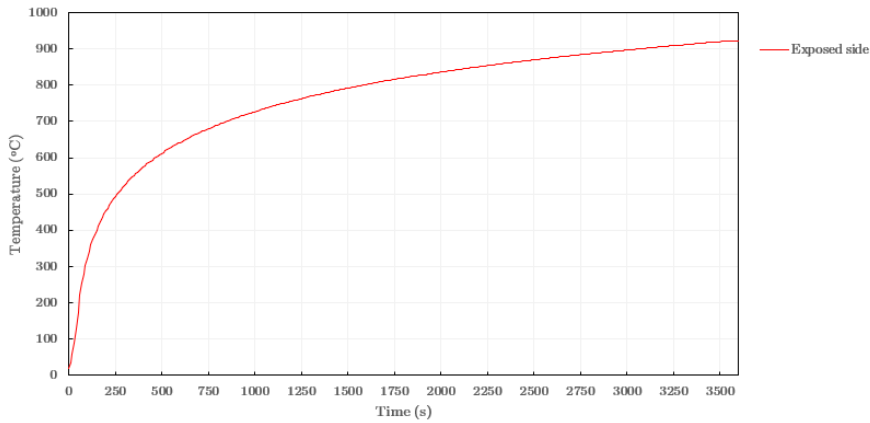


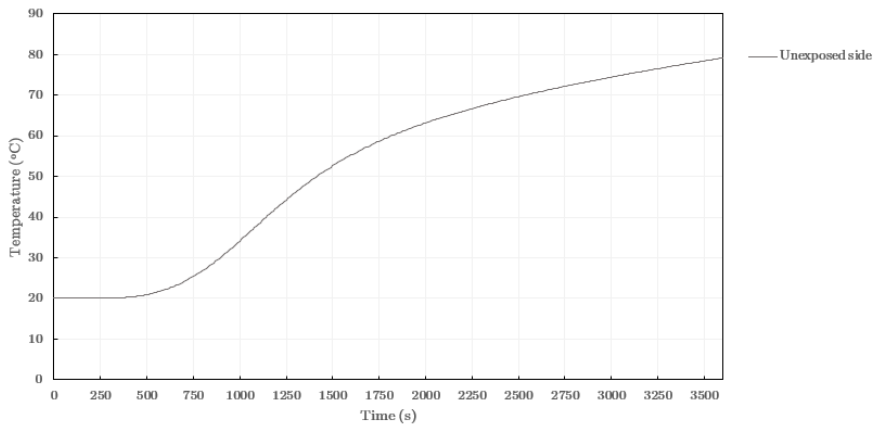**Figure 5.7** Exposed side temperature distribution obtained from the Thermal Model.



**Figure 5.8** Unexposed side temperature distribution obtained from the Thermal Model.
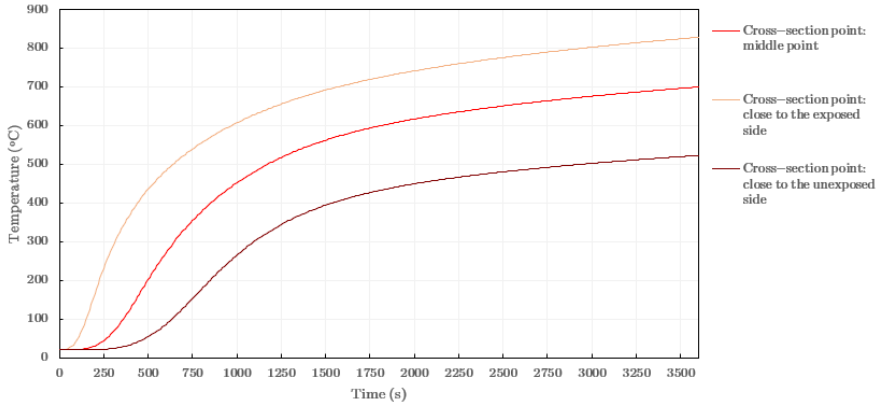
**Figure 5.9** Cross-section side temperature distribution obtained from the Thermal Model.

Regarding the initial imperfection, there are several ways of introducing it. One of them is to add an imperfection factor to the first eigenmode, then the imperfection will followed a sinus shape and will have the same shape as the first eigenmode. The maximum imperfection will be located in the middle of the loaded frontal plate.
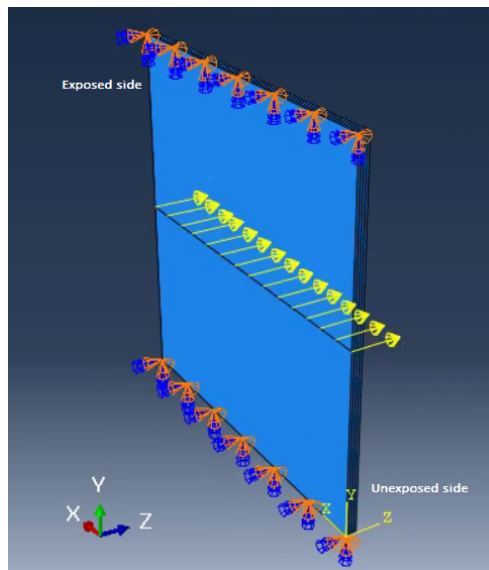


**Figure 5.10** Initial load method to introduce the initial imperfection in the model.

However, this way is really optimal for simpler structures like a beam or a single

plate but for this case some irregularities appear when this method was used. For this reason the imperfection was introduced by applying in a preliminary step a small distributed load along the middle of the loaded frontal plate, Figure 5.10.

This load has to be small enough to produce a small initial imperfection of the model. The imperfection value and the initial load applied was calibrated in order to obtain the best results. The maximum initial deflection is located in the middle of the plate and it has a value of 0.1 mm, which is equivalent to 10% of the thickness of the plates.

## 5.3   Model 1: Simply supported at top and bottom

This first final model has the same geometrical properties and boundary conditions of Model 4, from Chapter 4. The door will be simply supported at top and bottom in only one of the frontal plates, this restrictions will simulate the effect of the rails of the door.
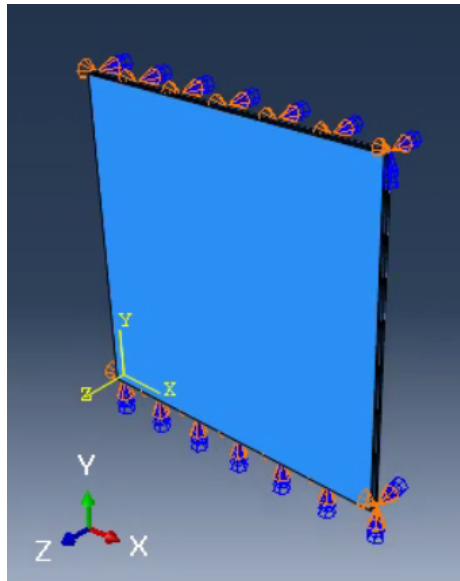


**Figure 5.11** Boundary conditions of the first final model analysed.

Two different analysis will be performed, one Eigenvalue analysis to find the critical temperature at which the system buckles and a statically incremental analysis to study the post-buckling behavior.

### 5.3.1  Eigenvalue analysis

The Eigenvalue analysis was ran for the model explained before. In this analysis the first three buckling modes were calculated obtaining the critical temperature at which the system starts buckling and the mode shapes.
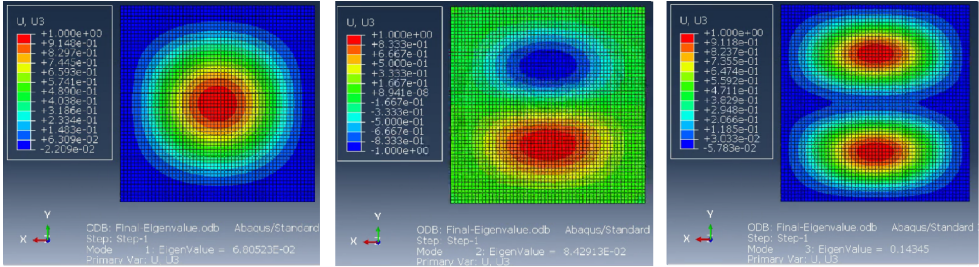


**Figure 5.12** Eigenmodes of the loaded frontal plate, frontal view.

In Figure 5.12 and 5.13 the first three mode shapes are shown. The only plate that will buckle is the one that have the boundary conditions and the temperature field acting. So, the rest of the structure does not buckle.
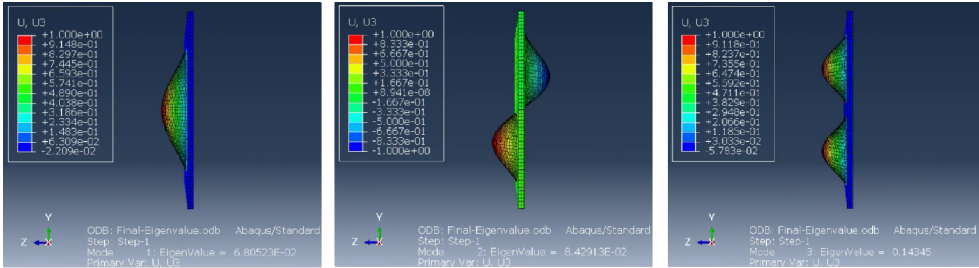


**Figure 5.13** Eigenmodes of the loaded frontal plate, side view.

In Table 5.1 the critical temperature obtained is displayed. As it can be observed, the buckling temperature is the same as in Model 4 in Chapter 4. The buckling temperature is so low because the two frontal plates are not connected so they do not behave as a whole. However, the sides provide stiffness to the system and connect the external sides of the two main plates. For this reason, the critical temperature is higher than in Model 1 in Chapter 4, where a single steel plate was analysed.

| Abaqus results | Eigenvalue 1 | Eigenvalue 2 | Eigenvalue 3 | |
|:---:|:---:|:---:|:---:|:---:|
| $\Delta T_{cr}$ | 0.068 | 0.084 | 0.143 | ºC |
| $T_F$ | 20.068 | 20.084 | 20.143 | ºC |

**Table 5.1** Eigenvalue analysis results: critical temperature of the first three eigenmodes.

### 5.3.2 Post-buckling

The post-buckling analysis is going to be performed using the statically incremental analysis. In this analysis, the temperature data of the different nodes extracted from the thermal model [5] are going to be used. First, the initial imperfection is add to the system by using a small distributed load in the middle of the frontal plate, as it was explained before. This initial deformation can be observed in Figure 5.14, it has the same shape as the first eigenmode and the maximum displacement it is located in the middle with a value of 0.15 mm.
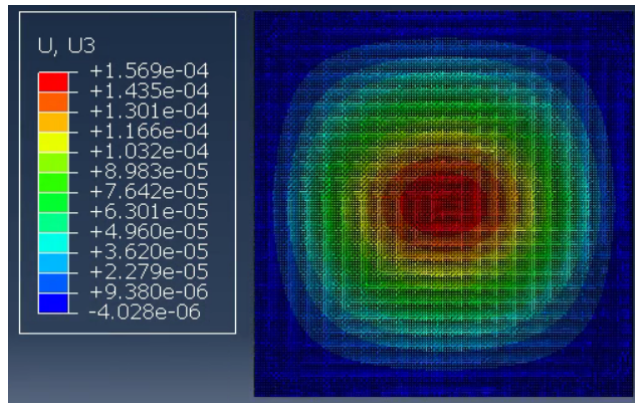


**Figure 5.14** Initial imperfection on the frontal steel door, exposed side.

Then, the analysis is ran. In Figure 5.15 it can be seen the deformation process followed on the exposed side while in Figure 5.16 it can be seen the unexposed side.

At first the deformation on the exposed side follows the first eigenvalue mode shape, but when the critical buckling temperature is surpassed the behaviour changes. This change is related with how the thermal load acts. Because, the stresses produce by the thermal load moves with the displacement of the plate while a mechanical distributed load would remain vertical. Also the influence of the boundary conditions and the rigidity of the sides plates influence this behavior.
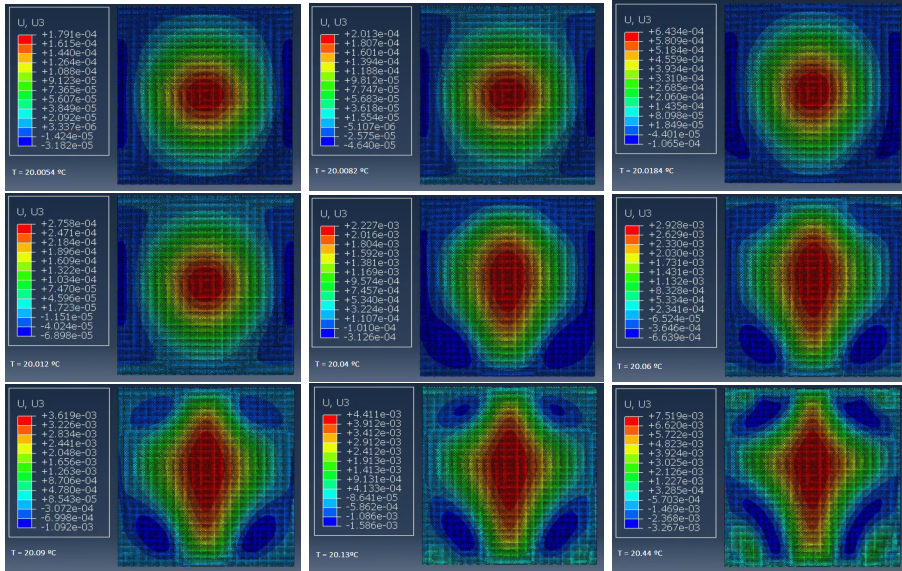
**Figure 5.15** Deformation process of the exposed side during the statically incremental analysis. The temperatures goes from 20ºC till 20.4ºC.

In the unexposed side the deformation starts later because according to the fire curve introduce into the unexposed side, it takes more time to be heated. However, due to the small buckling temperature the unexposed side does not experience more than 20ºC during this analysis before it aborts. So, the deformation observed is effect of the sides deformation due to the action of the exposed side increase on temperature.
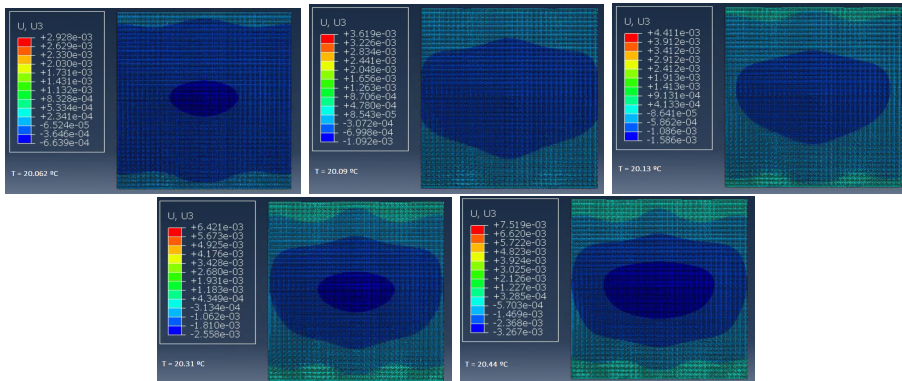


**Figure 5.16** Deformation process of the unexposed side during the statically incremental analysis. The temperatures goes from 20.06ºC till 20.4ºC.

In Figure 5.17 the deformation of the door observed from the side is shown, the scale has been augmented x25. The maximum deformation is located in the middle of the plate with a value of 0.751 centimeters.
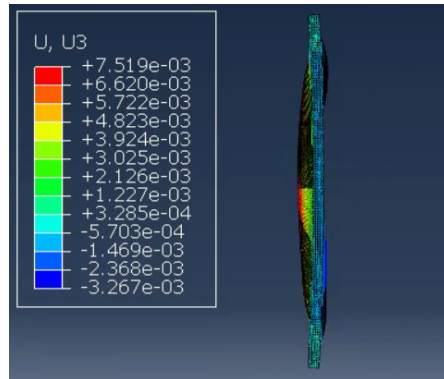


**Figure 5.17** Out of plane deformation of the door at 20.44ºC. Scale augmented x25.

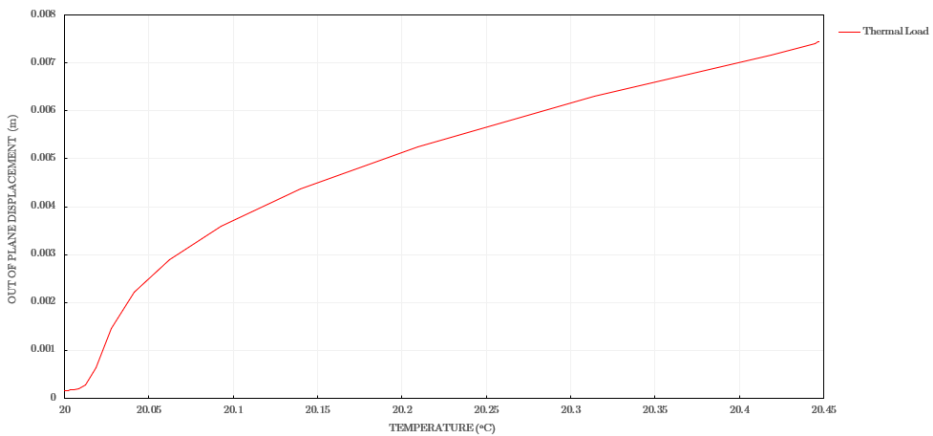In Figure 5.18 the temperature-displacement curve has been plotted for the middle point of the exposed plate.



**Figure 5.18** Temperature-displacement curve of the exposed side.

## 5.4 Model 2: Simply supported at top and bottom and restrained on the sides

This model have the same geometric properties than the previous one but the boundary conditions are different. First of all, in order to understand the decisions made regarding the support conditions of the door it is necessary to have in mind Section 2.2, where it was briefly explained the mechanism of the sliding steel door.



**Figure 5.19** Industrial sliding fire resistance steel door. Picture extracted from Samson doors official website [6]

In Figure 5.19 a industrial steel door is shown, it can be seen that the right side of the door fits in the frame when its close. But, the left side would not be in contact with the frame along all its surface. However, the left side edge and the top border of the panel would be in contact with the frame and the wall behind the door, when its close, and this would restrict its horizontal movement. The boundary conditions are shown in Figure 5.21 and in Figure 5.20 a sketch of the door configuration is shown to fully understand the boundary conditions decision.
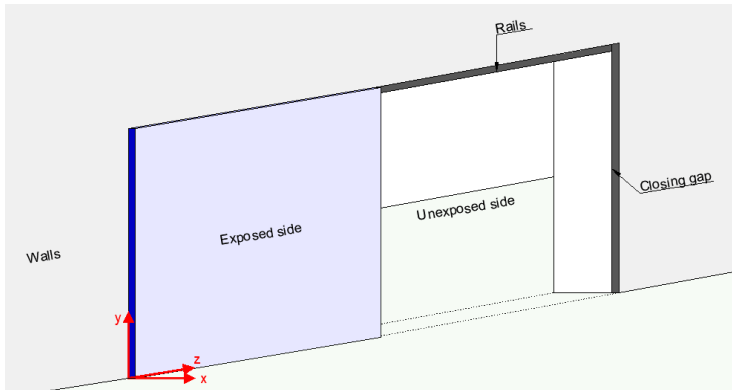
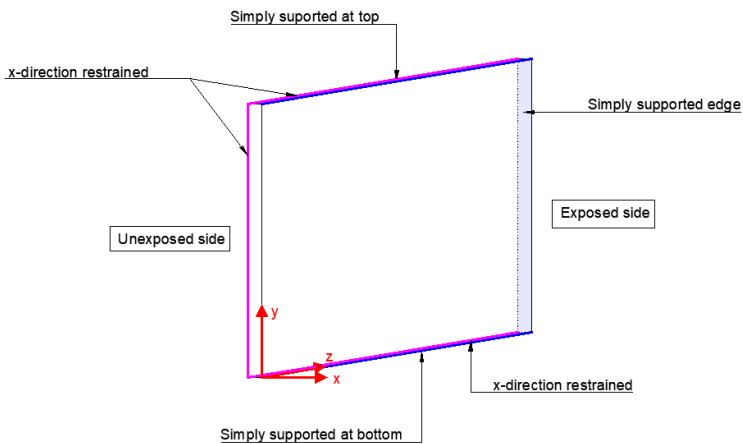**Figure 5.20** Sketch of the door configuration, based in Figure 5.19.



**Figure 5.21** Boundary condition of the door model.

## 5.4.1 Eigenvalue analysis

The Eigenvalue analysis is performed and the first three eigenmodes are shown in Figure 5.22 and 5.23. The shape of the first two eigenmodes is the same as in the previous case. However, the third mode shape is different due to the influence of the restrained side at the right of the plate. The critical temperature is registered in Table 5.2 and its values are slightly lower than in the previous case.
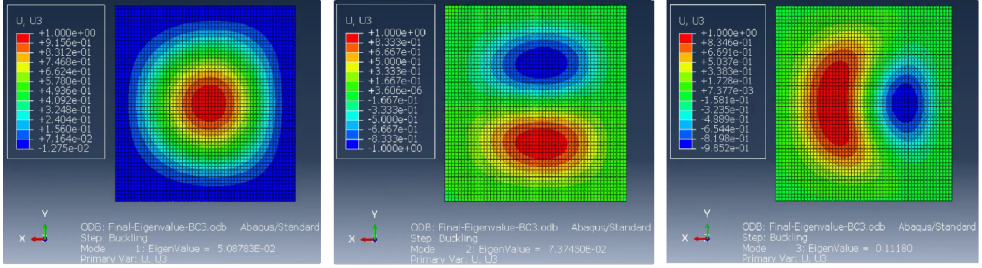
**Figure 5.22** Eigenmodes of the loaded frontal plate, frontal view.
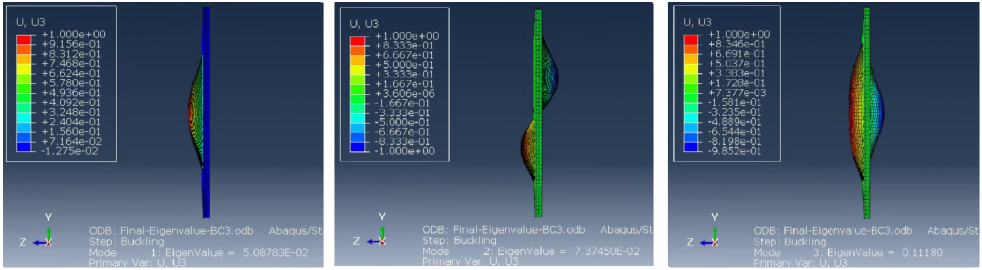


**Figure 5.23** Eigenmodes of the loaded frontal plate, side view.

| Abaqus results | Eigenvalue 1 | Eigenvalue 2 | Eigenvalue 3 | |
|:---:|:---:|:---:|:---:|:---|
| $\Delta T_{cr}$ | 0.050 | 0.073 | 0.111 | ºC |
| $T_F$ | 20.050 | 20.073 | 20.111 | ºC |

**Table 5.2** Eigenvalue analysis results: critical temperature of the first three eigenmodes.

## 5.4.2  Post-buckling

Now, the post-buckling behaviour is studied. The initial imperfection is introduced as it was explained before, adding a small distributed load along the middle of the loaded plate. In figure 5.24 is shown the initial deformation and the maximum value is located in the center of the plate, being equal to 0.15 mm.
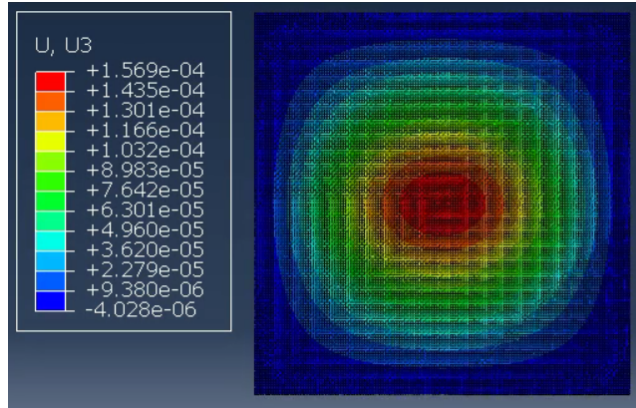
**Figure 5.24** Initial imperfection of the frontal steel door, exposed side.

Then the analysis was ran and the deformation process from 20ºC till 20.89ºC is registered in Figure 5.25. It can be observed that the initial deformation is equal to the one obtained for the first Eigenvalue, but as the temperature increase and surpasses the buckling temperature this shape changes. The deformation grows towards the restricted edges, simply supported, because the thermal expansion is not allowed there thus the stresses are bigger.
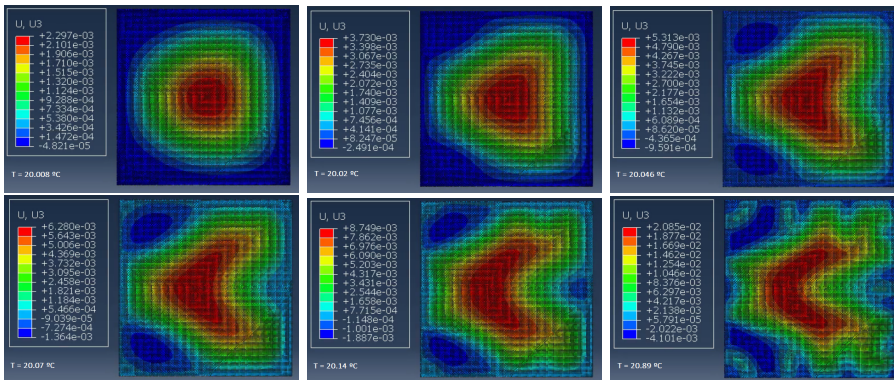


**Figure 5.25** Deformation process of the exposed side during the statically incremental analysis. The temperatures goes from 20ºC till 20.89ºC.

In Figure 5.26 the side view of the door deformation is shown at 20.89ºC, with a augmented scale of x10. The maximum deformation registered is located at left side of the door with a maximum deformation of 2.08 centimeters.
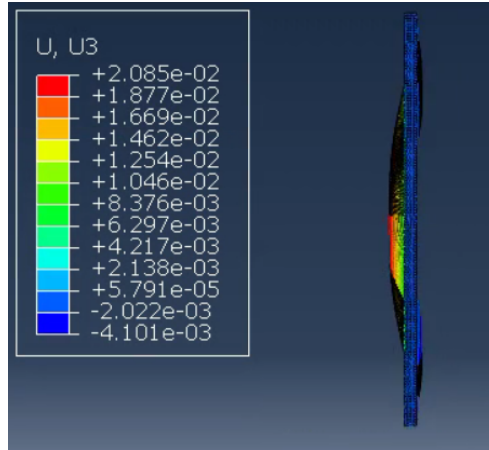
**Figure 5.26** Out of plane deformation of the door at 20.89ºC. Scale augmented x10.

Then the temperature-displacement curve is plotted in Figure 5.27. At first sight, this graph look different than the previous model, but if the initial part of the curve is expanded it can be seen that that is not accurate. The start of the curve is not vertical it has a small slope but it is so small that in the global graph it cannot be noticed. This could be because of the different boundary conditions between the previous model and this model.
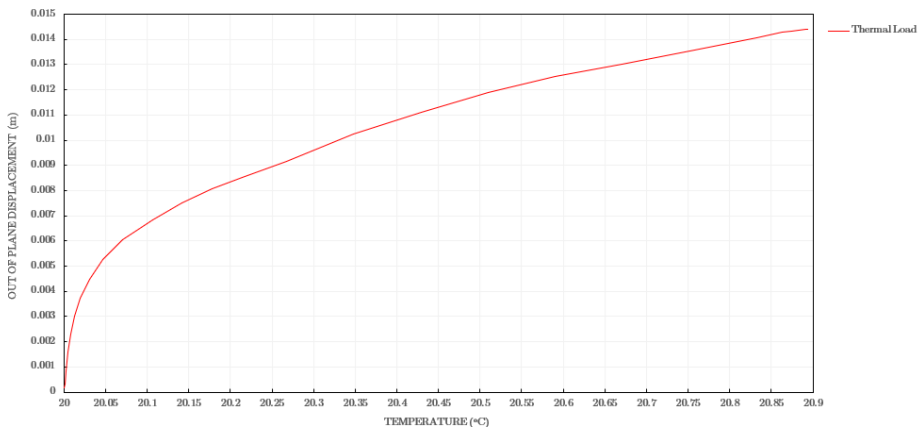


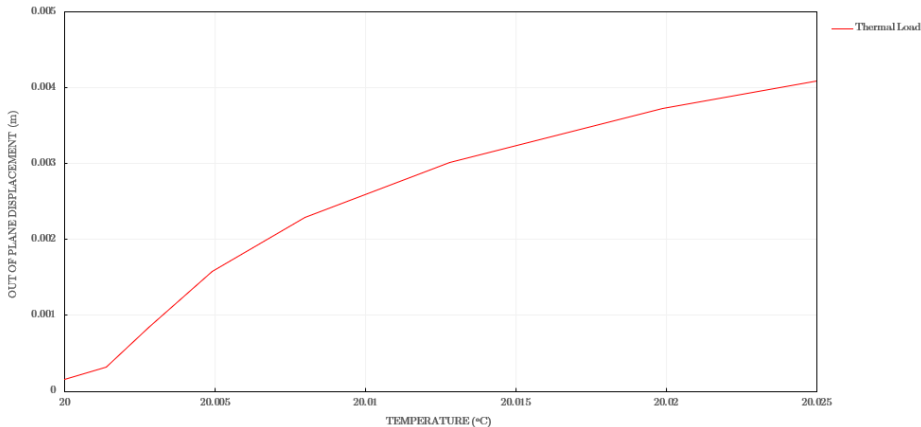**Figure 5.27** Temperature-displacement curve of the exposed side.

**Figure 5.28** Expanded temperature-displacement curve of the exposed side.

## 5.5   Model with connectors between plates

As an extra of this chapter it would be developed a model with intermediate connectors between the two frontal plates. The objective of this section is to shown how connecting the two frontal plates provides a higher structural resistance for fire situations.

For this task the geometrical properties, boundary conditions and load state of the first model analysed on this Chapter are going to be used. Then, connectors along the surface of the frontal plate are going to be add to the model. The aim of the model is to show the increase in resistance as the two plates are more connected, not to show a real model of a door. In reality, a door design cannot have a lot of connectors because they are a thermal bridge between the exposed side and the unexposed side and this can be counterproductive for the door's resistance. So, in reality the disposition of the connectors is a real problem and a balance has to be reached between the increase of mechanical resistance and the influence of thermal bridges in the model.

Only an eigenvalue analysis would be developed for this study, the post-buckling behaviour is not going to be studied. The connectors would be place every 0.2 meters, so the total number used is 169. First a non rigid type of connectors would be used, a link connector which only merge the movement of the master surface to the slave surface. The second type of connectors used would be weld connection, which

approaches more to the real type of connections used in this type of structures. Besides connecting the movement of the two surface it also gives rigidity to the structure. To know more about the connectors used, in Chapter 3, Section 3.3 its characteristics are explained.
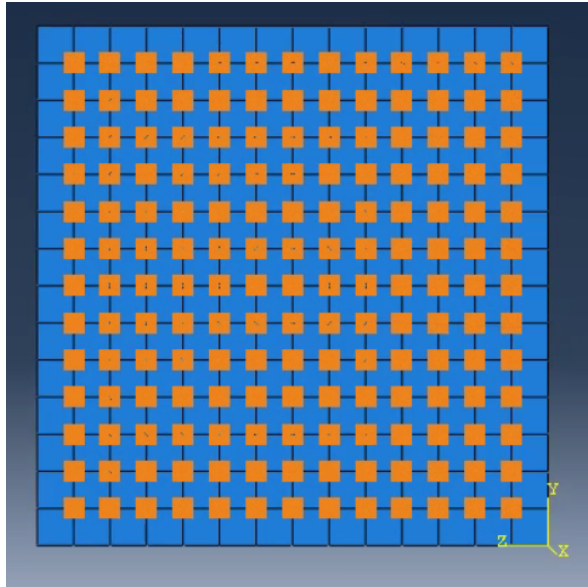


**Figure 5.29** Connectors disposition in the frontal plate.

In Figure 5.30 the first three buckling mode shapes and the critical buckling temperatures are shown. As it can be seen the critical temperature value has been increased from 20.068ºC to 20.14ºC. This increase it is not really big, but one of the reason could be that the connectors only connect movement and does not provide rigidity to the system.
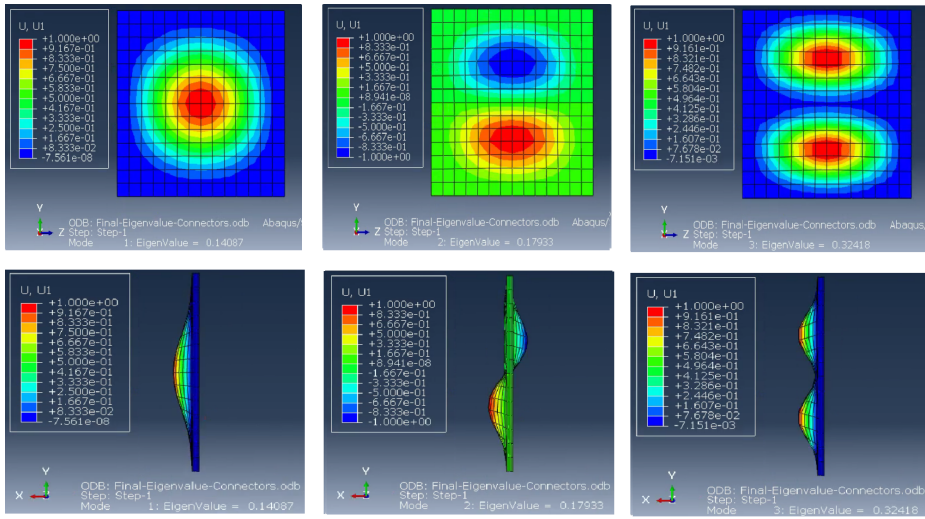
**Figure 5.30** Eigenvalue analysis results for the model with link connectors.

Then, weld connections were used in the model. This type provide rigidity and connects all the degrees of freedom between the master surface and the slave surface. The results are shown in Figure 5.31 where it can be seen the increase in temperature for the first eigenmode from 20.068ºC till 58ºC.
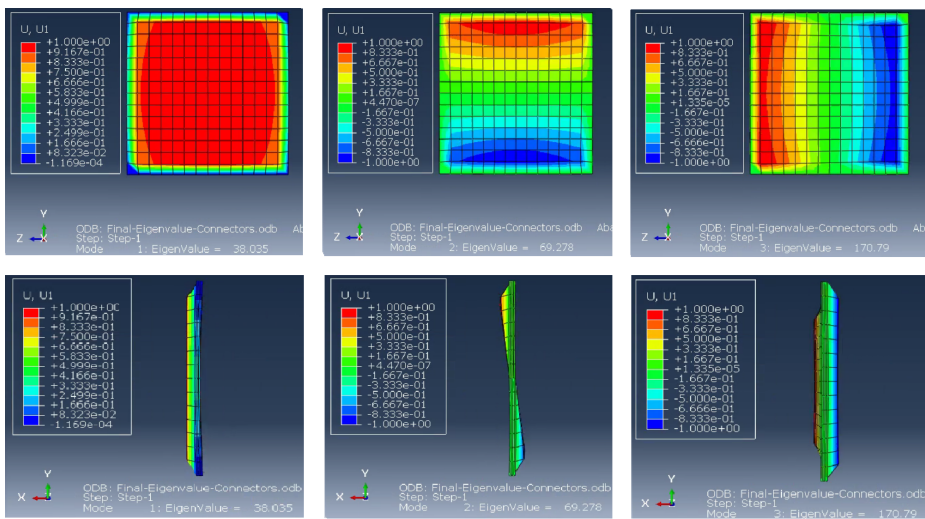


**Figure 5.31** Eigenvalue analysis results for the model with weld connectors.

As it can be seen connecting the two main plates between them provides extra rigidity to the system. However, it is important to choose well how many connectors and were to locate them in order to provide the maximum rigidity and not add too much thermal bridges. Another possibility instead of connectors could be to use inside stiffeners, they would provide more resistance and for a door of this dimensions they could be a better solution. However, the mode shape of the buckling modes can change depending were they are located.

5

CHAPTER 6

# Conclusion

This Thesis was written to develop a mechanical model that represents the behaviour of a wide sliding fire-resistance steel door. As it is established in *Fire Test Procedures Code (FTP code) of the International Maritime Organization (IMO)*[1], when a fire door is larger than those which can be accommodated in the standard specimen size (2.4x2.5 m) two alternatives can be followed to approve the door, accommodate it into a larger test furnace or use the procedure established in the code for evaluation of the fire performance.

Accommodating the door into a larger furnace can be a challenging and expensive task, for this reason applying the method established can be a good alternative for the industry. The methodology used to extrapolate the fire test results include three steps:

- Perform a standard fire test to a specimen to obtain reference temperature and structural displacement. This specimen could be a door already certified which has an identical design to the door that wants to be a study or a specially-built specimen where FEM modelling is performed to extrapolate the results from the tested door to the bigger size door.

- Perform a FEM analysis of the door to calibrate the thermal and mechanical boundary conditions.

- Perform a FEM analysis of the door using the model calibrated assuming the differences in geometry and dimensions between the real door and the specimen door does nos significantly influence the results.

As a summary, performing a FEM analysis that represents the real behaviour of the steel door can be useful for the industry, for this reason, the objective of this thesis was to develop a FEM model that approaches to a big dimension door model. However, no analytical data was available, and the ideal situation would be to have a real

door design to develop a FEM model that can be compared with the fire-test results of an equivalent door.

So, this Thesis have its limitations and, after all the modelling process followed several conclusions were made regarding the door model and the behaviour observed.

First of all, the external structure of the steel door by itself does not provide a lot of mechanical resistance against buckling. When the frontal plates are not connected the buckling load approaches more to the buckling load of single steel plate than the whole door acting as a set. For this reason, it is important to have connectors or stiffeners that connect the two frontal plates that conform the door to provide enough stiffness to the model.

A proper definition of the boundary conditions is fundamental to analyse the behaviour of the door and approach it to its real performance.

For this type of steel doors, the common failure mechanism is buckling so the calculus and analysis should be focus on this topic. Especially when the width and the height of the door are bigger than a pedestrian door because as the slenderness augment the buckling load gets lower.

After testing different analysis, it was found that the Riks analysis in Abaqus is the best one to analysed the post-buckling behaviour of structures. However, this analysis has its limitations when a temperature field that follows the standard fire curve wants to be introduced in the model. Because this analysis only processes linear temperature fields.

Regarding the merge of the thermal model and the mechanical model, it was found that running a one way coupled analysis in Abaqus provides as good results as the models merged. So, this could be useful because instead of running two analysis only one can be processed. This can save a lot of work because the meshing compatibilities problems can be avoided by running a single model.

## 6.1   Further work

In this Thesis, several studies of the material behaviour under fire were performed and several models were developed to ensure the validation of the final model. The objective was to understand the behaviour, validate the model and developed a simple final model of the steel door. For this reason, there is a lot of improvements that can be made to expand the investigation in a way that approaches it to a more realistic model.

First of all, only the external steel structure was modelled so one of the improvements could be to add the frame, the sliding mechanism and the walls that surround the door. It is also possible to model the mineral wool that goes inside the door, but this would not provide a lot of improvement because it does not add stiffness to the system. However, the internal stiffeners could be added. It could also be possible to model the door with the stiffeners and developed a model that runs a coupled model, on this way it would not be necessary to run first a thermal analysis and then add the results to the mechanical model. A single analysis could be made instead of two, as it was shown in one of the chapters of this thesis.

Another interesting study that can be developed is how the stiffness of the weld joints that merge the steel structure of the door could be affected by the heat increase and how it would affect to the global behaviour of the door.

Also, a study of the influence of the stiffeners on the door deformation could be an interesting aspect to develop. Because adding stiffeners will add stiffness and resistance to the system due to the connection between the front plates. However, this connection transmits the heat from one plate to the other faster than the insulation. This is a real problem and the equilibrium between the stiffness increment and the heat transfer is the key to a good fire-resistance design of the door.

Lastly, if some experimental data of an equivalent door can be obtained the FEM model could be compared to it and made the proper modification to approach it to a more realistic model.

# Plastic analysis

## A.1    Introduction

In this section, it is going to be modelled in ABAQUS a steel beam with specific boundary conditions and load distribution. The objective is to perform a statically incremental analysis to study the behaviour of the beam. This results will be compared with the analytical solution of the problem to calibrate and validate the model. First, only the elastic properties of the material will be included and afterwards, in the second analysis, the plastic properties will be added.

It will be analysed a double clamped steel beam which has a punctual load acting close to the support A.
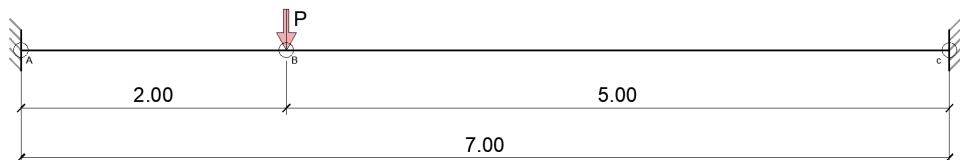


**Figure A.1** Case analysed: Double clamped beam with a punctual load.

The material used is structural steel S355 and the cross-section is rectangular, with a total eight of 50 cm and a width of 30 cm.

## A.2    Analytical solution

It is going to be carried an elastic and plastic analysis. The objective is to find the load at which the plastic hinges start developing and the final load where the system collapse. Due to its characteristics, boundary conditions, the beam will develop three

plastic hinges before failure, due to its grade of hyperstaticity, grade 3.

The moment diagram obtained from the elastic analysis is shown in the Figure A.2, where the maximum moment takes place at support A.
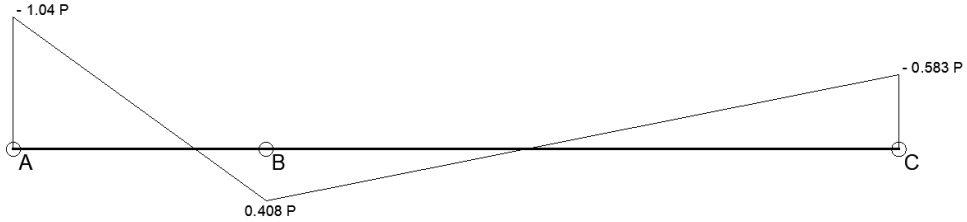


**Figure A.2** Moment distribution.

The maximum elastic moment that the beam can support before failure ($M_{el}$) is calculated, as well as the maximum plastic moment the system can take ($M_{pl}$).

$$W_{el} = \frac{I}{z} = 0.0125m^3 \tag{A.1}$$

$$M_{el} = W_{el}f_{yd} = 4437.5kNm \tag{A.2}$$

The plastic moment can be obtained stating that it will take place when the section reaches its yielding limit ($f_{yd}$), which for steel S355 is 355 MPa.

$$W_{pl} = A_{traction}z + A_{compression}\mathring{u}z = 0.01875m^3 \tag{A.3}$$

$$M_{pl} = W_{pl}f_{yd} = 6638.5kNm \tag{A.4}$$

The ultimate plastic moment has a greater value than the elastic one due to the plastic reserve of the beam. When the beam reaches its yielding point in the elastic analysis the ultimate bending load is reached, however in plastic analysis the load can still be increased.

In the plastic analysis, the first plastic hinge appears when a section of the beam starts yielding, after that the load still increases until another section of the element yields, and another hinge appears. The last plastic hinge can be found following the same procedure, increasing the load until a third section of the beam starts yielding. In the plastic hinge theory it is assumed that when the section yields it yields

completely, but in reality, is a step by step process where the yielding value is first reached by the external fibres and then it arrives at deeper layers of the cross-section.

The first plastic hinge will appear where the moment is greater which is in point A. Then, when the plastic moment is reached the load will be re-distributed and the boundary conditions will change. Due to this fact, the new moment diagram can be calculated as in elastic analysis having into account the new conditions.
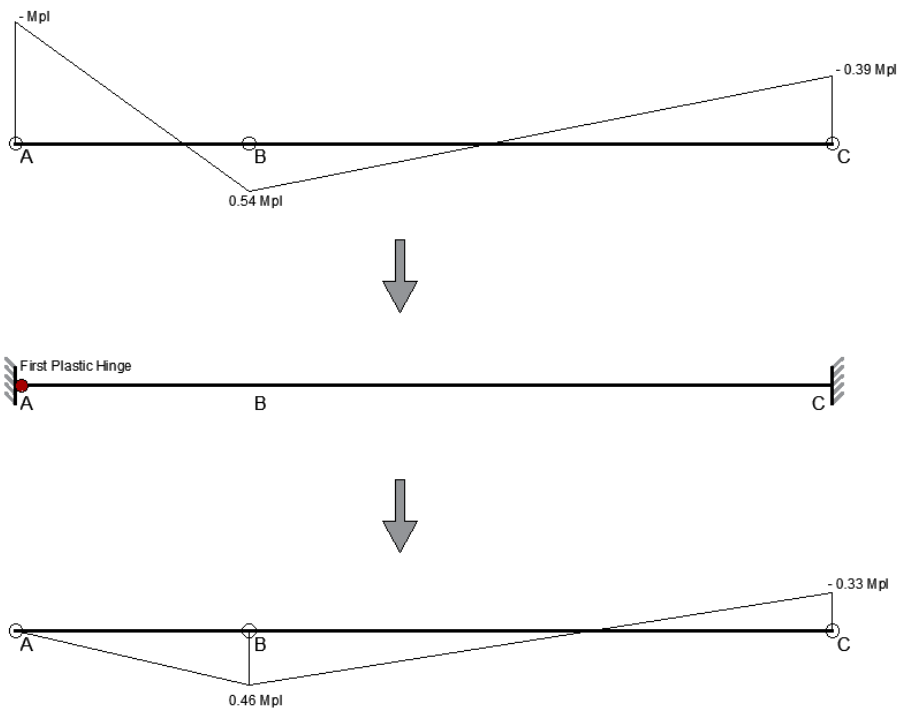


**Figure A.3** From top to bottom: Moment diagram, appearance of the first Plastic Hinge and load redistribution after the hinge appearance.
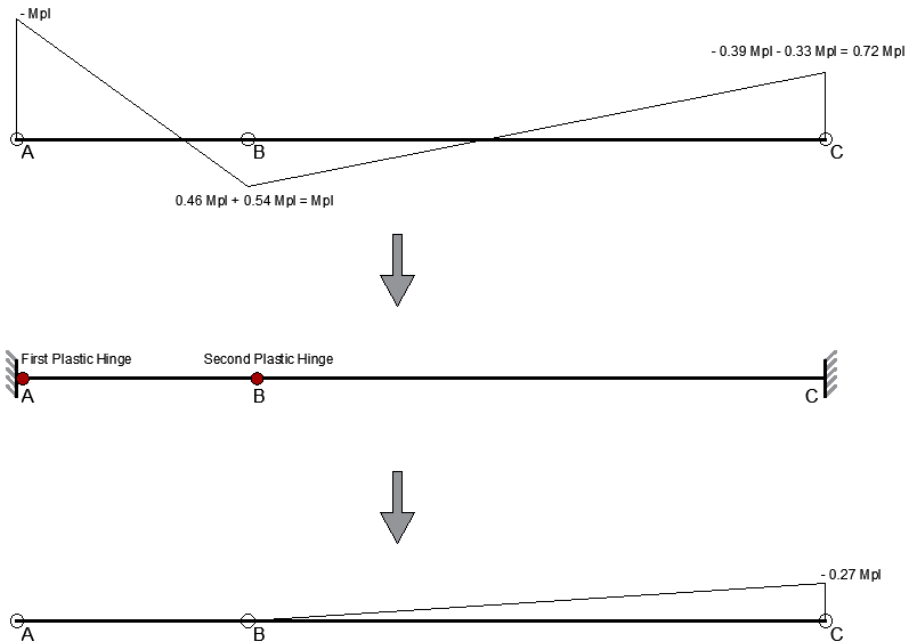
**Figure A.4** From top to bottom: Moment diagram when two points of the beam yield (two plastic hinges), appearance of the second Plastic Hinge and load redistribution after the hinge appearance.
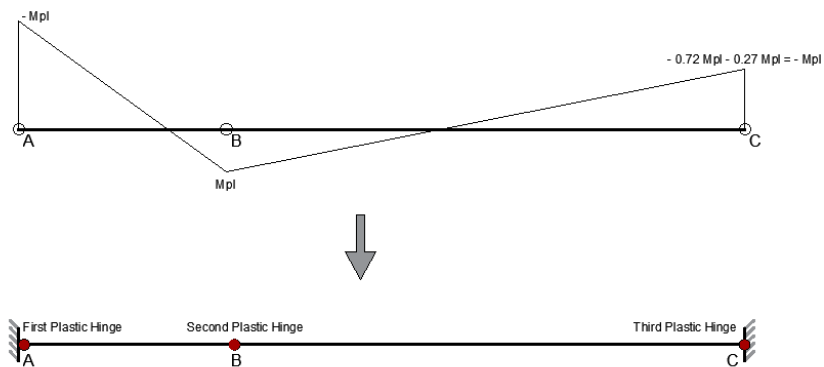


**Figure A.5** From top to bottom: Moment diagram when three points of the beam yield (three plastic hinges) and appearance of the third Plastic Hinge.

When the three plastic hinges appear, the system will collapse. The loads and the vertical displacement obtained for each one of the plastic hinges are showed in Table A.1.

| Plastic hinge | Load condition (kN) | Vertical displacement (m) |
|:---:|:---:|:---:|
| 1 | 6523 | 0.011 |
| 2 | 8977 | 0.022 |
| 3 | 9324 | 0.044 |

**Table A.1** Load condition at which the Plastic hinges appear and their corresponding vertical displacement.

The analytical values for the length of the three plastic hinges have been calculated in Equation A.5, A.6 and A.7. The first one has a length of 0.33 meters, the second one 1.1 meters and the third one 0.83 meters.

$$L_1 = \frac{2}{2}\left(1 - \frac{M_e l}{M_{pl}}\right) = 0.33m \tag{A.5}$$

$$L_3 = \frac{5}{2}\left(1 - \frac{M_e l}{M_{pl}}\right) = 0.83m \tag{A.6}$$

$$L_2 = L_1 + L_3 = 1.1m \tag{A.7}$$

## A.3   Abaqus modelling

The material characteristics are defined at the beginning of the model. For this case, it was characterized by the Young Modulus and Poisson's ratio (Elastic properties) and the stress-strain curve of the material (Plastic properties). In this Exercise, no hardening was considered for the stress-strain curve so the material behaviour can be considered as perfectly plastic. Their value can be observed in Figure A.6.
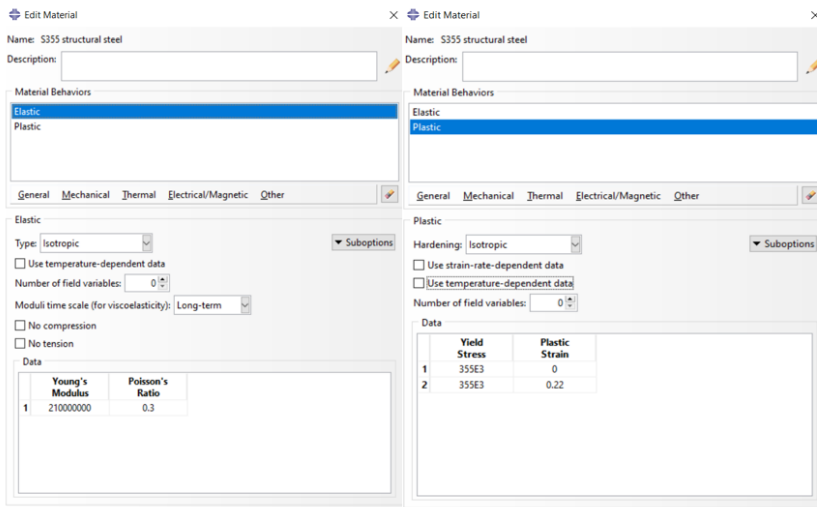
**Figure A.6** Material editing tab in Abaqus.

The type of element used for meshing the beam is B22, which is a 3-node quadratic element. This element has more computation weight than other elements, but for this case, it gives more accurate results. This element is also known as Timoshenko beams and it is suitable for modelling slender and non-slender beams. The cross-sections of these elements behave in the same manner as the cross-sections of the thick shell elements.
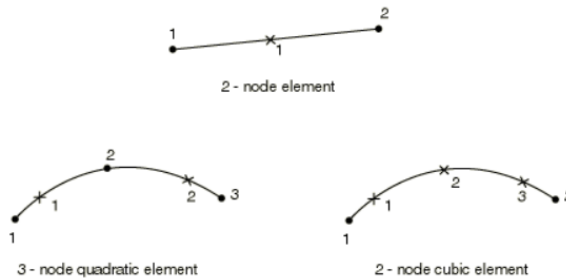


**Figure A.7** Type of beam elements in Abaqus.

Then the load is applied to the beam step by step until collapsed occurs. The deformation, stresses and strains are recorded for each time step, allowing to develop the load-deformation curve for the element. This curve is compared with the one obtained with the analytical analysis, checking if the plastic hinges develop at the same loading.

The main difference between the analytical procedure and Abaqus, for the plastic analysis, is that the hinge-theory is considered in the hand-calculations. This means that, when the yielding occurs, the plastic hinge will be located in one unique point instead of having a length, as it happens in Abaqus.

It is also important to consider that Abaqus accuracy is also affected by the number of integration points of the section that are considered in the analysis. The integration points are the locations of the section where the stresses are calculated, if the number of points is insufficient or excessive, the yielding stress results would not be correct.
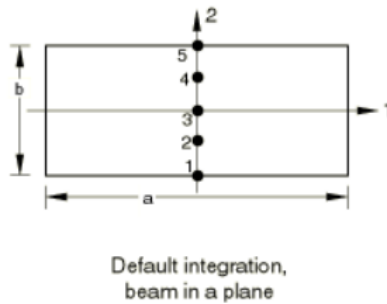


Default integration,
beam in a plane

**Figure A.8** Default integration points in Abaqus, Simpson points.

The default number of integration points are five and, after the analysis, it was proven as an insufficient number because the analytical solution results were far from the values obtained.

The way of changing the integration points in the program is editing the keyword, where you can get access clicking with the right button of your mouse in the Model tab and selecting Edit Keywords.

In the keywords tab, the number of integration points has to be added in the third line under *Beam Section, material="S355 structural steel". To gather the results of the

Mises stresses, it has to be written under *Output, history, variable=PRESELECT the following lines: *EL PRINT, the number of integration points, MISES.



```
*Part, name=Part
*Element, type=B22
** Section: Section  Profile: Section
*Beam Section, elset=_PickedSet2, material="S355 structural steel", temperature=GRADIENTS
0.3, 0.5
0.,0.,-1.
31
*End Part

** HISTORY OUTPUT: H-Output-1
**
*Output, history, variable=PRESELECT
*ELPRINT
1,2,3,4,5,6,7,8,9,10,11,12,13,14,15,16,17,18,19,20,21,22,23,24,25,26,27,28,29,30,31
MISES
*End Step
```

**Figure A.9** Procedure followed to change the number of integration points, in this case it was chosen 31 points.

## A.4   Analysis of results

### A.4.1   Calibration and validation

The default number of integration points are five and, after the analysis, it was proven as an insufficient number because the analytical solution was far from the values obtained.

The number of integration points was increased and the model was calibrated by augmenting the number of points in the section until the solution converges. The convergence was found for 31 integration points, as it can be observed in Figure A.10 and Figure A.11.
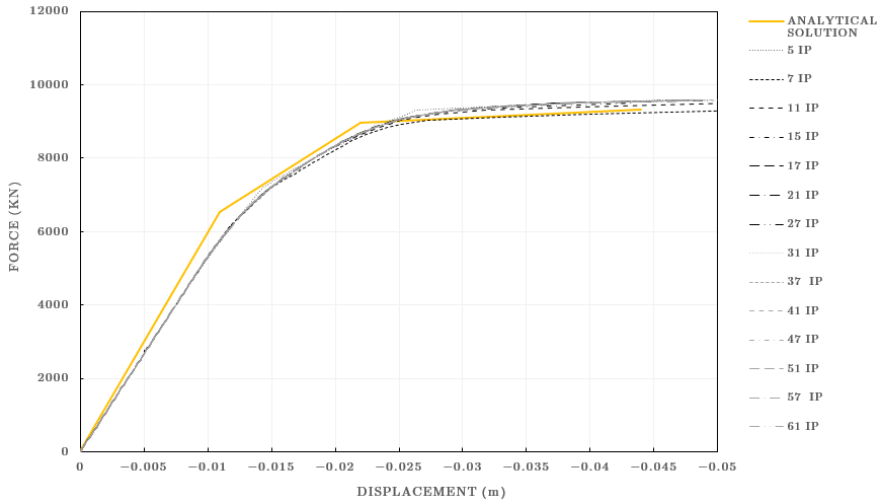
**Figure A.10** Load versus displacement for different number of integration points.
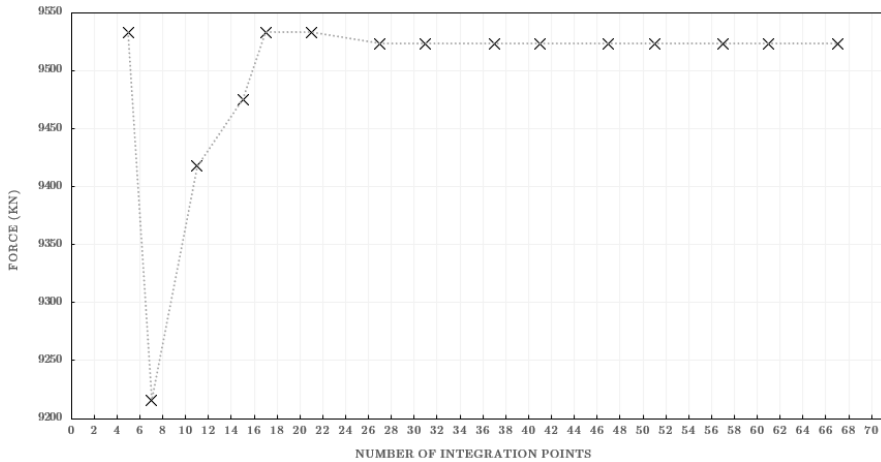


**Figure A.11** Load versus number of integration points.All the values corresponds to an specific deformation of the graph represented in A.11, 0.04m

Now the model has been calibrated, the next step is to validate it with the Analytical solution. The results obtained for 31 integration points were compared with the analytical results, Table A.2 and Table A.3.

| Plastic Hinge | Analytical Solution (kN) | Abaqus results (kN) |
|:---:|:---:|:---:|
| 1 | 6523 | 6336 |
| 2 | 8977 | 8640 |
| 3 | 9324 | 9312 |

**Table A.2** Load condition at which the plastic hinges appear. Validation between Abaqus solution and the analytical solution.

| Plastic hinge | Analytical solution (m) | Abaqus results (m) |
|:---:|:---:|:---:|
| 1 | 0.011 | 0.0123 |
| 2 | 0.022 | 0.0228 |
| 3 | 0.044 | 0.0497 |

**Table A.3** Vertical displacement produce due to the plastic hinges appearance. Validation between Abaqus solution and the analytical solution.

The results obtained with the Abaqus model are really close to the ones obtained analytically, so it can be said that this difference is acceptable and the model can be validated. The deformation values are higher due to the type of element chosen, B22, which takes into account the shear deformation (Timoshenko theory).

The type of element chosen gives higher deformation than, for example, element B23 which is also known as the Euler Bernoulli beam element. The Euler-Bernoulli element would provide closer results between the analytical solution and the Abaqus results for the vertical deformation. However, for this case, B22 was also adequate and its theory has fewer simplifications because it takes into account the shear flexibility of the section. Usually, when B23 and B22 are both adequate to solve a problem the element chose is the one with less computational weight, which is B23. But for this problem, it was considered interesting to use B22 because due to the beam characteristics the computational time needed to process B22 is practically the same than B23.

The increase in the number of integration points gives a better approximation to the plastic behaviour of the section, as it can be seen in Figure A.12, where the stress in the section is represented when the plastic hinge is fully developed. It is noticed that, as the number of integration points increases the stress diagram gets closer to a perfect plastic stress distribution. The yielding starts in the external fibres of the beam and as the load increase, the yielding goes deeper in the cross-section.
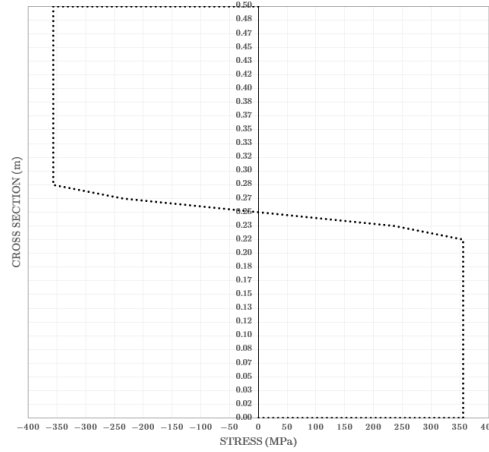
**Figure A.12** Stress distribution in the cross-section for the first plastic hinge. Number of integration points used: 31.

The deformation of the model directly depends on the number of elements of the mesh. If the mesh is denser, then the results are more accurate to the real behaviour. For this reason, the mesh is going to be calibrated, Figure A.13, A.14 and A.15. In the graph, it is shown how the length of the plastic hinge changes depending on how many elements the mesh has. The value tends to an asymptotic value as the number of elements increase. The result converges for a mesh of 70 elements.
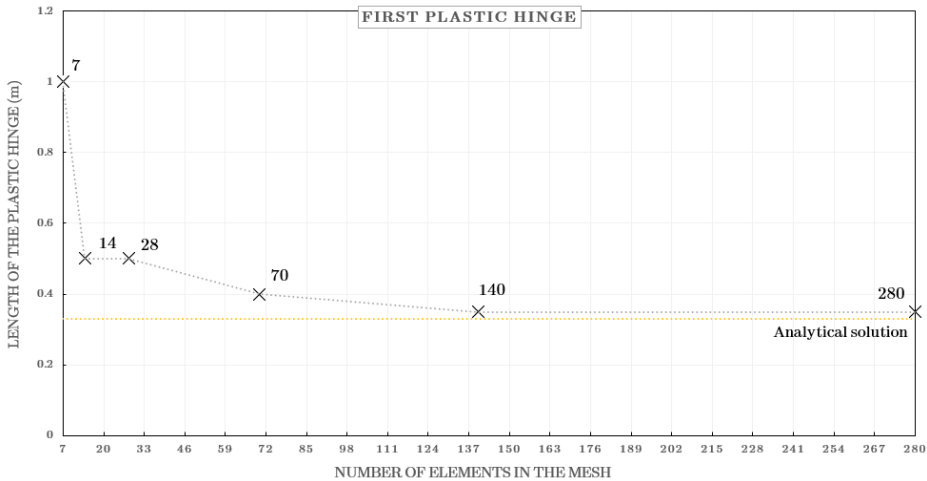


**Figure A.13** Variation of the First plastic hinge length depending of the mesh discretization.
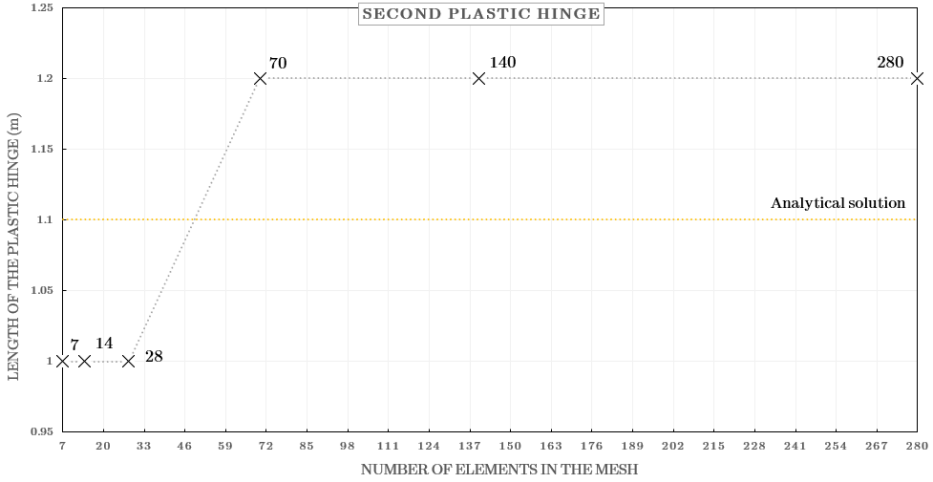
**Figure A.14** Variation of the Second plastic hinge length depending of the mesh discretization.
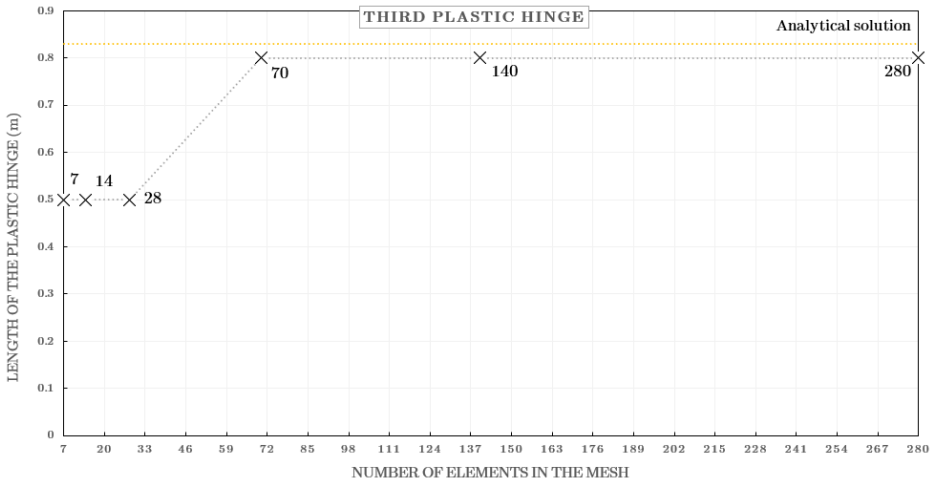


**Figure A.15** Variation of the Third plastic hinge length depending of the mesh discretization.

The analytical values for the three Plastic hinges length have been calculated in Section A.2 and its values are sum up in Table A.4.

| Plastic hinge | Length (m) |
|:---:|:---:|
| **1** | 0.33 |
| **2** | 1.1 |
| **3** | 0.83 |

**Table A.4** Analytical solution obtained for the length of the different plastic hinges.

The validation of these results is shown in Table A.5, where the different values of the hinge length for the different number of mesh elements have been compared with the analytical results, showing the error between them. The error decreases as the number of elements increases, becoming small enough to consider it acceptable.

| Nº of mesh elements | $1^{st}$ PH (m) | Error % | $2^{nd}$ PH (m) | Error % | $3^{rd}$ PH (m) | Error % |
|:---:|:---:|:---:|:---:|:---:|:---:|:---:|
| 7 | 1 | **2.03** | 1 | **0.09** | 0.5 | **0.4** |
| 14 | 0.5 | **0.52** | 1 | **0.09** | 0.5 | **0.4** |
| 28 | 0.5 | **0.52** | 1 | **0.09** | 0.5 | **0.4** |
| 70 | 0.4 | **0.21** | 1.2 | **0.09** | 0.8 | **0.04** |
| 140 | 0.35 | **0.06** | 1.2 | **0.09** | 0.8 | **0.04** |
| 280 | 0.35 | **0.06** | 1.2 | **0.09** | 0.8 | **0.04** |

**Table A.5** Plastic hinge length and relative error comparing with the analytical solution.

# Temperature dependent data

This exercise is going to be divided in two different cases, the first one is simple supported steel beam with a roller and the second one is a simple supported beam with the horizontal displacement restricted.

The loads applied are a constant temperature field and a punctual load at mid span.

### B.0.1    Case 1: Simple supported beam with a roller support.

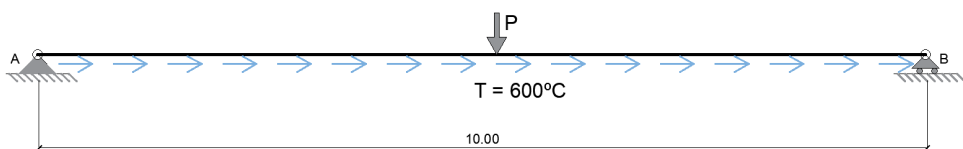The boundary conditions and the load characteristics of the beam analysed are represented in Figure B.1.



**Figure B.1** Simple supported beam with a roller support.

The punctual load P has a value of 100 KN for the first part of the analysis, when the Non linear geometry (large displacement theory) is considered the load will be increase until 1000 KN. This increase is necessary to appreciate this effect.

Regarding the temperature field, the standard fire curve ISO 834 is going to be implemented in the model. So, the temperature will increase through time following this fire curve, Equation B.1 and Figure B.2.
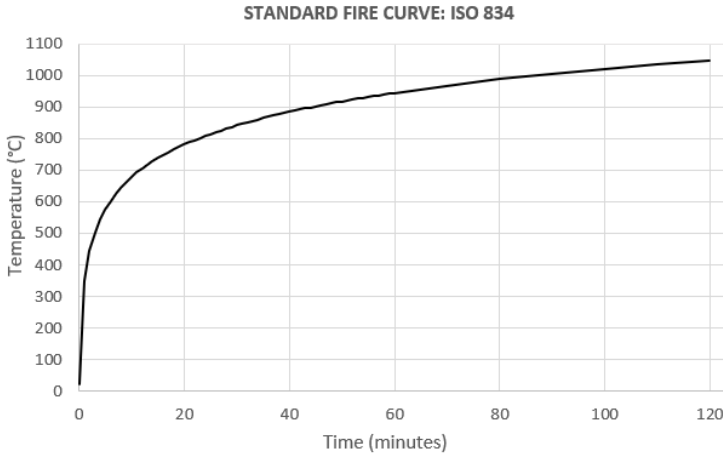


**Figure B.2** Standard fire curve, ISO 834.

$$T = T_o + 345 \log(8t + 1) \tag{B.1}$$

The maximum temperature reached will correspond to 100 minutes of fire, $T_{100} = 1021.75C$.

### B.0.1.1 Elastic analysis

The elastic and expansion properties of the material are specified in the material definition tab. The Young modulus and the Poisson ratio are established in Mechanical>Elasticity>Elastic and the thermal expansion coefficient in Mechanical>Elasticity>Expansion.

The coefficient of linear thermal expansion ($\alpha$) of steel followed a temperature dependence linear distribution, with the initial ($1.22E^{-5}$ $^oC^{-1}$) and final values ($1.51E^{-5}$ $^oC^{-1}$) extracted from EC-3.

Firstly, it is going to be analysed the behaviour of the beam when the temperature field is acting; secondly, the distributed load will be introduced and lastly, the temperature field and the load will be acting at the same time.

The results obtained for the three steps will be analysed and compared, being the last step results the sum of the previous ones (superposition). The Abaqus model used was validated comparing the values obtained with the analytical solution, checking that the results were practically the same (small error).

| | Temperature | Bending | Temperature & bending | Analytical solution | |
|---|---|---|---|---|---|
| $R_{ay}$ | 0 | 50 | 50 | 50 | kN |
| $R_{by}$ | 0 | 50 | 50 | 50 | kN |
| $M_{max}$ | 0 | -250 | -250 | 250 | kN $\cdot$ m |
| $M_{min}$ | 0 | 0 | 0 | 0 | kN $\cdot$ m |
| $V_a$ | 0 | -50 | -50 | -50 | kN |
| $V_b$ | 0 | 50 | 50 | 50 | kN |
| $U_{horizontal}$ | 0.12 | 0 | 0.12 | 0.12 | m |
| $U_{vertical}$ | 0 | 0.00317 | 0.00317 | 0.00317 | m |

**Table B.1** Results for the three different cases for the Elastic analysis: Temperature, bending and temperature plus bending.

The analytical solution for the reactions ($R_{ay}$, $R_{by}$) and forces ($M_{max}$, $M_{min}$, $V_a$, $V_b$) in the system were determined by equilibrium of forces. The thermal expansion was calculated using Equation B.2.

$$\frac{\Delta L}{L} = \alpha \Delta T \tag{B.2}$$

The reference temperature of the air surrounding the beam is 20ºC, the temperature of the steel beam is 600ºC and the length equal to 10 m. This formulation gives the value for ΔL, which represents the displacement (expansion) in 1-axis (U1).

The deflection due to the action of the punctual load was determined with internal equilibrium of the system, Equation B.3.

$$U_2 = \frac{PL^3}{48EI} \tag{B.3}$$

### B.0.1.2 Material degradation

Then the material degradation due to the increase of temperature was implemented in the material properties.

According to EC-3, the degradation slope followed by the material depends of the reduction factor for stress-strain relationship of carbon steel at elevated temperatures. It can be observed that the degradation does not influence the first case, because its effects does not affect to expansion of the material in the horizontal direction when the movement is allowed. In Case 2, the results are the same as the previous exercise because no thermal field was introduced. However, the effect of the degradation can be noticed in Case 3, where the temperature field and the distributed load are applied. Then due to the lower value of E and the corresponding reduction in stiffness of the material, the vertical displacement ($U_{vertical}$) is higher than the one obtained without degradation.

The value corresponding to E for 1021.75ºC is 8.4E6 KPa.

| | Temperature | Bending | Temperature & bending | Analytical solution | |
|---|---|---|---|---|---|
| $R_{ay}$ | 0 | 50 | 50 | 50 | kN |
| $R_{by}$ | 0 | 50 | 50 | 50 | kN |
| $M_{max}$ | 0 | -250 | -250 | 250 | kN · m |
| $M_{min}$ | 0 | 0 | 0 | 0 | kN · m |
| $V_a$ | 0 | -50 | -50 | -50 | kN |
| $V_b$ | 0 | 50 | 50 | 50 | kN |
| $U_{horizontal}$ | 0.12 | 0 | 0.12 | 0.12 | m |
| $U_{vertical}$ | 0 | 0.00317 | 0.0793 | 0.0793 | m |

**Table B.2** Results for the three different cases with E degradation: Temperature, bending and temperature plus bending.

### B.0.1.3 Plastic analysis

Plasticity properties are going to be add to the model by editing the material properties of the steel S355, which yields at 355 Mpa. The plasticity is introduced in the material characteristics, mechanical> plasticity>plastic, no hardening was considered.
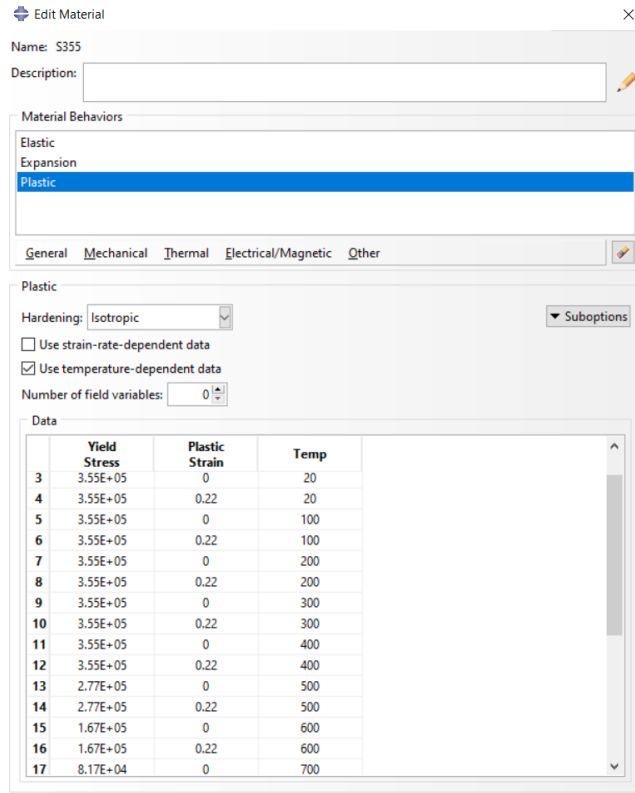
**Figure B.3** Plastic tab in Abaqus, Editing the material.

It can be noticed that the reduction of the yielding point due to temperature variation was also included in the plastic properties. As the temperature of the steel increases, the yield strength decreases. This effect was represented in Figure **??**.

The non linear geometry (large displacements theory) shall be considered now, in order to approximate the behavior of the element as close as possible to reality. This affects to the deformation of the beam because now the vertical and horizontal displacement will be coupled, they will influenced each other.

However, the punctual load applied is not sufficient to appreciate this effect and its value shall be increase. The new load is 1000 KN, which is sufficiently large to appreciate the non linear geometry effect.

When there is only one of the loads applied, the thermal load or the punctual load, this effect cannot be appreciate because they only generates one direction displacement, horizontal for the thermal load and vertical for the punctual load. For this reason, the case where the thermal and the punctual load are applied at the same time is the one that will be analysed.

The results obtained are compared with the ones when the non linear geometry is not considered, Table B.3. The maximum temperature reached is approximately 820ºC before the structure collapses due to yielding. All the results showed corresponds to that final temperature and to a punctual load value of 260 KN.

| | With NLG | Without NLG | Analytical solution | |
|---|---|---|---|---|
| $R_{ay}$ | 130 | 130 | 130 | kN |
| $R_{by}$ | 130 | 130 | 130 | kN |
| $M_{max}$ | 657.1 | 650 | 650 | kN · m |
| $M_{min}$ | 0 | 0 | 0 | kN · m |
| $V_a$ | -130 | -130 | -130 | kN |
| $V_b$ | 130 | 130 | 130 | kN |
| $U_{horizontal}$ | 0.112 | 0.115 | 0.115 | m |
| $U_{vertical}$ | 0.126 | 0.118 | 0.118 | m |

**Table B.3** Comparission between the results with NLG, without NLG and the analytical solution.

The vertical displacement is the same with NLG than without because both cases takes into account the plastic behaviour of the material. However, the run-away phenomenon only occur with NLG. This effects appears when the beam cannot carry the load anymore due to the lost of stiffness. Then the roller support is "pulled" towards its initial position.For this reason the horizontal displacement is lower with NLG than without.This effect is explained in Figure B.4.
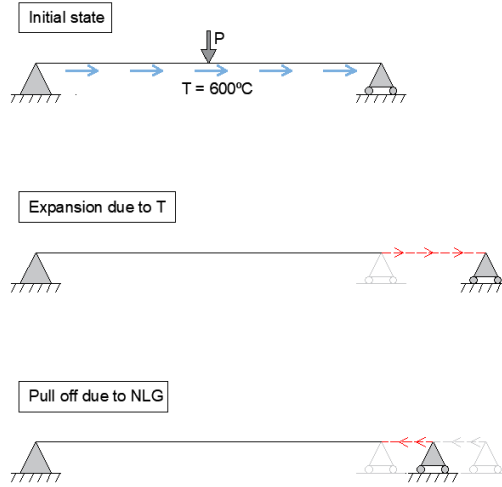
**Figure B.4** Non-linear geometry effect.

This effect is shown in Figure B.5, B.6 and B.7. In all the graphs it has been plotted the horizontal displacement of the roller versus the time. In the first one the Non linearity is not considered, for this reason the beam keeps expanding until failure. However, in the second and the third, the non linearity effect is taken into account. Due to this fact, the pull off of the roller appears when the beam starts yielding, long displacement theory.
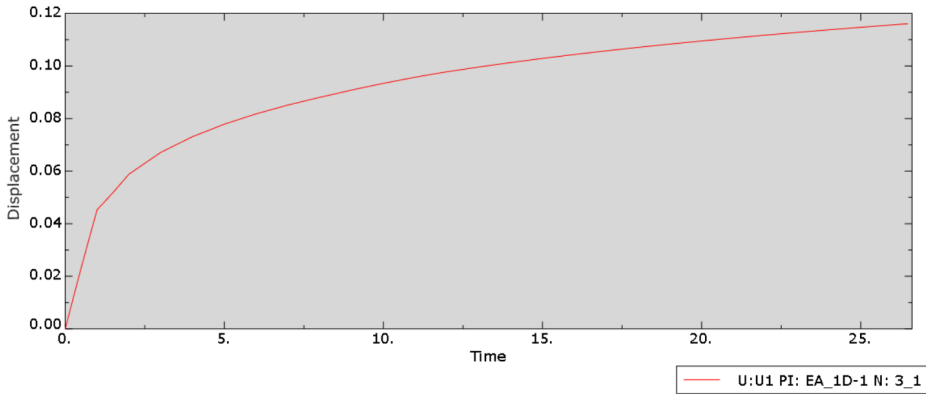


**Figure B.5** Roller displacement until failure, non linearity not considered.
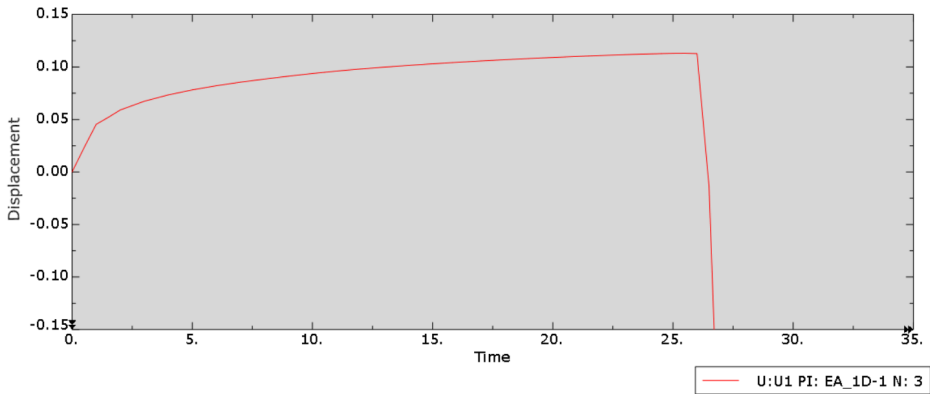
**Figure B.6** Roller displacement until yielding, non linearity considered.
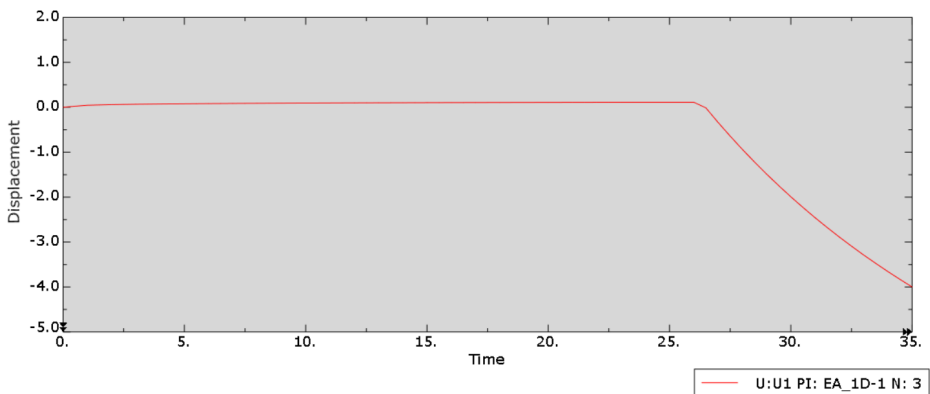


**Figure B.7** Roller displacement , non linearity considered.

## B.0.2   Case 2: Simple supported beam with horizontal displacement restricted.

The boundary conditions changes respect the previous exercise, but the load case is the same. The only change is that the support B restricts the movement in the vertical and horizontal direction.
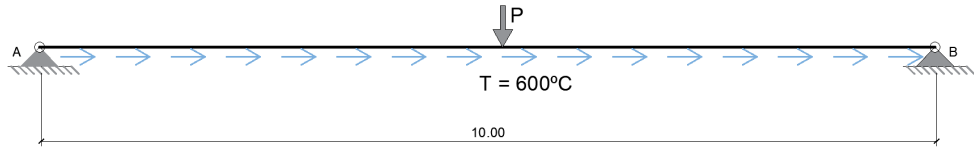
**Figure B.8** Simple supported beam with horizontal displacement restricted.

### B.0.2.1 Elastic analysis

The procedure is the same as the one followed in Exercise 2.1. First, the temperature field is applied, then the distributed load and finally both loads actuates in the beam at the same time.

The main change in the results obtained are reflected in the support reaction forces. Due to the restriction of horizontal displacement, when the temperature field is applied the expansion and the consequent displacement cannot occur. Instead of the displacement a horizontal force appears, and its value is the equivalence of the displacement that should take place when the horizontal degree of freedom is free.

On the other side, for Case 2, there are not changes in the results and, as it was explained before, the values for Case 3 are the combination of the previous cases. All this results are gathered in Table B.4

| | Temperature | Bending | Temperature & bending | Analytical solution | |
|---|---|---|---|---|---|
| $R_{ay}$ | 0 | 50 | 50 | 50 | kN |
| $R_{by}$ | 0 | 50 | 50 | 50 | kN |
| $R_{ax}$ | 25.7E4 | 0 | 25.7E4 | 25.7E4 | kN |
| $R_{bx}$ | -25.7E4 | 0 | -25.7E4 | -25.7E4 | kN |
| $M_{max}$ | 0 | -250 | -250 | 250 | kN · m |
| $M_{min}$ | 0 | 0 | 0 | 0 | kN · m |
| $V_a$ | 0 | -50 | -50 | -50 | kN |
| $V_b$ | 0 | 50 | 50 | 50 | kN |
| $U_{horizontal}$ | 0 | 0 | 0 | 0 | m |
| $U_{vertical}$ | 0 | 3.17E-3 | 3.17E-3 | 3.17E-3 | m |

**Table B.4** Results for the three different cases for the Elastic analysis.

The analytical solution for the equivalent force in x-axis is determined using Equation

B.4.

$$\Delta L = \frac{FL}{AE} \tag{B.4}$$

Where $\Delta L$ is the expansion that should have take place if the horizontal movement was allowed, A is the area of the cross section, E is the Young modulus and F is the equivalent force.

### B.0.2.2  Material degradation

Then, the material degradation properties where introduced in the previous model. The influence of this reduction of stiffness reflects in the equivalent horizontal force that appears in support B. The force is lower because the stiffness has been reduced. Besides, in Case 3, the vertical displacement is also higher, as it was explained in the previous section.

|  | Temperature | Bending | Temperature & bending | Analytical solution | |
|---|---|---|---|---|---|
| $R_{ay}$ | 0 | 50 | 50 | 50 | kN |
| $R_{by}$ | 0 | 50 | 50 | 50 | kN |
| $R_{ax}$ | 7.9E4 | 0 | 7.9E4 | 7.9E4 | kN |
| $R_{bx}$ | -7.9E4 | 0 | -7.9E4 | -7.9E4 | kN |
| $M_{max}$ | 0 | -250 | -250 | 250 | kN · m |
| $M_{min}$ | 0 | 0 | 0 | 0 | kN · m |
| $V_a$ | 0 | -50 | -50 | -50 | kN |
| $V_b$ | 0 | 50 | 50 | 50 | kN |
| $U_{horizontal}$ | 0 | 0 | 0 | 0 | m |
| $U_{vertical}$ | 0 | 0.00317 | 0.01024 | 0.01024 | m |

**Table B.5** Results for the three different cases with E degradation: Temperature, bending and temperature plus bending.

### B.0.2.3  Plastic analysis

The plasticity properties of the material and the Non linear geometry are going to be implemented in the model. The process is analogue to the one followed in Section 4.1.3.

At first, the load applied was the same as in the previous case, temperature field equal to 600ºC and load of 1000 kN. But, when the plasticity was implemented in the model and the temperature add the structure collapsed due to yielding. The lost in stiffness and the decrease of the yielding point as temperature increases was enough to make the system collapsed, forming a plastic hinge in mid span.

For this reason, the temperature was lowered in order to appreciate the effect of plasticity plus non linear geometry in this system. The new temperature is 140ºC, which lowers the stiffness and the yielding point but the values are really close to the initial ones, E equal to 2.02E5 Mpa and the yielding point is still the same 355 MPa. The punctual load keeps the same value as before, 1000 kN.

The results obtained are shown in Table B.6 and, as it can be noticed, the run-away effect can also be appreciate in this case. However, due to the restriction of movement in the horizontal direction, this effect is reflected in the decrease of the horizontal force that appears as a reaction of the beam trying to expand (due to temperature).

| | PLASTICITY + NLG | | | | |
|---|---|---|---|---|---|
| | Temperature | Bending | Temperature & bending | Analytical solution | |
| $R_{ay}$ | 0 | 500 | 500 | 500 | kN |
| $R_{by}$ | 0 | 500 | 500 | 500 | kN |
| $R_{ax}$ | 5.26E4 | 0 | 1.742E4 | 5.51E4 | kN |
| $R_{bx}$ | -5.26E4 | 0 | -1.742E4 | -5.51E4 | kN |
| $M_{max}$ | 0 | 2476 | -5620 | -500 | kN·m |
| $M_{min}$ | 0 | 0 | 0 | 500 | kN·m |
| $V_a$ | 0 | -499 | -1284 | 0 | kN |
| $V_b$ | 0 | 499 | 1284 | 0.1024 | kN |
| $U_{horizontal}$ | 0 | 0 | 0 | 0 | m |
| $U_{vertical}$ | 0 | 3.16E-2 | 0.1792 | 3.16E-3 | m |

**Table B.6** Results for the simple supported beam with horizontal displacement restricted, considering NLG and plasticity.

The analytical solution was calculated without considering the NLG and the plasticity of the material.

# Structural stability: buckling

## C.1 Introduction

The buckling instability appears suddenly producing the collapse of a structural member subjected to high compression load (axial load). The importance of this analysis relays in the fact that the buckling load is lower than the maximum axial load a structure can withstand before yielding. This instability affects slender structures subjected to high axial load.

In this Appendix a 10 meters long steel column will be analysed. Four different cases will be studied, two with concentrated elasticity and two with distributed elasticity. The material and geometric characteristics of the structure will remain the same while the boundary conditions will be changed for each case.

The total length of the column is 10 meters with a square cross section of 0.15 m with. It is compose of structural steel, S355. For all the cases analysed, the material degradation due to temperature effects will be not considered. In addition, the type of elements used will employ Euler theory, no shear deformation will be taken into account.

### C.1.1 Abaqus modelling

In order to perform a buckling analysis in Abaqus it is necessary to carry out two different procedures. The first one is an eigenvalue buckling analysis which estimates the critical buckling load (bifurcation point). The second one is a post-buckling anal-

ysis that calculates the unstable, geometrically nonlinear collapse of a structure, it is also known as Riks analysis. However, the postbuckling analysis can also be performed using the Statically Incremental analysis, which allows to add a temperature field with a defined relation time-temperature, like the standard fire curve.

### C.1.1.1  Eigenvalue buckling analysis

It is a linear analysis used to determine the critical buckling load of a structure. The output is the value of the critical load for each eigenvalue and the mode shapes. From this buckling mode shapes it can also be obtained the stresses and strains, however these are perturbation values not absolute results. In order to calculate the real results, the post-buckling analysis must be performed.

Firstly, the geometry of the structure and the elastic properties of the material have to be defined. Then, a new step will be created, Figure C.1: Create step > Procedure type, Linear perturbation > Buckle. Then the number of eigenvalues requested is chosen, in this case with the first three will be sufficient, Figure C.2. Each eigenvalue result corresponds to the buckling mode shapes.

Lastly, the keyword will be modified in order to store the information related to the eigenmodes for each node of the structure. This file will be used after, in the Riks analysis to add an imperfection to the model. The lines have to be add at the end of the file, where the output is defined, Figure C.3.
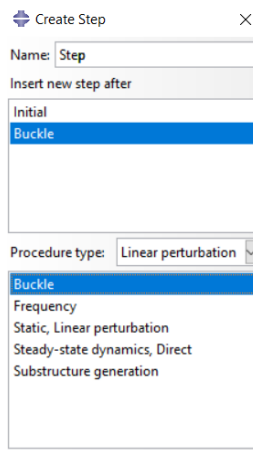
**Figure C.1** Create step in Abaqus: Buckle
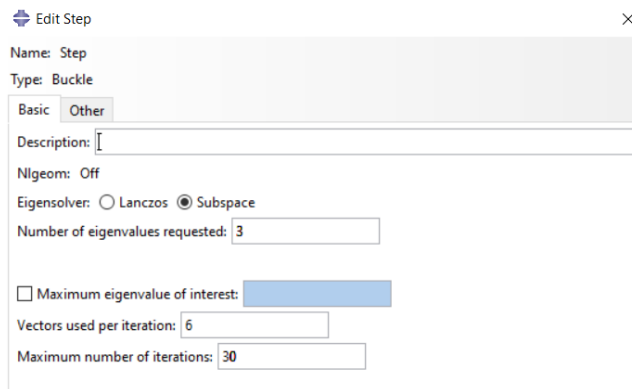


**Figure C.2** Edit Buckle step: number of eigenvalues.



**Figure C.3** Keyword modification to store the eigenmodes information.

### C.1.1.2 Post-buckling analysis: Riks analysis/Statically Incremental analysis

**Riks analysis**

After obtaining the values of the critical loads $P_{cri}$ and the different buckling mode shapes, the post-buckling analysis can be performed. The Riks analysis is going to be used, which predicts unstable, geometrically nonlinear collapse. Buckling is a geometrically nonlinear static problem. The riks method is used for both stable and unstable postbuckling behavior.

A new step has to be created, it is a static general Riks analysis, Figure C.4. Then the non linear geometry (NLgeom) has to be considered, Figure C.5, and the increment length especified, Figure C.6.
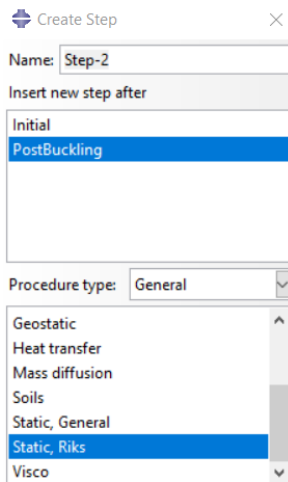


**Figure C.4** Create Riks analysis step
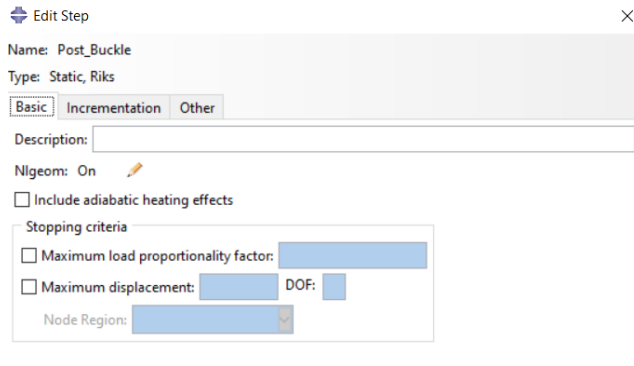
**Figure C.5** Edit Riks step: NLgeom ON
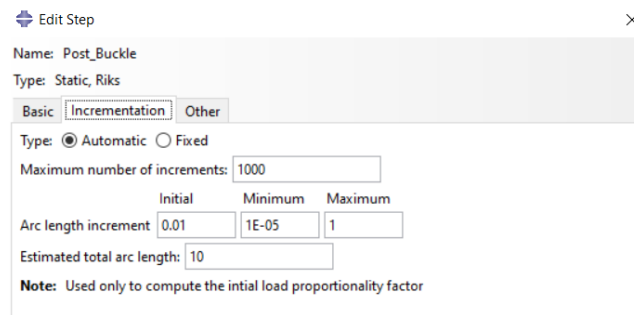


**Figure C.6** Edit Riks step: arch length increment.

Then, an imperfection must be add to the structure in order to perform the analysis. The exact post-buckling problem usually cannot be analysed directly because of the bifurcation point that appears when the buckling load ($P_{cri}$) is reached. Then, an imperfection must be included in the structure geometry to turn it into a problem with continuous response, without bifurcation. This imperfection added to the perfect geometry will produce some response in the buckling mode before arriving to the critical load.

There are three different ways of introducing this imperfection: as a linear superposition of buckling eigenmodes, from the displacements of static analysis or implementing the exact values of the imperfection directly to each node. However, the most common way of adding the imperfection is by superposition of the buckling modes because for the other methods it is necessary to know the precise shape of the

imperfection.

In this case, the superposition of the eigenmodes was the method chosen to add the imperfection to the perfect geometry, only the translational degrees of freedom are modified. The imperfection is implemented using the keyword, where the file created in the Eigenvalue analysis carried before has to be called using the command "FILE", Figure C.7. The lowest buckling mode is usually the one that provides the most critical imperfection, for this reason the higher imperfection value is add to this mode (second line of the keyword script). Adding only the imperfection to one of the modes usually gives non-conservative results so, the best way is to add imperfection to the first three or two eigenmodes. For these modes the value of the imperfection is lower.

```
** ----------------------------------------------------------------
**
*IMPERFECTION, FILE=Buckling, STEP=1
1, 12.5e-3
2, 6.25e-3
3, 3.1e-3
** STEP: Post_Buckle
**
*Step, name=Post_Buckle, nlgeom=YES, inc=1000
*Static, riks
0.01, 1., 1e-05, 1., ,
```

**Figure C.7** Edit keyword post-buckling analysis: imperfection added to the first three buckling modes.

The imperfection magnitude is usually chosen as a percentage of the cross-section dimensions. However, it is necessary to perform a sensitivity analysis before determining this value, specially for the structures which has many buckling modes closely spaced because they are usually imperfection sensitive. If the imperfection is too small the deformation will be also small and below the critical load. The response will grow fast close to $P_{cri}$ introducing a rapid change behavior. Nonetheless, if the imperfection is large the response will grow steadily until $P_{cri}$ is reached, the transition to post-buckled behavior is smooth.

After performing the sensitivity analysis and choosing an adequate value for the imperfection, it can be add to the geometry.

**Statically incremental analysis**
The main advantage of using this method instead of Riks analysis is that a time de-

pendent temperature field can be add to the model while in Riks this is not possible. That does not mean that in Riks analysis a temperature field cannot be add, it is possible but it will not followed a specific distribution over time. For this reason, the statically incremental analysis is fundamental when the standard fire curve wants to be implemented in the model.

However, it has its drawbacks, it perfectly represents and process stable buckling behaviour while the unstable not. This can be improved by decreasing the time step and the number of steps. A comparison between this different analysis will be performed in Section 3.2.

## C.2   Imperfection sensitivity analysis and calibration

A sensitivity analysis was performed for the case studied in Section 3.1.2, where a rigid rod with translational spring at the top is represented. The postbuckling response is unstable, the curve after reaching $P_{cri}$ will decrease. The load decreases as the deformation augment.

Different imperfections where introduced and then represented in a graph in Figure C.8. The value chosen, $\theta$ equal to 0.005, which is equivalent to an initial displacement on top of the column of 50 mm. With this imperfection the buckling load decreases 5% and, as it can be observed in the graph, for this value the solutions already converge.
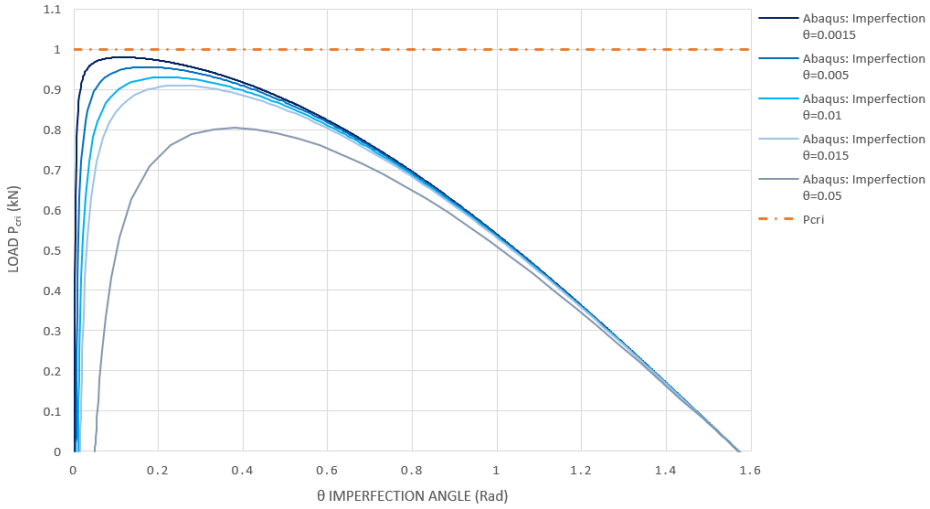
**Figure C.8** Sensitivity analysis.

Furthermore, the imperfection was applied in two different ways in order to calibrate the model. The first method was the one explained before, by adding a deformation to the buckling shape calculated before. The second one consists in dividing the post-buckling analysis in two different steps. In the first step a small load is applied to the top of the column, its value is the equivalence of the initial displacement that is intro-duce as an imperfection. In the second step the postbuckling analysis is performed to the deformed shape.

The results have been represented in Figure C.9 where it can be noticed that the values obtained are practically the same. So, it can be said that both methods are equivalent and the result obtained will be equal.
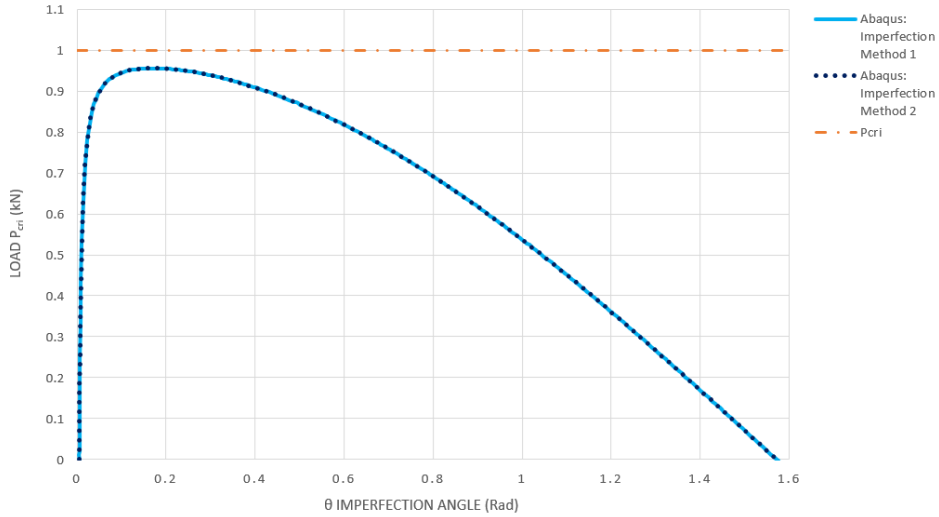
**Figure C.9** Imperfection method validation.

## C.3   2D Column modelling

Four different models are going to be developed in this section, the first two have concentrated elasticity while the second two have distributed elasticity.

The concentrated elasticity models are characterised by an elasticity modulus really high in comparison to its spring constant value. While the distributed elasticity models do not have springs and the stiffness is equally assigned.

### C.3.1   Concentrated elasticity

#### C.3.1.1   Rigid rod with rotational spring at the bottom

The geometric and material properties of the rod are the same as the ones described in the introduction of this Appendix. The material is structural steel, S355, with a Young modulus of 210 GPa. The rotational spring stiffness is equal to 10 KN/m.

Firstly, it is going to be analysed and ideal rod and secondly a rod with an initial imperfection. The imperfection was added as a superposition of the buckling modes

with the scalar factor obtained from the sensitivity analysis performed in Section 2, equal to 0.05. The ideal rod system is represented in Figure C.10.
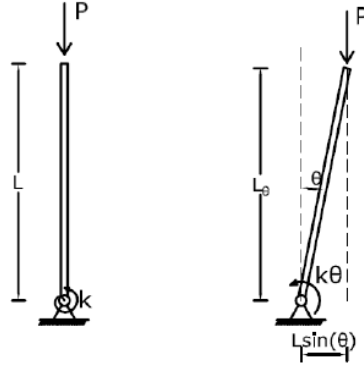


**Figure C.10** Ideal rod with rotational spring at the bottom.

The system depends directly of the angle $\theta$, which is the degree of freedom that describes the configuration of the system. The equilibrium of the rod in the deformed position is shown in Equation C.1.

$$PL \sin \theta = k\theta \tag{C.1}$$

If the assumption of small displacements is taken into account, the value of $\sin \theta$ can be approximated to $\theta$, $\sin \theta \approx \theta$. So, the equation can be rewrite, Equation C.2.

$$PL\theta = k\theta \tag{C.2}$$
$$\theta(PL - K) = 0 \tag{C.3}$$

There are two solutions, the trivial solution where $\theta$ is equal to 0, it corresponds when the rod is vertical and there are not any rotation. The second one corresponds to the buckling load, when buckling appear, Equation C.4.

$$P_{cri} = \frac{k}{L} \tag{C.4}$$

Both solution have into account the small displacements theory, however if the dis-

placements cannot be considered under this assumption, the solutions are not valid. If the displacements are considered as large displacements the simplifications made cannot be used, $\sin\theta \approx \theta$. So, the solution that corresponds to large displacements is shown in Equation C.5.

$$P_{cri} = \frac{k}{L}\frac{\theta}{\sin\theta} \tag{C.5}$$

Now, the assumption of an ideal rod is removed and an imperfection is introduced in the system. In this case an initial angle of rotation is added, Figure C.11. The value of $P_{cri}$ obtained for the imperfection case will be lower than in the ideal case.
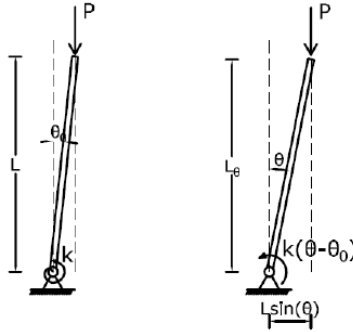


**Figure C.11** Imperfect rod with rotational spring at the bottom.

Taking into account this initial rotation the equilibrium can be established as it was done before, Equation C.6. There will be only one solution, there is not trivial solution for this case.

$$PL\sin\theta = k(\theta - \theta_o) \tag{C.6}$$

If the hypothesis of small displacements is taken into account the result is obtained in Equation C.7.

$$P_{cri} = \frac{k}{L}\left(1 - \frac{\theta_o}{\theta}\right) \tag{C.7}$$

Then, if the last assumption is removed and the displacement is considered as large

displacement the value obtained for $P_{cr}$ is shown in Equation C.8.

$$P_{cri} = \frac{k}{L}\left(1 - \frac{\theta_o}{\theta}\right)\frac{\theta}{\sin\theta} \tag{C.8}$$
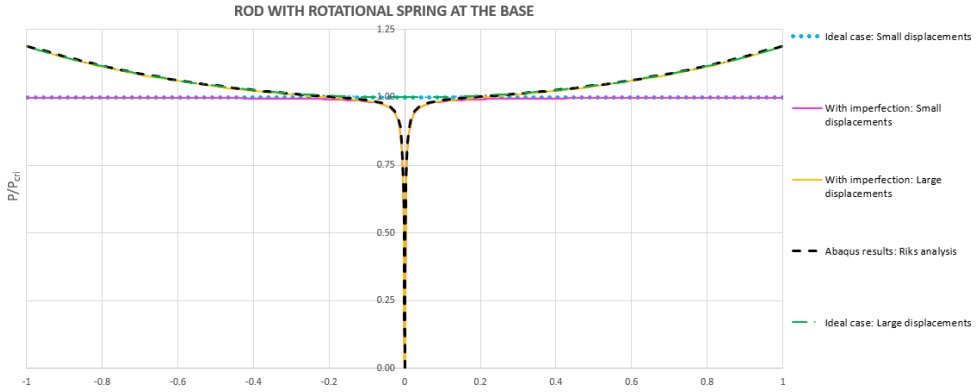


**Figure C.12** Equilibrium paths for rod with rotational spring at the bottom.

The solution obtained for the ideal rod and the imperfect rod was plotted in Figure C.12 as well as the solution obtained using the program Abaqus. The result provided by Abaqus has into account large displacements and non linear behavior. As it can be seen the solutions show a stable post-buckling behaviour when the large displacement theory is used.

### C.3.1.2 Rigid rod with translational spring at the top

In this case, the bottom of the rod is pinned and the top of it has a trasnlational spring, with a translational stiffness $k$. The problem is analogue to the one analysed in Section 3.1.1, the system is also described by the angle $\theta$.
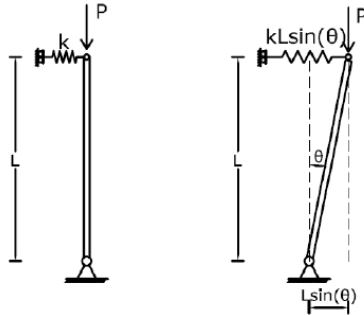
**Figure C.13** Ideal rod with translational spring at the top.

The reaction force of the spring is described in Equation C.9 and the equilibrium in the deformed possition is expressed in Equation C.10.

$$F = kL\sin\theta \tag{C.9}$$

$$PL\sin\theta = FL\cos \tag{C.10}$$

$$PL\sin\theta = L^2 k\sin\theta\cos \tag{C.11}$$

Firstly, the small displacement theory is considered, some simplifications can be made: $\cos\theta \approx 1$ and $\sin\theta \approx \theta$. Then the equilibrium equation can be solved, Equation C.12, there are two solutions, the trivial solution with $\theta$ equal to 0 and the solution that corresponds to the buckling load, Equation C.14.

$$P\theta = Lk \tag{C.12}$$

$$\theta(P - kL) = 0 \tag{C.13}$$

$$P_{cri} = kL \tag{C.14}$$

If instead of small displacements it is considered the large displacement theory the result will be change, Equation C.15.

$$P_{cri} = kL\cos\theta \tag{C.15}$$

Then, after obtaining the solution for the ideal rod an imperfection is going to be introduced in the model, an initial rotation $\theta_o$, Figure C.14.
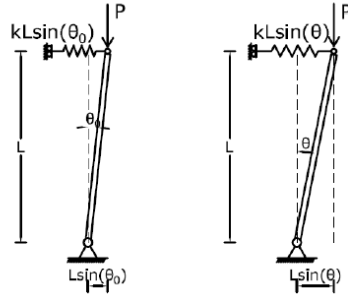
**Figure C.14** Imperfect rod with translational spring at the top.

The procedure that evaluates the equilibrium of the deformed system is the same as the one followed in the previous section. However, the solution obtained with the imperfection is unique, there is not trivial solution. The equivalent force of the spring is shown in Equation C.19, the equilibrium equation in Equation C.17, the solution obtained for small displacements in Equation C.18 and the one for large displacements in Equation C.19.

$$F = kL(\sin\theta - \sin{}_o) \tag{C.16}$$

$$PL\sin\theta = kL^2(\sin\theta - \sin\theta_o)\cos\theta \tag{C.17}$$

$$P_{cri} = kL\left(1 - \frac{\theta}{\theta_o}\right) \tag{C.18}$$

$$P_{cri} = kL\left(1 - \frac{\sin\theta}{\sin\theta_o}\right)\cos\theta \tag{C.19}$$
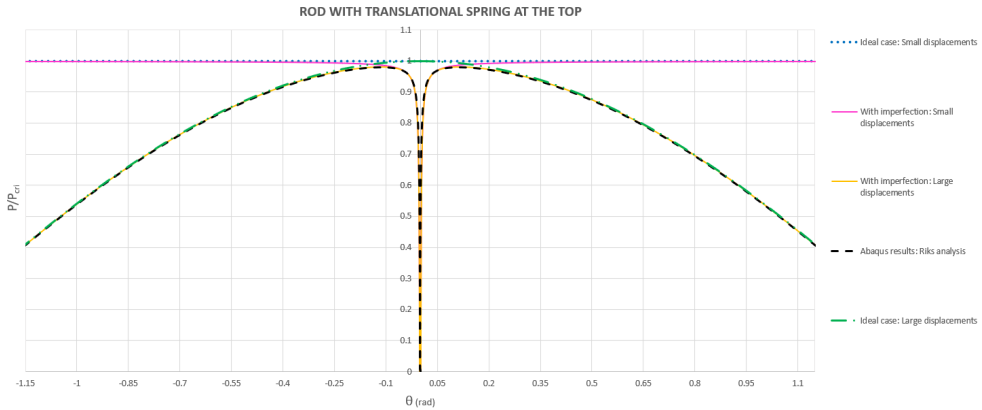


**Figure C.15** Equilibrium paths for rod with translational spring at the top.

The results of these equations have been plotted in Figure C.15, where it was also plotted the solution obtained with the software Abaqus. The solutions that takes into account large displacements clearly show the unstable post-buckling behaviour of the system.

## C.3.2 Comparison between Riks analysis and Statically incremental analysis

The postbuckling analysis performed in the previous sections where made using Riks analysis method. In order to compare the results obtained using different methods the Static Incremental analysis was used with the same cases: rod with roatational spring at the bottom and rod with translational spring at the top.

The results, Figure C.16 and C.17, are practically the same specially for the first case. The main reason is that this analysis represents perfectly the postbuckling behaviour for the stable cases, however when the buckling is unstable the analysis stopped at some point. This analysis cannot fully represent the unstable behavior produce by buckling like Riks analysis does. Nevertheless, adjusting the time step and the number of step it has the results can be improved.

As a conclusion, Statically incremental analysis gives as good solution as Riks analysis for stable buckling behavior but for unstable not, however the solution is good enough.
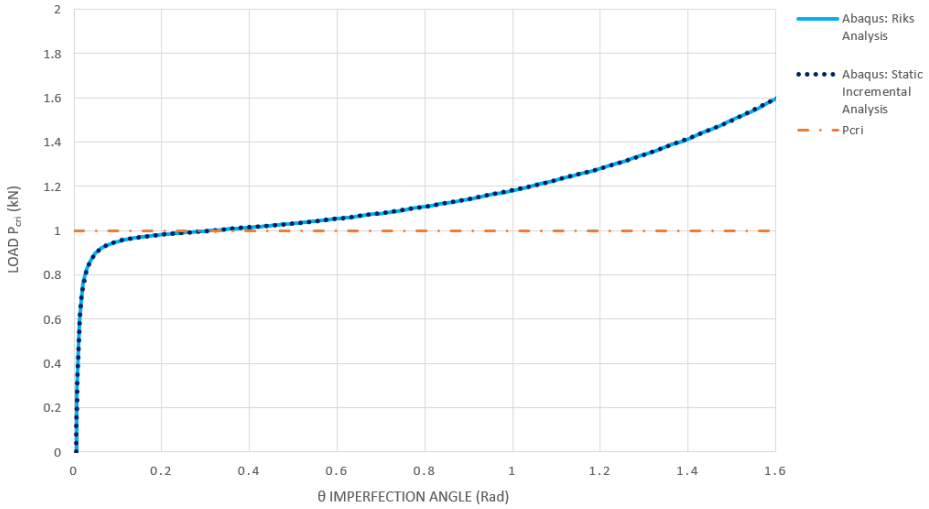
**Figure C.16** Comparison between Riks and Statically incremental for the rod with rotational spring at the bottom. Stable buckling behavior.
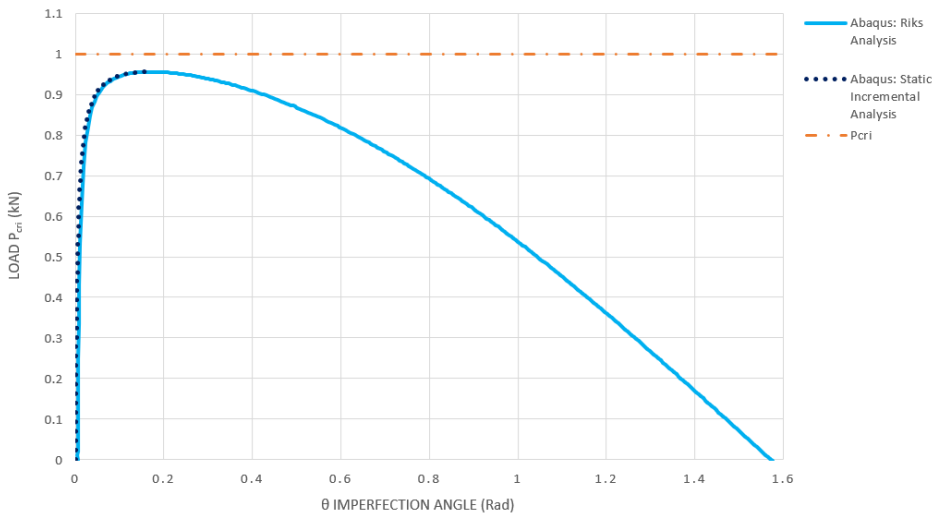


**Figure C.17** Comparison between Riks and Statically incremental for the rod with translational spring at the top. Unstable buckling behavior.

### C.3.3 Distributed elasticity

The material properties remain the same as for the concentrated elasticity cases. However the geometry is different, the section is rectangular with a width of 200 mm and the column has a total height of 5 m. The boundary conditions change, now a simply supported beam will be analysed. The Euler load or buckling load for this case is equal to 11054 KN.

Two different analysis will be developed, Riks analysis and Statically Incremental analysis. It will be demonstrated that, for stable buckling behavior the incremental analysis gives good solutions.
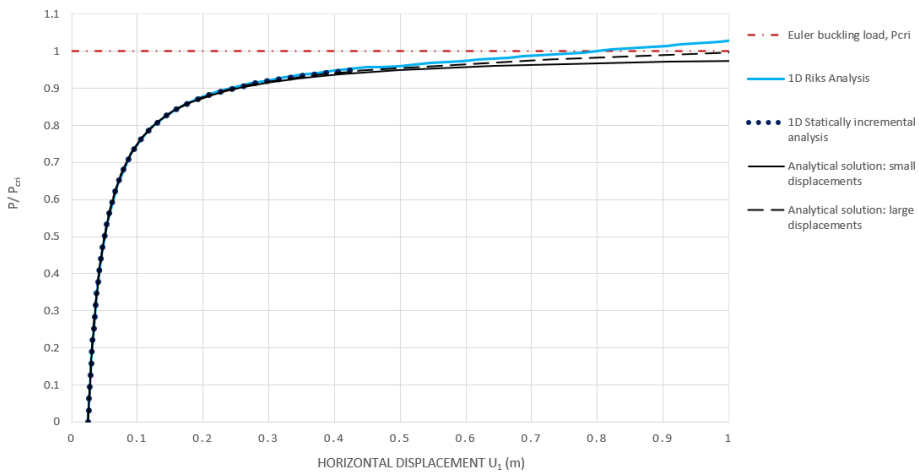


**Figure C.18**

It can be observed that in Riks analysis, Statically incremental analysis and in the Analytical solution the Load-displacement has the same behaviour until approximately 92% of the critical load. Beyond this point, the analytical solution grows asymptotically towards the Euler load while the Riks analysis pass this load in a stable postbuckling path.

### C.3.4 Thermal buckling

Now, a not time dependent temperature field will be introduce in the model. The punctual load will be removed and the vertical expansion limited. The buckling phenomenon will occur due to the axial load that will appear because the beam is trying

145

to expand when the temperature is raising but the boundary conditions does not let it. The thermal expansion coefficient of the material is added and the maximum temperature of the temperature field is 1000ºC.

In Figure C.19 the load versus temperature is represented, the curve form looks similar to the load-displacement curve for buckling. It can also be seen the horizontal displacement process as a function of temperature, Figure C.20.
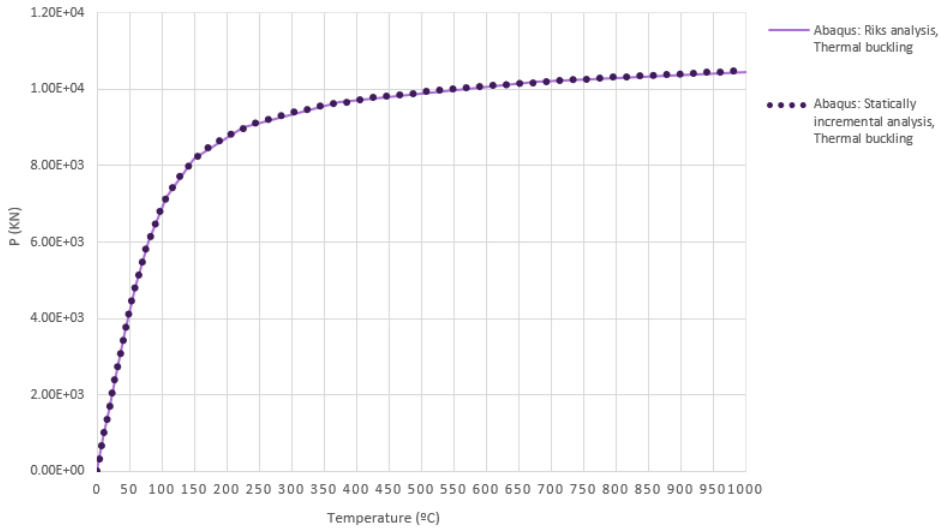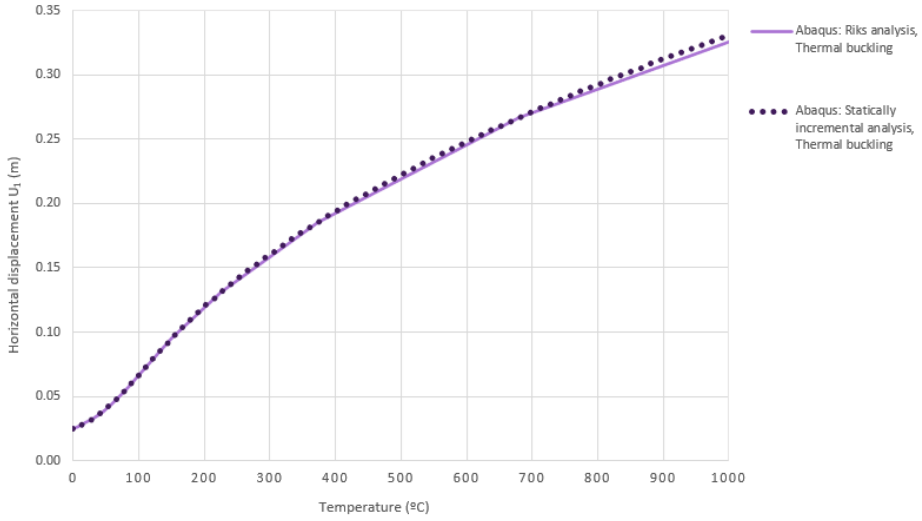


**Figure C.19** Load versus temperature.

**Figure C.20** Horizontal displacement versus temeprature.
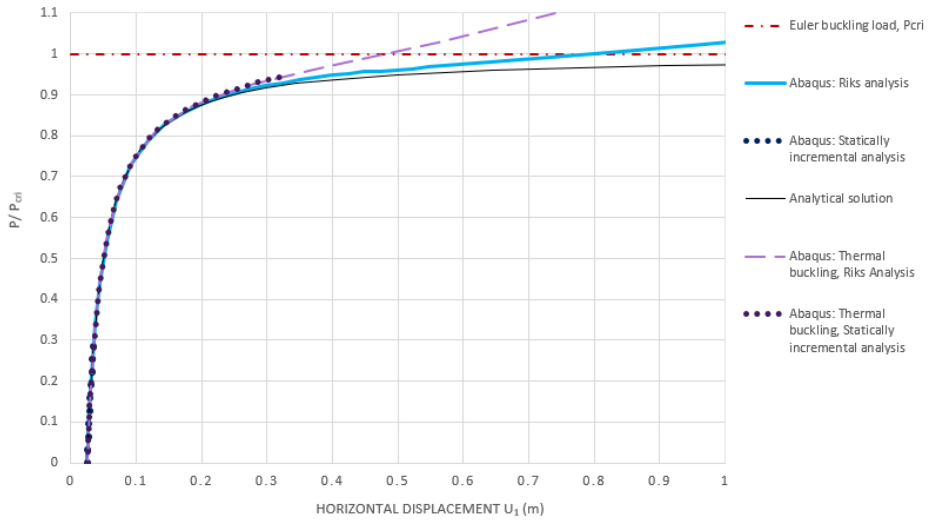


**Figure C.21** Load versus horizontal displacement.

Lastly, in Figure C.21, the Load versus horizontal displacement was plotted. The blue lines refer to the case where there is only temperature acting on the model while in the orange lines the model has no temperature but a punctual load.

It can be noticed that the curve is practically the same for both cases, at least until the 92% of the buckling load is reached. However the thermal buckling model presents a stiffer behavior.

It was calculated the critical temperature at which the beam will buckle, finding that the values is 109.66ºC. This temperature can be considered as low and maybe incorrect at first, specially if the graphs plot before are observed. However, this value is correct and the main reason why it is lower than expected is because it does not have into consideration the initial imperfection. If the same problem is analysed with smaller imperfection the graph plotted represents perfectly that the buckle starts at approximately 108ºC As the value of the imperfection is getting smaller the buckling temperature observed gets closer to the critical value calculated.
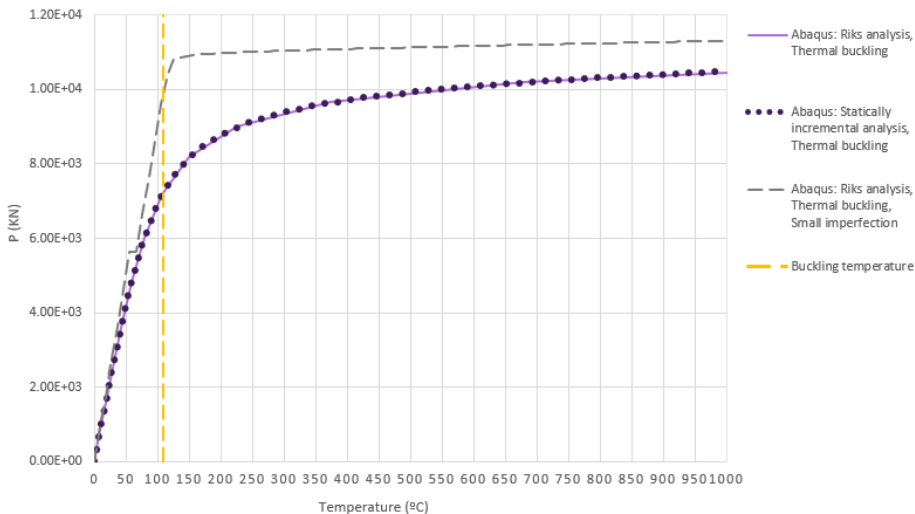


**Figure C.22**

### C.3.4.1   Material degradation

The Young modulus degradation curve used is the one developed by Kristian Hertz and it corresponds of a 0.2% stress reduction of cold worked steel sections.
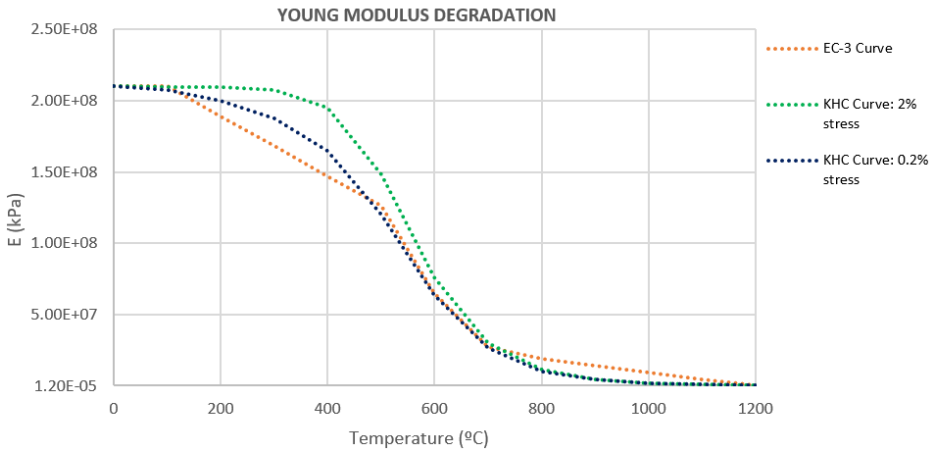
**Figure C.23** E degradation curves
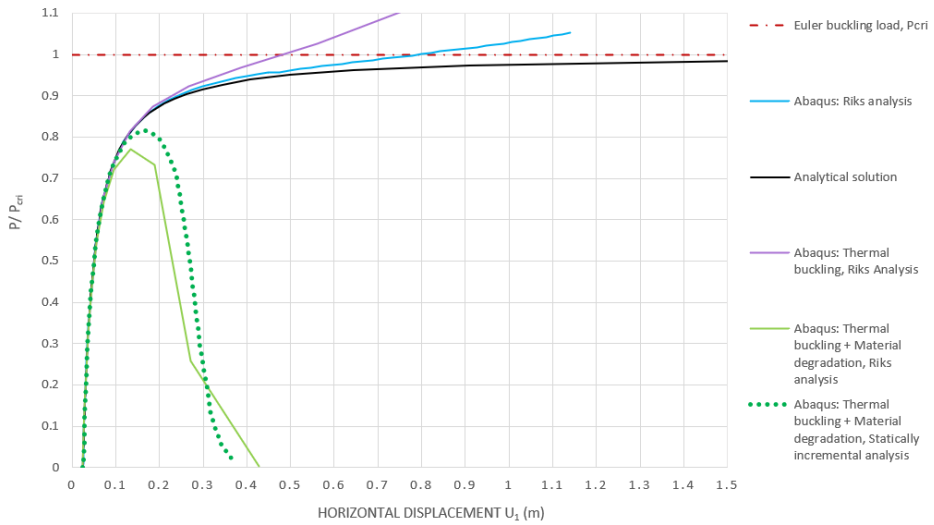


**Figure C.24** E degradation effect.

## C.3.5   2D Column modelling

The same case as before was modelled in 2D using solid elements. The objective is to reproduce the same problem with a different model and compare the results. The 2D structure created is a 5 meters beam with a width of 0.2 meters, Figure C.28.
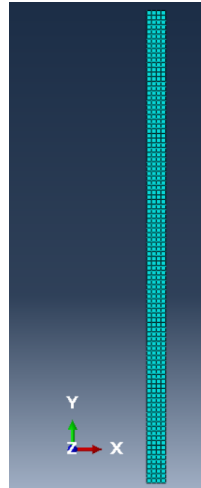
**Figure C.25** 2D model.

The element chosen is CPS4I which corresponds to the type of solid continuum elements with plane stress. It is a quadrilateral element with 4 node-bilinear and incompatible modes, Figure C.26. The thickness of the element is 0.2 meters, the same as the width. The main reason why it was chosen a full integration element with incompatible modes is to avoid shear locking and hourglass phenomena, eliminating parasitic shear stresses.
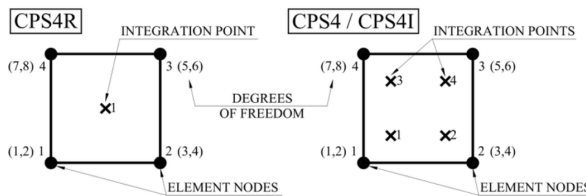


**Figure C.26** Type of element chosen.

The hourglass phenomena appears in reduce integration elements where it cannot be detected strains at the integration point due to bending. Regarding the shear locking, it is caused due to the linear nature of quadrilateral elements, which do not accurately model the curvature present in the material caused by bending. Then, a shear stress is introduce causing that the element reach equilibrium with smaller displacements, which gives stiffer results than in reality. This phenomenon affects mainly to pure

bending problems, but due to the initial imperfection introduce in the beam this issue can also affect to the case of study.

It is fundamental for the model to establish the proper boundary conditions. If they are not well introduced the system will not behave as a simple supported beam. The bottom of the structure is pinned and the restriction of the horizontal and vertical displacement is only applied in the central node of the base. With this boundary condition the rotation is allowed but not the translation. The top of the beam boundary conditions are also applied to the central node, where the horizontal displacement is not allowed. Instead of applying the boundary conditions to the border they were applied to the central nodes to reproduce the simple supported beam behaviour.
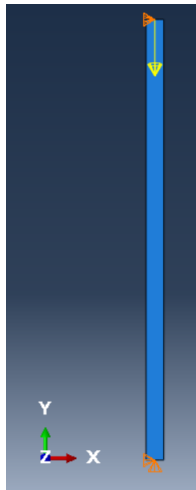


**Figure C.27** 2D model boundary conditions.

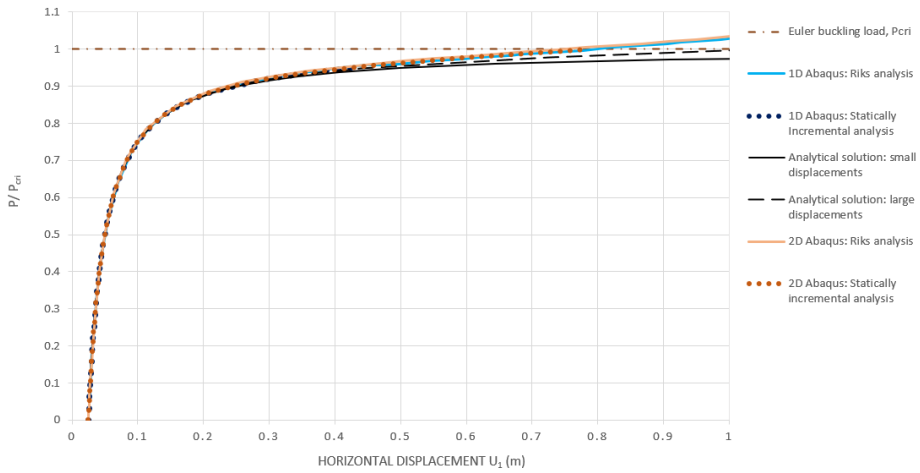As it can be observed in Figure C.28 the behaviour of the 2D model is the same as the one obtained for the 1D model.

**Figure C.28** Load versus horizontal displacement comparison for 1D and 2D model.

## C.3.6  3D Column modelling

Lastly the beam was modelled using 3D elements. The type of element used is S4, which is a homogeneous shell element, 4-node with full integration method. Now the beam has 6 degrees of freedom per each node and this should be considered when the boundary conditions are established. At the top of the beam a roller has to be placed being the restricted DOF U1, U3 and UR3. While at the bottom there is a pinned support which restricts the DOFs: U1, U2, U3 and UR3. The DOF UR3 refers to the rotation arround the Z-axis.
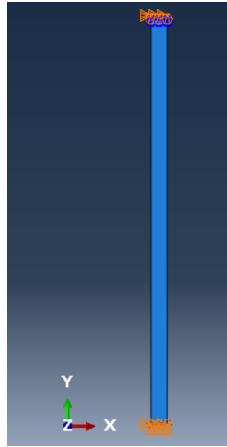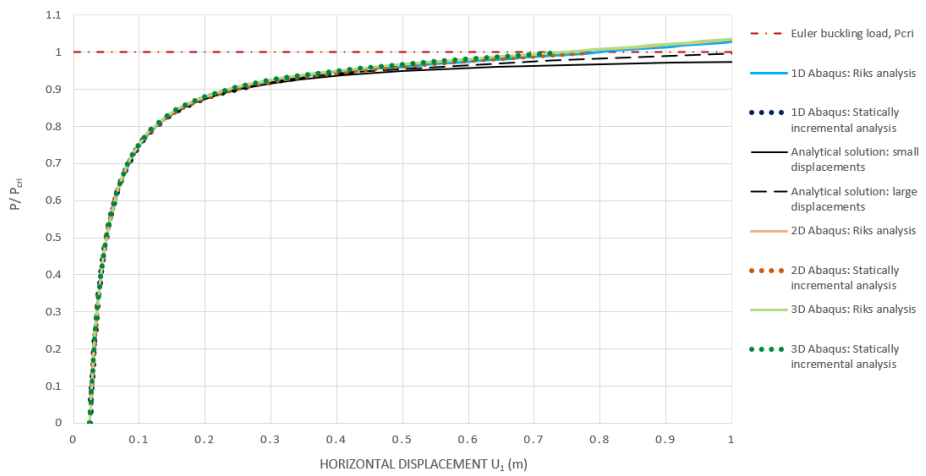
**Figure C.29** 3D model boundary conditions.



**Figure C.30** Load versus horizontal displacement comparison for 1D, 2D and 3D model.

# Buckling of plates: validation and calibration

### D.0.1 Single steel sheet model

The objective is to run Abaqus model and check with the analytical solution calculated that the behaviour of the plate corresponds to the one expected. This will validate this initial model and will serve as a first step towards the final model.

### D.0.2 Characteristics of the model

The model consists of a single plate with 2.8 meters height, 2.8 meters length and 2 millimetres thick, Figure D.1. The mechanical characteristics of the door will be the same as the ones that are going to be used for the final model, described in Section 2.4. But, for this validation, it is only going to be considered the elastic properties of the material. It also would not be considered the thermal dependent data.
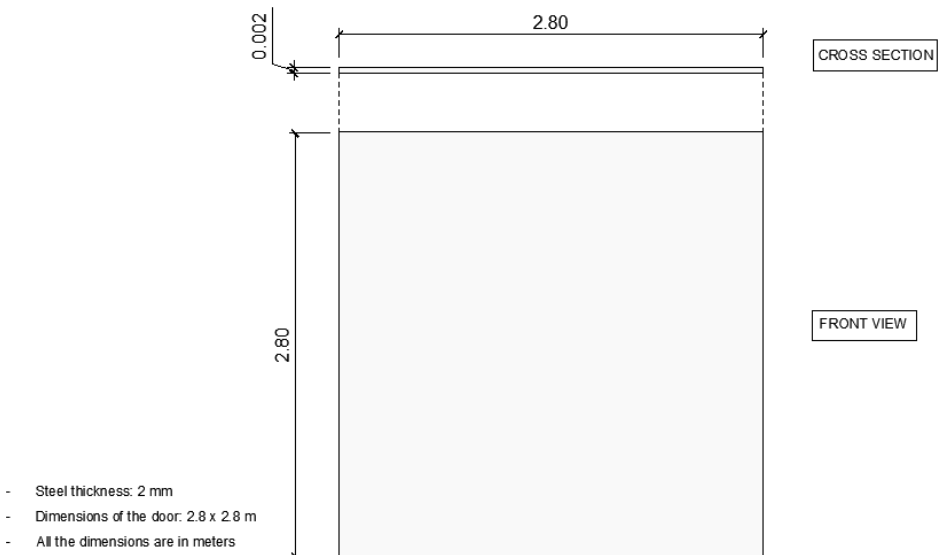
**Figure D.1** Geometrical characteristics of the single steel plate model.

The boundary conditions will correspond to a simply supported plate with free sides. The displacement at the bottom will not be allowed and only the rotation around the horizontal axis will be free. At the top, all the degrees of freedom will be restricted except the vertical displacement and the rotation around the horizontal axis. Besides, when the thermal load is acting also the vertical displacement at the top will be restricted.

Due to the characteristics of the model, it is going to be used the general-purpose shell element, S4, described in Section 3.2.2.1. This element was chosen because is the most appropriate for this case. However, a thin shell element like STRI3 could also be used due to the small thickness of the shell as opposed to the wide of the element. Its thickness is less than 1/15 of the shell width, so it can be considered as a thin shell.

### D.0.2.1  Analytical solution for steel plates axially loaded

First, the critical load and the critical temperature at which the plate will start to buckle will be calculated.

To calculate the buckling load of a simply supported plate Equation D.1 is used. This formulation comes from the Euler buckling theory and its equation for calculating the critical buckling load in beams. The formula used is a variation that allows calculating buckling in plates and shells [19].

$$P_{cri} = \frac{\pi^2 EI}{(1 - \nu^2)L^2} \tag{D.1}$$

The value of $E$ is 210 GPa, $\nu$ is equal to 0.3, $L$ corresponds to the height of the plate which is 2.8 meters and $I$ is the inertia modulus which has a value of $1.86 \cdot 10^{-9}$ $m^4$. The value at which the shell starts buckling is 54.23 Newtons.

Now, the critical temperature at which the system starts buckling can be estimated using Equation D.2. The value of $\alpha$ is $12.2 \cdot 10^{-6}$ $C^{-1}$ which its the coefficient of thermal expansion, E is the Young modulus and $A$ is the cross-section area that is equivalent to 0.056 $m^2$. The temperature at which the model will start buckling is $3.7 \cdot 10^{-2}$ ºC.

$$\Delta T = \frac{P_{cri}}{AE\alpha} \tag{D.2}$$

The values obtained are really low so it can be said that the model does not practically have mechanical resistance by itself. The reason is that the steel sheet is really thin and by itself, it does not have much resistance.

Lastly, the equation used to calculate analytically the displacement as a function of the load applied is shown in Equation D.3 [21].

$$w(x, y) = \frac{\delta}{1 - \frac{P}{P_{cri}}} \sin \frac{\pi x}{L} \sin \frac{\pi y}{B} \tag{D.3}$$

The letter $\delta$ refers to the initial imperfection introduce in the model, for this case it is equal to 0.005 meters. Regarding x and y, they are the coordinates of the point analysed, the value of x refers to the horizontal axis and y to the vertical axis. The length of the plate is referred to as L and the width as B.

### D.0.2.2   Mechanical load model

The plate was loaded with a uniform axial load along its width and two different analysis were run. First, the eigenvalue analysis to find the buckling modes and shapes, and lastly the statically incremental analysis to study the post-buckling behaviour.

**Eigenvalue analysis**

The Eigenvalue analysis was run and the first buckling loads calculated corresponds perfectly to the analytical solution, in shape and load. The first buckling load obtained in Abaqus is equal to 52 Newtons, which is practically the same as the analytical critical load calculated before. The error is less than 3% which is acceptable. The shape is the one expected for a simply supported square plate with axial load.
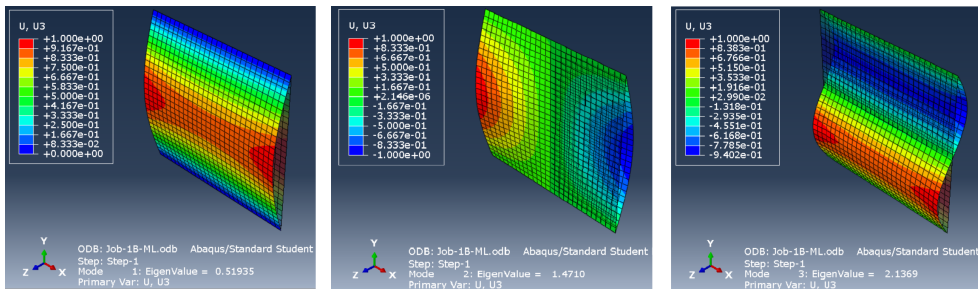


**Figure D.2** First three buckling modes of a 2 mm thick shell that is axially loaded.

**Statically incremental analysis**

Afterwards, post-buckling behaviour was analysed. The middle point of the shell was used for this study of the steel sheet behaviour. The diagram force-displacement was plotted and it was compared with the analytical solution for this specific case. The results can be observed in FigureD.3, where it can be observed that the behaviour is the one expected. So, it can be said that the model used has been verified.
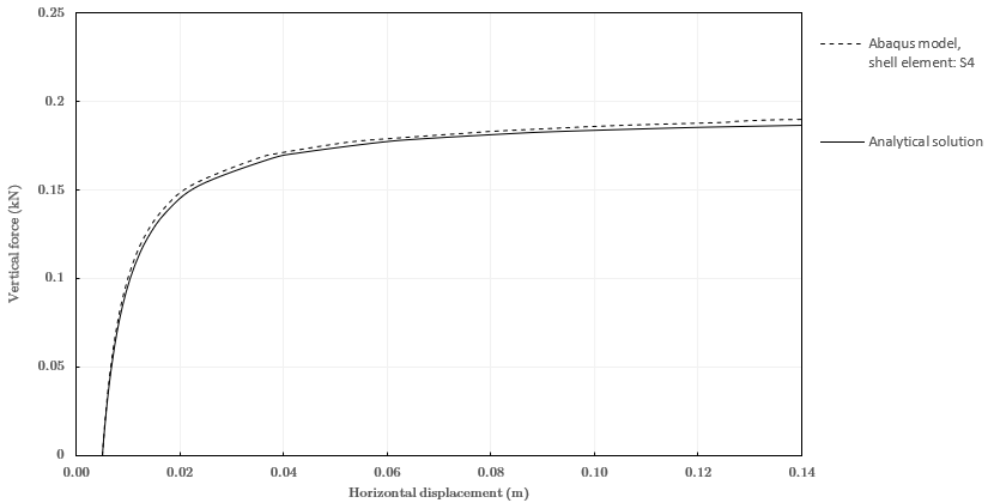
**Figure D.3** Graph vertical force versus displacement. Post-Buckling behaviour of a 2 mm thick shell that is axially loaded.

## D.0.3   Thermal load model

The plate is going to be subjected to a thermal load instead of a mechanical load. The load will be acting on the whole surface and, to allow thermal buckling, the vertical expansion of the steel will be restricted.

It was observed that, due to local buckling, the post-buckling behaviour could not be validated with the analytical solution for this case. However, the objective is to check if the model is working fine for this load condition with the specific boundary conditions specified before. So, to do that it was performed a second analysis with a 3 cm thick door to avoid local buckling and check if the post-buckling behaviour corresponds to the one expected.

**Eigenvalue analysis**

First, the Eigenvalue analysis for the panel with 2 mm thickness was run and it was checked that the first buckling modes correspond to the analytical solution. The first critical temperature at which the panel buckles is equal to $3.7 \cdot 10-2^{\circ}$C and the value obtained with Abaqus is $3.27 \cdot 10-2^{\circ}$C. The shape of the first three buckling modes corresponds to the ones expected and they also match the shapes obtained

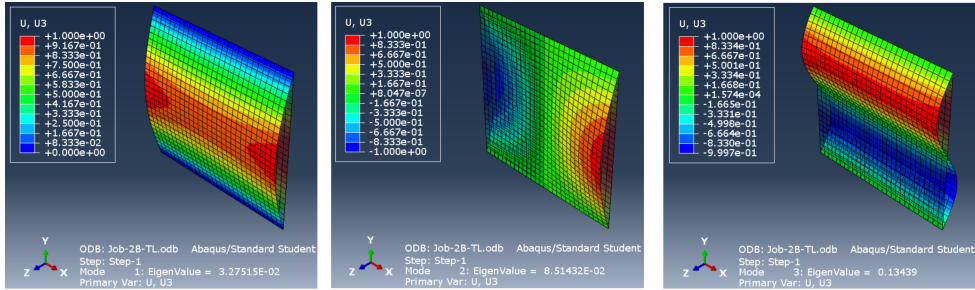with the model where the mechanical load was acting.



**Figure D.4** First three buckling modes of a 2 mm thick shell that thermally loaded.

Then the 3 mm thick panel was analysed. The analytical value obtained for the critical temperature for the first buckling mode is equal to 7.73ºC. This value matches with the one obtained in Abaqus, which is 7.36ºC, approximately 5% error. The first three buckling shapes obtained are the same as the ones obtained with the 2 mm thick case.
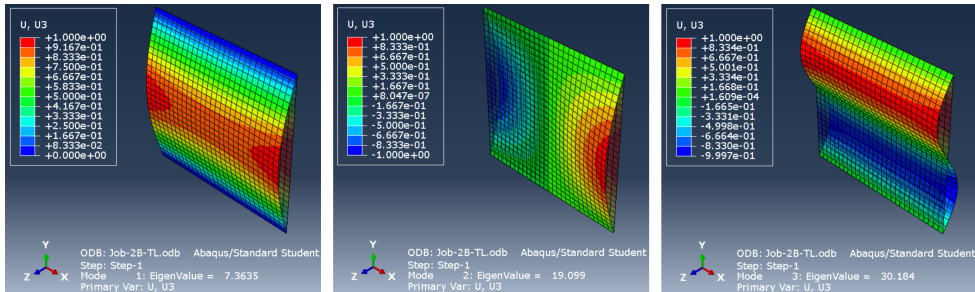


**Figure D.5** First three buckling modes of a 3 cm thick shell that thermally loaded.

**Statically incremental analysis**

To analysed the post-buckling behaviour a statically incremental analysis was run. However, it was noticed that due to local buckling the analytical formulation used is not correct for this validation. However, for a stiffer plate, it is useful so the model was validated with the 3 cm thick shell. As it can be observed in Figure D.6 the result practically matches the analytical solution. The vertical force that the graph refers to is the total vertical force produce at the borders when the steel tries to expand due to temperature and the boundary conditions did not allow it. It is the total axial load at the borders.
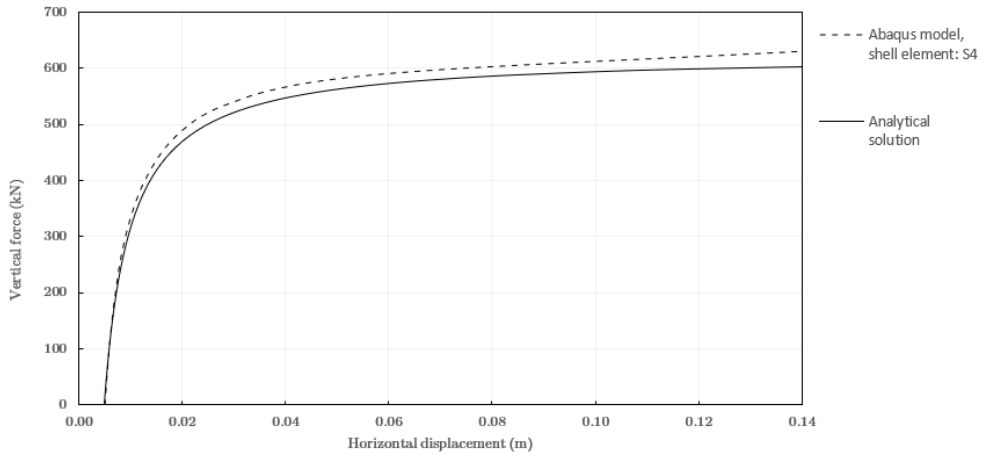
**Figure D.6** Graph vertical force versus displacement. Post-Buckling behavior of a 3 cm thick shell that is axially loaded.

# Analysis of the different elements in Abaqus

The objective of this appendix is to analyse the different types of element in Abaqus to chose the adequate one for the analysed case.

## E.0.1 Shell elements

After analysing the different types of shell elements available in Abaqus it was chosen three different ones to model a plate with the door characteristics. The element S4, STRI3 and CSS8 were used.

The characteristics of the element are the same for all the models, it is a plate with 2.8 meters length and 2.8 meters high with a thickness of 0.1 meters. It was chosen a big thickness for this first analysis but it was also checked that for a thinner thickness (2 mm, steel plate dimensions of a door) the results corresponds to what it was expected.

The plate is doubled pinned at the top and at the bottom. The mesh used is composed of 28 x 28 square elements, with a side length of 0.1 meters.
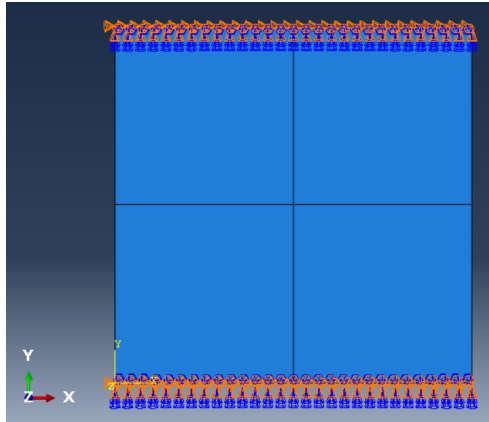
**Figure E.1** Plate geometric characteristics and boundary conditions.

### E.0.1.1   General-purpose conventional shell elements

This type of element corresponds to S4 and it was considered as appropriate for this specific case because it uses both, thin and thick shell theory, depending of the shell's thickness. So the shell was modelled with this type of element to compare its results with the ones obtained with the other models. It is a 4-node shell element that uses full integration. It considers shear deformation. The mesh used is composed with quadrilateral elements.
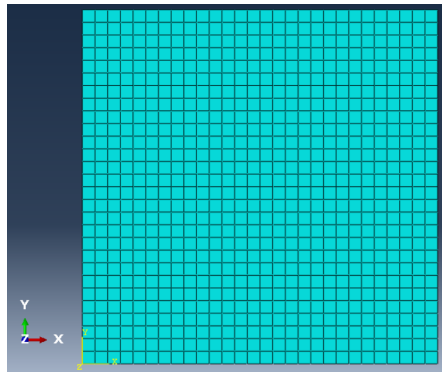


**Figure E.2** General-purpose conventional element mesh, S4.

### E.0.1.2   Thin conventional shell elements

Thin conventional shell elements were considered adequate because the thickness of the plate is smaller than 1/15 of the characteristic length of the shell, being this characteristic length the distance between supports. This element neglects the transverse shear flexibility and fulfills Kirchhoff requirement, having six degrees of freedom on each node. The mesh used is triangular.
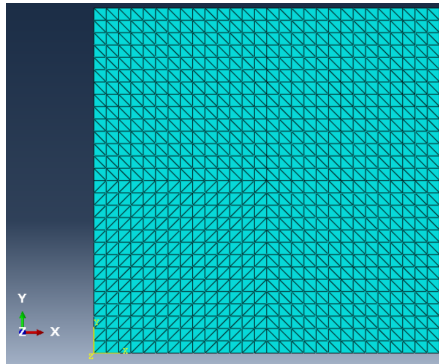


**Figure E.3** Thin conventional shell element mesh, STRI3.

### E.0.1.3   Continuum shell elements

Continuum shell elements were chosen to modelled the structure because allows to discretize the structure in 3D. The main advantage is that the thickness can be analysed better with this model. In the previous elements explained the shell was discretize from a reference surface. The mesh is a 3D quadrilateral element.
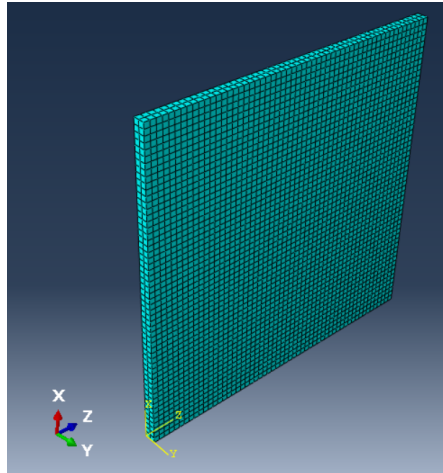
**Figure E.4** Continuum shell element mesh, CSS8.

## E.0.1.4  Comparison of results

## E.0.1.5  Eigenvalue analysis: buckling temperature

The buckling temperature calculated analytically corresponds to a temperature of 86º C. The temperatures obtained are slightly different but they get really close to this value, better results can be found as the mesh gets thinner.

The elements STRI3 and S4 have a really similar value while CSS8 not. This could be because CSS8 needs a better mesh discretization. The shapes obtained for the three cases is the same, as it was expected.
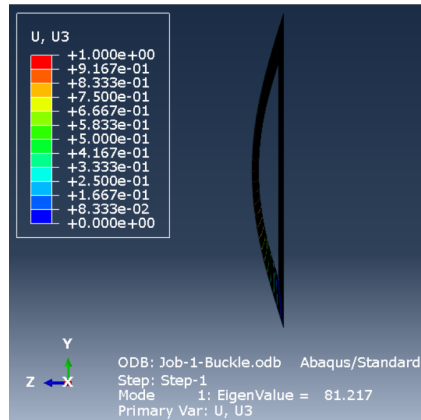
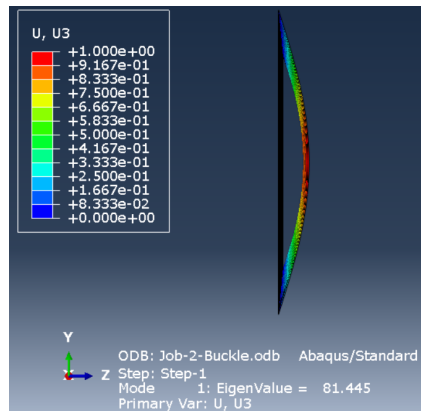**Figure E.5** Thermal buckling temperature for STRI3 element.



**Figure E.6** Thermal buckling temperature for S4 element.
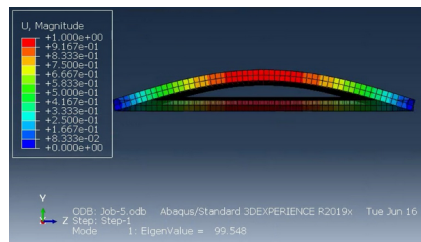


**Figure E.7** Thermal buckling temperature for CSS8 element.

Statically incremental analysis: post-buckling behaviour In order to analyse the behaviour of the different elements after buckling a comparative graphic has been plotted. There are two different graphs that allows to compare the performance of the elements, the first one plots the horizontal displacement versus the vertical load while the second one plots the temperature versus horizontal displacement. One way to validate the model is to compare the results obtained from a beam model with the rest of the elements.

The beam model is a simple 1D model of a beam, developed in a 2D space. The element employed is B23 and the analysis is elastic. This is the simpler model it can be developed, where the steel sheet is treat as a beam. The geometrical properties are the same as the ones used in the shell model, the height corresponds to the height of the door and the cross-section is equivalent to the dimensions of the top view of the door.
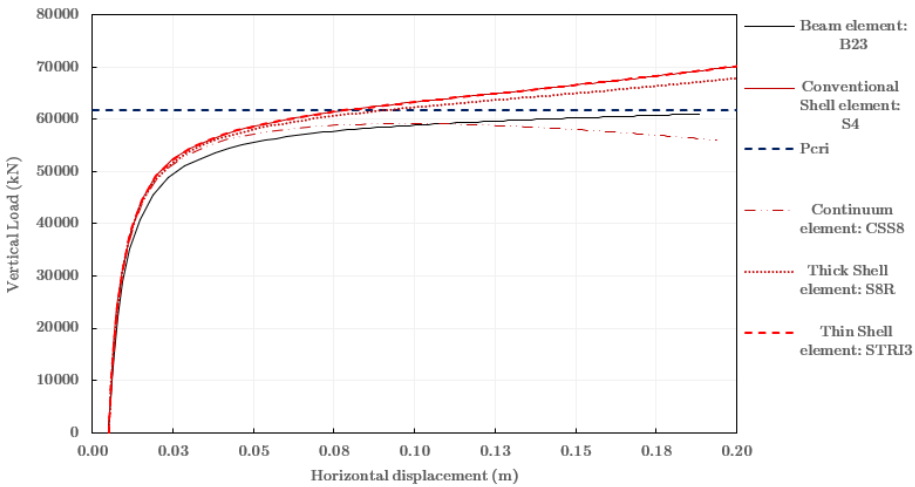


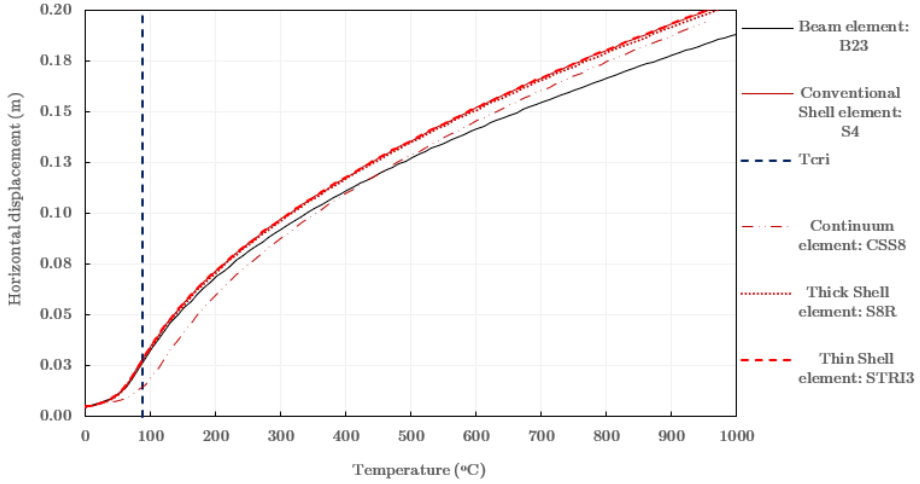**Figure E.8** Horizontal displacement versus Vertical load.

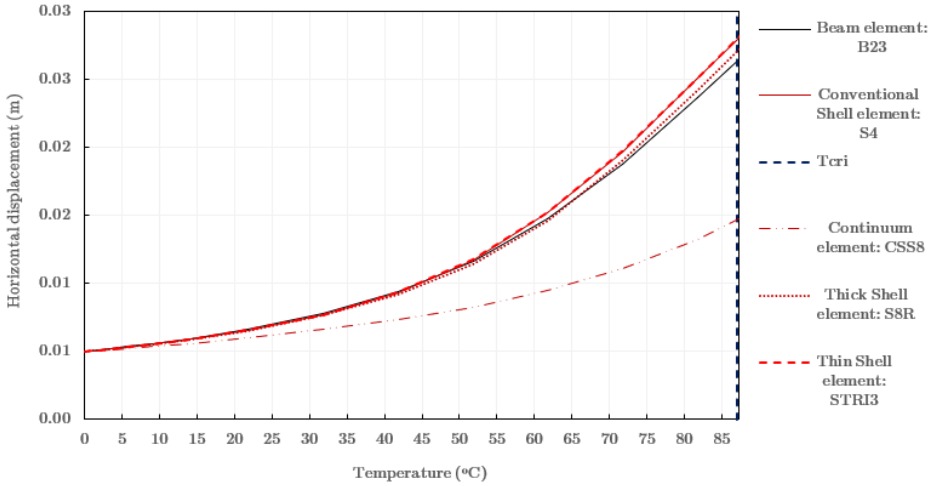**Figure E.9** Temperature versus horizontal displacement.



**Figure E.10** Temperature versus horizontal displacement zoom view.

As it can be observed before buckling the behavior is exactly the same as in the beam element. However is in the post-buckling analysis when the results follow a different path.
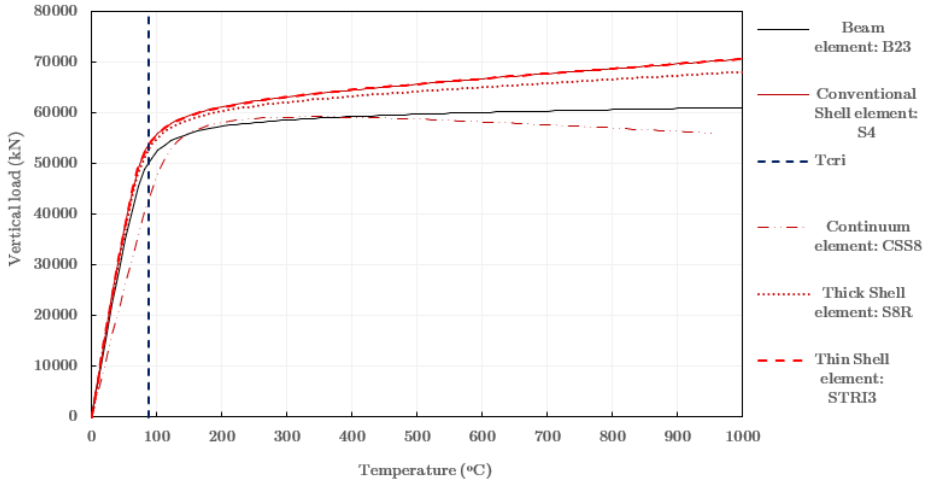
**Figure E.11** Temperature versus Vertical load.

# Bibliography

[1]  International Maritime Organization (IMO). *Fire Test Procedures Code (FTP code).* FTP Code sub-section 5.3 and Annex 1, Part 3 – Test for "A", "B", and "F" class divisions. 2010.

[2]  International Maritime Organization. *Recommendation for the evaluation of fire performance and approval of large fire doors.* MSC.1/Circ.1319. 2009.

[3]  Moro L De Bona F Gasparetto A Novak J Boscariol P. *Thermo-mechanical analysis of a fire door for naval applications.* Journal of fire sciences, 2014.

[4]  Joeux D. *Experimental investigation of fire door behaviour during a natural fire.* 14. Springer Science, 2001.

[5]  Ainara Sofía Franco Vergara. *Numerical model of the thermal behaviour of steel-doors in fire.* Master Thesis, Department of Civil Engineering. DTU, 2020.

[6]  *Samson Doors.* www.samsondoors.co.uk.

[7]  Matweb. *Material propety data.* http://www.matweb.com.

[8]  Directive 2004/18/EC The European Union Per Regulation 305/2011 Directive 98/34/EC. *Eurocode 2: Design of concretestructures - Part 1-1: General rules and rules for buildings.* EN 1992-1-1. 2004.

[9]  Directive 2004/18 The European Union Per Regulation305/2011 Directive 98/34/EC. *Eurocode 3: Design of steelstructures - Part 1-2: General rules - Structural firedesig.* EN 1993-1-1. 2005.

[10] Luisa Giuliani and Kristian Hertz. *Slides of the course: 11023 Structural Fire Safety Design.* DTU (Danmarks Tekniske Universitet), 2019.

[11] Hui Liu Yongxiang Wang Minghua Haim Waisman. *Strength and ductility performance of concrete-filled steel tubular columns after long-term service loading.* researchgate.net, 2015.

[12] R. Cook. *Concepts and Applications of Finite Element Analysis.* 1996.

[13] Robert M. Jones. *Buckling of bars, plates and shells.* Bull Ridge Publishing, 2006.

[14] Douglas Wright. *Notes on: Design and analysis of machine elements.* Buckling. Department of Mechanical and Materials Engineering. The University of Western Australia, 2005.

[15] Eduard Ventsel and Theodor Krauthammer. *Thin Plates and Shells. Theory, Analysis, and Applications.* Massachusetts Institute of Technology: MIT Open-CourseWare. Marcel Dekker Inc, 2001.

[16] DavidW.A.Ree. *Mechanics of optimal structural design: Minimum Weight Structures.* School of Engineering and Design, Brunel University, Uxbridge, UK. John Wiley  Sons, Ltd, 2009.

[17] Simulia. *Abaqus Analysis user's manual.* Abaqus 6.10.

[18] Simulia. *Abaqus/CAE User's manual.* Abaqus 6.10.

[19] Adam Wosatko Maria Radwánska Anna Stankiewicz and Jerzy Pamin. *Plate and Shell Structures. Selected Analytical and Finite Element Solutions.* Cracow University of Technology, Poland. Wiley  Sons Ltd, 2017.

[20] Josshua Sebastián Panchi Díaz. *Diseño y simulación de una puerta cortafuego peatonal batiente de simple hoja.* Trabajo de titulación previo a la obtención del título de Ingeniero mecánico. Escuela Politécnica Nacional (Ecuador). Facultad de Ingeniería Mecánica, 2018.

[21] Tomasz Wierzbicki. *2.080J Structural Mechanic. Lecture 11: Buckling of Plates and Sections.* Massachusetts Institute of Technology: MIT OpenCourseWare. https://ocw.mit.edu. License: Creative Commons BY-NC-SA, Fall 2013.